UNIVERSITÀ
DEGLI STUDI
FIRENZE

DOTTORATO DI RICERCA IN
SCIENZE BIOMEDICHE

CICLO XXIX

COORDINATORE *Prof. Dello Sbarba Persio*

STRUCTURAL DETERMINATION OF TOXIC AND NONTOXIC HYPF-N OLIGOMERS BY FRET

Settore Scientifico Disciplinare BIO/10

Dottorando
Dott.ssa Capitini Claudia

Tutore
Prof. Chiti Fabrizio

Coordinatore
Prof. Dello Sbarba Persio

Anni 2013/2016

To everyone I love

Table of Contents

Summary

The aggregation and accumulation of proteins into extracellular deposits of amyloid fibrils or into intracellular inclusions with amyloid-like properties is the hallmark of several human disorders, such as Alzheimer's disease, Parkinson's disease, type II diabetes and amyloidosis. It is nowadays accepted that oligomeric intermediates, rather than mature amyloid fibrils, are considered the primary pathogenic species in many protein deposition diseases.

The ability of the N-terminal domain of the bacterial HypF protein from *E. coli* (HypF-N) to produce oligomers with different biological properties when incubated in different solution conditions allowed to focus the attention on the parameters that determine a higher or a lower capacity of the oligomers to cause cell dysfunction. Previous data revealed that toxic HypF-N oligomers present a high degree of solvent-exposure and flexibility of the hydrophobic cores, necessary to interact and permeabilize the cellular membrane and, subsequently, determine an increase of calcium influx, production of ROS, activation of caspase-3, and, finally, cellular death.

This thesis work aims at contributing to elucidate the structural differences between toxic type A and nontoxic type B HypF-N oligomers with a level of detail higher than that obtained in previous studies. In a first set of experiments 12 mutational variants of HypF-N carrying a single cysteine residue located at different positions along the polypeptide chain were labelled with the fluorescent dye 1,5-IAEDANS and, then, were allowed to form oligomers under conditions A and B. The maximum fluorescence emission (λ_{max}) of this dye is influenced by the dielectric constant of the medium in which it is located. Thus, it is indicative of the hydrophilic/hydrophobic environment around the labelled residue in the oligomer. The results show that the hydrophobic regions of the sequence are more solvent-exposed in type A oligomers than in type B oligomers, in agreement with the PM excimer ratio analysis previously performed.

As a second set of experiments, a structural investigation of such toxic and nontoxic HypF-N oligomers was carried out using Förster Resonance Energy Transfer (FRET), using the 1,5-IAEDANS and 6-IAF dyes, that have the necessary prerequisites to be considered a suitable pair of donor/acceptor probes of FRET. Thus, all the single cysteine variants were labelled with 1,5-IAEDANS (donor) and 6-IAF (acceptor) and combined in a 1:1 molar ratio to form toxic and nontoxic oligomers. By calculating the FRET

efficiency from the donor to the acceptor, it was possible to determine and compare the degrees of intermolecular interaction between various residues in the oligomers.

The results show that FRET efficiency values are generally higher in the toxic oligomers than in the nontoxic oligomers. This means that the intermolecular distances between pairs of labelled residues in adjacent protein molecules in the oligomer are lower in the case of type A oligomers, indicating that these aggregates are more compact and structured than the oligomers B. However, most of the hydrophobic interactions appear to be less structured in the toxic type A oligomers, allowing the key solvent-exposed residues to be identified in the toxic assemblies.

Chapter 1

Introduction

1.1 Protein misfolding diseases

1.1.1 Principles of protein folding, misfolding and aggregation

Proteins are biological macromolecules which play an essential role in the cellular maintenance, growth and functioning of living systems, interacting each other in order to ensure the efficient and correct functioning of every chemical process. Following their biosynthesis as unstructured linear chains of amino acids fulfiled by ribosomes, the majority of proteins spontaneously converts into a tightly compact structure, that is fundamental for the proper performance of the protein functions. Although the majority of proteins folds in the cytoplasm or in specific cellular compartments, in some cases this process initiates during the translation, that is while the nascent polypeptide chain is still attached to the ribosome [Hardesty and Kramer, 2001; Hartl and Hayer-Hartl, 2002; Dobson, 2003]. The resulting three-dimensional structure, that represents the "native state" of the protein, corresponds to the most thermodynamically stable conformation that the protein achieves under physiological conditions among all possible monomeric conformations. Experimental and theoretical studies have shown that the process necessary for reaching the native structure, called "folding", involves a stochastic search of many conformations accessible to a given polypeptide chain, until the most energetically favourable one is found [Levinthal, 1968; Karplus, 1997; Dobson *et al.*, 1998; Dobson, 2004].

Before reaching the final native structure, protein molecules pass through incompletely folded states that expose critical regions of structure to the solvent, normally buried in the native state because of their tendence to interact inappropriately with the other surrounding molecules [Ellis, 2001]. Moreover, protein folding is made more difficult *in vivo* by the crowded environment of the cell, where proteins must assume their correct conformation while being constantly bombarded by high-energy collisions with neighboring proteins [Ellis and Minton, 2006]. In order to prevent the formation of these wrong interactions, but also to maintain the folded state after it is achieved, living

organisms have evolved a network of control and regulation systems of the folding process [Dobson, 2003]. Examples are molecular chaperones, that include the heat shock proteins (HSPs), which control the folding at a translational or post-translational stage, often working in tandem to guarantee a more efficient folding [Bukau and Horwich, 1998; Hartl and Hayer-Hartl, 2002; Voellmy and Boellmann, 2007]; folding catalysts, which accelerate some potentially slow steps during the folding process, in order to prevent aberrant interactions [Schiene and Fischer, 2000]; the unfolded protein response (UPR) and the endoplasmic reticulum associated degradation (ERAD), for proteins delivered to various organelles, to the cell surface, or to the extracellular environment [Kapoor and Sanyal, 2009; Hoseki *et al.*, 2010; Fu and Gao, 2014]; the ubiquitin-proteasome and the autophagy-lysosome, which are the two major protein degradation systems in all eukaryotic cells and act when it becomes clear that a misfolded protein cannot be properly refolded [Bejarano and Cuervo, 2010; Claessen *et al.*, 2012; Cohen-Kaplan *et al.*, 2016].

Despite these control systems, a broad range of human diseases is associated with the failure of the folding process, namely "misfolding", of specific peptides or proteins. This occurs primarly because of aging [Koga *et al*., 2011; Labbadia and Morimoto, 2015; Balchin *et al*., 2016], environmental stress and certain aspects of 'lifestyles', such as obesity [Zraika *et al*., 2010; Labbadia and Morimoto, 2015; Singh *et al*., 2015; Balchin *et al*., 2016], sustained increases in protein concentration [Hinton *et al*., 1997; Itoh-Watanabe *et al*., 2013; Singh *et al*., 2015], ingestion or iatrogenic transmissin of pre-formed aggregates [Collinge and Clarke, 2007], mutations [Benson *et al*., 2001; Canet *et al*., 2002; De Gracia *et al*., 2006; Caubet *et al*., 2010; Raimondi *et al*., 2011; Solomon *et al*., 2012; Spillantini and Goedert, 2013; Flagmeier *et al*., 2016], or aberrant proteolytic cleavage [Raimondi *et al*., 2011; Solomon *et al*., 2012]. All of these factors can act either independently of each other or simultaneously [Uversky, 2014]. These pathological conditions are generally referred to as "protein misfolding diseases" or "protein conformational diseases", in which an impairment in the folding efficiency causes the incapability of a protein to fold into its globular and functional state, or to remain correctly folded, favouring the acquisition of an alternative conformation to the native one. In some protein misfolding pathologies, a specific protein adopts a misfolded state that compromises the implementation of its normal function, as in the case of cystic fibrosis disease [Amaral, 2004], or determines an impairment of its translocation in the correct site, as in the early-onset pulmonary emphysema [Lomas and Carrell, 2002]. Many of these pathologies are familial, because the probability of misfolding is often higher in

mutational variants. The largest group of misfolding diseases is related to proteins with a high propensity to misfold that determines the loss of their soluble state and the consequent formation of fibrillar aggregates that accumulate within cells or, more commonly, in the extracellular space [Stefani and Dobson, 2003; Chiti and Dobson, 2006]. For this reason, this type of pathologies are also called "protein deposition diseases".

Protein aggregates, known as "amyloid fibrils", represent one of the possible aggregate forms that can be adopted by a monomeric protein (Figure 1.1). Fully or partially unfolded structures, as well as fragments of proteolysed proteins, are particularly prone to form disordered aggregates due to their interaction through hydrophobic moieties exposed to the solvent, normally buried in the native state. Disordered aggregates can then evolve in more organized fibrillar structures. In addition, even a native protein can associate to form aggregates, but with different features relative to the amyloid type ("native-like aggregates"). However, a folded protein, in some circumstances, can be converted in a non-native, partially, or fully unfolded state, that can facilitate intermolecular interactions and, therefore, the formation of amyloid fibrils (Figure 1.1) [Uversky and Fink, 2004; Chiti and Dobson, 2006].

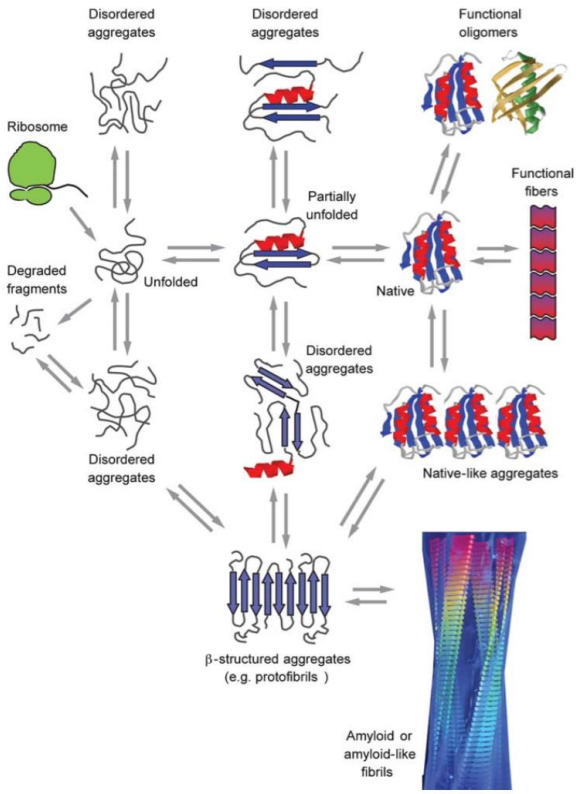

Figure 1.1. Schematic representation of some of the many conformational states that can be adopted by a polypeptide chain and of the means by which they can be interconverted. Amyloid fibrils are one of the possible aggregate forms. All of these different conformational states and their interconversions are carefully regulated in the biological environment, by using machineries, such as molecular chaperones, degradation systems, and other quality control processes. Conformational diseases will occur when such regulatory systems fail. Figure taken from Chiti and Dobson, 2006.

It is well known that the aggregation process leading to amyloid formation is characterized by a "nucleated growth" mechanism. The time course in which a peptide or protein converts into its fibrillar form typically consists of a lag phase followed by a rapid exponential growth phase [Naiki *et al*., 1997; Serio *et al*., 2000; Pedersen *et al*., 2004]. The lag phase is the time required for the formation of "nuclei", and is considered to be the rate-limiting step [Orte *et al*., 2008; Morris *et al*., 2009]. Once a nucleus is formed, fibril growth proceeds rapidly by further association of either monomers or oligomers with the nucleus [Chiti and Dobson, 2006]. Oligomers are complexes of a few number of molecules with a typical diameter of 2-5 nm, which present a transient, unstable and heterogeneous conformation [Chiti and Dobson, 2006; Stefani, 2010]. Initially disordered oligomers can then reorganize into an ordered β-sheet structure and further associate with each other to form amyloid protofibrils, which can appear as either isolated spherical beads of 2-5 nm in diameter or chains of beads again having a diameter of 2-5 nm. Protofibrils can also be able to associate and function as precursors for longer protofilaments and mature fibrils, which represent the final products of the aggregation process, characterized by a high thermodynamic stability (Figure 1.1) [Jahn and Radford, 2008].

1.1.2 Diseases caused by improper protein degradation

Cellular degradation systems, such as ERAD, ubiquitin-proteasome and the autophagy-lysosome, are essential for preventing the accumulation of non-functional misfolded proteins [Kapoor and Sanyal, 2009; Bejarano and Cuervo, 2010; Hoseki *et al.*, 2010; Claessen *et al.*, 2012; Fu and Gao, 2014; Cohen-Kaplan *et al.*, 2016]. However, they can sometimes cause disease by being overactive, degrading improperly proteins that, although mutant, retain some functionality. A canonical example is provided by the cystic fibrosis, which is caused by mutations in the gene of cystic fibrosis transmembrane conductance regulator (CFTR), a plasma membrane chloride channel. The most common causative mutation observed in patients with cystic fibrosis is the deletion of the phenylalanine residue at position 508 (ΔF508) [Qu *et al*., 1997]. This mutation causes the protein to be misfolded and targeted for degradation. Maturation and degradation of CFTR require its association with several chaperones and co-chaperones. When the function of these chaperones is compromised, mutant CFTR can escape its degradation. For instance, experiments of knockdown of AHA1, a co-chaperone that works together with HSP90 altering the maturation of CFTR, determine a more stability and a partially

more funtionality of CFTR ΔF508 [Wang *et al*., 2006]. In addition to AHA1, a co-chaperone of HSP70, named CHIP, aids in the ubiquitylation and later degradation of mutant CFTR. It was observed that the block of CHIP function might also allow more CFTR to mature and function [Meacham *et al*., 2001]. These studies suggest that inhibition of chaperone systems could be therapeutically beneficial to individuals with this mutation.

A related example of this category of improper protein degradation diseases is provided by Gaucher's disease, the most common lysosomal storage disease [Futerman and van Meer, 2004; Cox and Cachón-González, 2012]. Gaucher's disease is caused by a number of mutational variants of the lysosomal β-glucosidase, an enzyme that plays a role in metabolism of the lipid glucosylceramide. Defects in this enzyme result in intracellular accumulation of its substrate, particularly in white blood cells. Patients with Gaucher's disease can display a high degree of symptom variability, such as bone lesions and enlarged spleen and liver [Grabowski, 2008]. It was supposed that this variability may be related to the extent of degradation of β-glucosidase in the ER [Ron and Horowitz, 2005], that in some cases can implicate a correct trafficking of the functional protein to the lysosome, even in individuals carrying disease-associated mutations. For this reason, it was proposed the upregulation of chaperones that assist in the correct folding of β-glucosidase as a useful intervention for the disease [Sawkar *et al*., 2006]. Indeed, some drugs identified as "pharmacological chaperones" have demonstrated their efficacy in cells derived from individuals with the disease, in which they mimic the activity of chaperones by binding to the β-glucosidase and stabilizing its fold, in order to allow its transfer to the lysosome, *i.e.* the site of activity [Sawkar *et al*., 2002; Sawkar *et al*., 2005]. Currently, enzyme replacement is one of the main treatment options for Gaucher's disease. However, this requires intravenous delivery and is quite expensive. These recent advances suggest that small-molecule-based therapy, which is potentially cheaper and easier to administer than enzyme delivery, could provide an alternative strategy.

1.1.3 Diseases caused by improper protein localization

The fact that many proteins must fold correctly in order to be trafficked properly to their specific organelles wherein they act, imply that mutations destabilizing the correct folded state can cause an improper subcellular localization of the protein. This can result in dysfunction via both loss of function of the protein at its normal location and gain of function if the protein acquires a toxic effect in a wrong site where it accumulates. As an

example of this dual behaviour, the secreted protease inhibitor α1-antitrypsin, when mutated, causes emphysema in a recessive loss of function manner and liver damage in a dominant gain of function manner [Perlmutter, 2011]. The misfolding of the mutant forms of this protein determines its block in the ER of hepatocytes, that is the site of its synthesis. Moreover, the misfolded protein is not degraded, unlike other misfolded proteins, so it accumulates in the ER of hepatocytes resulting in liver damage [Lomas *et al*., 1992; Hidvegi *et al*., 2005]. Since mutated α1-antitrypsin is not secreted in its native form, it is also unable to perform its normal biological function, which is to inhibit the action of proteases, including neutrophil elastase, in the lung. As a consequence, the lung's connective tissue is extensively damaged, even if this condition can be controlled with enzyme replacement therapy [Mohanka *et al*., 2012]. In the liver, because α1-antitrypsin aggregates are degraded by macroautophagy, drugs that enhance autophagy, including rapamycin and carbamazepine, alleviate the hepatic toxicity induced by these protein aggregates [Hidvegi *et al*., 2010].

1.1.4 Diseases caused by dominant-negative mutations of protein

Another way by which protein misfolding can cause disease is through a dominant-negative mechanism, which occurs when a mutant variant of a protein antagonizes the function of the wild-type form, causing a loss of protein activity even in a heterozygote. An example of this class of pathologies is epidermolysis bullosa simplex, an inherited connective tissue disorder in which mutant forms of KRT5 and KRT14, two types of keratin proteins, lead to severe blistering of the skin in response to injury [Chamcheu *et al*., 2011]. Keratin forms long intermediate filaments that provide structure to the epidermis of the skin. The mutated keratin in the pathology undergoes misfolding and aggregation, particularly in response to mechanical stress [Russell *et al*., 2004; Werner *et al*., 2004]. Since a filament is formed by several keratin molecules, a heterozygote individual presents filaments containing both wild-type and mutant forms of the protein. The dominant nature of the disease is therefore explained by the fact that the mutant protein forming these filaments does not function properly, thus compromising the function of the entire filament. This explains why epidermolysis bullosa simplex is a dominant nature pathology. In the recent years, research groups have identified chemical chaperones that could prevent the aggregation of mutant keratin or degrade aggregates already formed and, thus, alleviate symptoms of the disease [Chamcheu *et al*., 2012].

The homotetrameric transcription factor p53 ia a second example of dominant-negative mutation disease that involves protein misfolding [Lubin *et al*., 2010; Gavrin *et al*., 2012; Gong *et al*., 2015]. Mutations in p53 are one of the most common genetic alterations recurring in cancer [Gong *et al*., 2015]. Indeed, p53 is the regulator of multiple pathways involved in maintaining genome integrity, including apoptosis, DNA damage repair, cell cycle regulation and metabolism [Freed-Pastor and Prives, 2012], and mutations in its gene can have far-reaching effects due to a dominant-negative mechanism. When no genotoxic stresses are present in the cell, p53 is rapidly degraded by the proteasome in a process depending on the ubiquitin ligase MDM2 [Kubbutat *et al*., 1997]. By contrast, in conditions of cellular stress, such as DNA damage, p53 is stabilized, forms a tetramer and acts as a stimulator of transcription of many target genes [Kamada *et al*., 2016]. Oncogenic mutations in p53 gene cause the destruction of the core domain of the protein, impeding the reaching of its correct fold [Lubin *et al*., 2010]. As a consequence, the expression of genes depending on p53, that are involved in the genome protection, is compromised and the risk of cancer increases. Mutant p53 is still able to associate with other p53 monomers, but the resulting tetramer does not function properly, even if a wild-type copy of p53 is present [Milner and Medcalf, 1991]. This explains the dominant-negative mechanism of dysfunctional p53 tetramers in a heterozygous state. Moreover, mutant p53 is not able to interact with MDM2, thus it cannot be degraded. Some compounds currently under clinical trials, called Nutlins, seem to prevent the degradation of correctly folded p53 by MDM2 [Vassilev *et al*., 2004]. Recently, because of the important involvement of p53 in different cancers, several research groups have discovered different compounds that restore function of mutant p53. One of these is pk7088, which binds and stabilizes p53 mutant Y220C, and restores its transcriptional functions similarly to the wild-type protein [Liu *et al*., 2013].

1.1.5 Diseases caused by gain of toxic function

In some cases, changes in protein conformation can induce the acquisition of a toxic function by a protein. The lipid transport apolipoprotein E (APOE) is an example: in the presence of the polymorphism APOE4, the protein is stabilized with an altered conformation [Dong and Weisgraber, 1996]. The other alleles of the protein have an extended domain structure that is compromised by an extra salt bridge in APOE4, consequently, the lipid affinity of APOE4 changes, mitochondrial function is disrupted and neurite outgrowth is impaired [Dong and Weisgraber, 1996; Chen *et al*., 2011; Nathan

et al., 1994]. The APOE4 allele has a worldwide frequency of 13.7%, but, interestingly, this frequency dramatically increased to ~ 40% in patients with Alzheimer's disease [Farrer *et al*., 1997]. Moreover, the APOE4 allele was found associated with increased levels of Aβ in the brain [Ma *et al*., 1994]. This reveals a strong implication of the polymorphism APOE4 in the pathogenesis of Alzheimer's disease. Possible therapeutic strategies focused on the prevention of the formation of the aberrant salt bridge are currently under study; compounds that correct APOE4 misfolding might also rescue APOE4-associated mitochondrial dysfunction and relieve inhibition of neurite outgrowth [Brodbeck *et al*., 2011].

Many oncogenic proteins involved in a high number of cancers acquire a different pathological function through mutation. The first one identified is a mutant of SRC (non-receptor tyrosine kinase), named v-SRC, which lacks the self-inhibitory phosphorylation site and promotes an uncontrolled cell proliferation [Xu and Lindquist, 1993; Whitesell *et al*., 1994; Bijlmakers and Marsh, 2000]. The mutant v-SRC is constitutively active, but it is much less stable than the wild-type c-SRC. However, the oncogenic form can be helped by the chaperone HSP90 to acquire its mature fold, localize to the membrane and avoid degradation. By contrast, wild-type SRC is much less HSP90-dependent [Xu and Lindquist, 1993; Whitesell *et al*., 1994; Xu *et al*., 1999; Bijlmakers and Marsh, 2000], thus, the excess capacity of HSP90 potentiates the evolution of v-SRC's malignant phenotype [Jarosz *et al*., 2010].

1.1.6 Diseases caused by amyloid deposition

The widest group of protein misfolding diseases regards those peptides or proteins that convert their soluble functional states into highly organized stable amyloid fibrillar aggregates (Table 1.1). The term "amyloidoses" is strictly referred to those pathologies characterized by the presence of extracellular protein deposits, known as "amyloid fibrils" or "amyloid plaques". However, in other diseases, similar aggregates are localized within cells, either in the nucleus or in the cytoplasm, generally termed "intracellular inclusions" [Stefani and Dobson, 2003; Westermark *et al*., 2005]. Despite the different location, extracellular and intracellular protein fibrils share similar morphological and structural features [Serpell *et al*., 2000c; Berriman *et al*., 2003].

The human diseases caused by the deposition of such aggregates in tissues can be divided into (i) neurodegenerative disorders, characterized by the presence of aggregates in the brain, (ii) nonneurophatic localized amyloidoses, in which the aggregation occurs

in a single type of tissue other than the brain, and (iii) nonneurophatic systemic amyloidoses, where proteins are able to produce deposits in multiple tissues [Chiti and Dobson, 2006]. Many of these pathological conditions can have either sporadic or hereditary etiology: the sporadic event is commonly due to the age-related decline of the cellular machinery, whereas the familial forms are associated with mutations that increase their aggregation rate, making them more susceptible to proteolysis or to other effects, and are generally characterized by early onset and aggressive symptomatology [Chiti and Dobson, 2006]. For instance, Alzheimer's and Parkinson's diseases are predominantly sporadic, although hereditary forms are reported, whereas lysozyme and fibrinogen amyloidoses are caused by specific mutations and are hereditary. Prion diseases, such as spongiform encephalopathies, in addition to the sporadic and hereditary forms, can also be transmissible in human and in other mammals, since the infectious capability of the disease-related protein aggregates. Finally, other diseases, such as hemodialysis related amyloidoses, originate from medical treatment [Chiti and Dobson, 2006].

Proteinaceous aggregates found in patients suffering from any amyloid disease contain a major protein that forms the core of the aggregates, to which other molecules are usually associated, such as metal ions, glycosaminoglycans, the serum amyloid P component, apolipoprotein E, collagen, and many others [Hirschfield and Hawkins, 2003; Alexandrescu, 2005].

Typically, peptides and proteins forming amyloid fibrils are small in size, even if they differ for their structure; indeed, large proteins have a high propensity to aggregate, but a low tendency to form amyloids [Ramshini *et al*., 2011]. Some of them are proteins, such as lysozyme, while others are peptides originating from larger proteins, as in the case of the islet amyloid polypeptide (IAPP) fragments obtained by the specific cleavage of the amyloid β peptide (Aβ), or the case of polyQ stretches produced by degradation of proteins with polyQ extensions, such as huntingtin, ataxins and the androgen receptor [Stefani and Dobson, 2003; Chiti and Dobson, 2006].

1.1.7 Diseases caused by non-amyloid aggregation

As an alternative possibility to the formation of amyloid fibrils, proteins can aggregate into disordered aggregates or native-like aggregates that can grow without conversion into β-structured species and give rise to large amorphous deposits or native-like assemblies, retaining the structure characterising the initial oligomers. Examples of diseases associated with the formation of this type of protein aggregates include Primary

Disease	Aggregating protein or peptide	Disease	Aggregating protein or peptide
Neurodegenerative diseases		**Nonneurophatic systemic amyloidoses**	
Alzheimer's disease[a]	amyloid β peptide	AL amyloidoses[a]	immunoglobulin light chains of fragments
Spongiform encephalopaties[a,c]	prion protein and fragments thereof	AA amyloidoses[a]	fragments of serum amyloid A protein
Parkinson's disease[a]	α-synuclein	Familial Mediterranean fever[a]	fragments of serum amyloid A protein
Dementia with Lewy bodies[a]	α-synuclein	Senile systemic amyloidoses[a]	wild-type transthyretin
Frontotemporal dementia with Parkinsonism[a]	tau	Familial amyloidotic polyneuropathy[b]	mutants of transthyretin
Amyotrophic lateral sclerosis[a]	superoxide dismutase I	Hemodialysis-related amyloidoses[a]	β_2-microglobulin
Hungtington's disease[b]	hungtingtin with polyQ expansion	ApoAI amyloidoses[b]	N-terminal fragment of apolipoprotein AI
Spinocerebral ataxias[b]	ataxins with polyQ expansion	ApoAII amyloidoses[b]	N-terminal fragment of apolipoprotein AII
Spinocerebral ataxia 17[b]	TATA box binding protein with polyQ expansion	ApoAIV amyloidoses[b]	N-terminal fragment of apolipoprotein AIV
Spinal and bulbal muscular atrophy[b]	androgen receptor with polyQ expansion	Finnish hereditary amyloidoses[b]	fragments of gelsolin mutants
Hereditary dentatorubral-pallidoluysian atrophy[b]	athrophin-1 with polyQ expansion	Lysozyme amyloidoses[b]	mutants of lysozyme
Familial British dementia[b]	ABri	Fibrinogen amyloidoses[b]	variants of fibrinogen α-chain
Familial Danish dementia[b]	ADan	Icelandic hereditary cerebral amyloid angiopathy[b]	mutant of cystatin C
Nonneuropathic localised diseases			
Type II diabetes[a]	islet amyloid polypeptide	Calcifying epithelial odontogenic tumors[a]	unknown
Medullary carcinoma of the thyroid[a]	calcitonin	Pulmonary alveolar proteinosis[b]	lung surfactant protein C
Atrial amyloidoses[a]	atrial nutriuretic factor	Inclusion-body myositis[a]	amyloid β peptide
Hereditary cerebral haemorrhage with amyloidoses[b]	mutants of amyloid β peptide	Cutaneous lichen amyloidoses[a]	keratins
Pituitary prolactinoma	prolactin	Cataract[a]	γ-crystallins
Aortic medial amyloidoses[a]	medin	Corneal amyloidoses associated with trichiasis[a]	lactoferrin

[a] Predominantly sporadic, although in some of these diseases hereditary forms associated with specific mutations are well documented
[b] Predominantly hereditary, although in some of these diseases sporadic cases are documented
[c] 5% of cases are infectious (iatrogenic)

Table 1.1. Diseases associated with the formation of extracellular amyloid fibrils or intracellular inclusions with amyloid-like properties.

hyperoxaluria type 1, where mutant forms of Alanine:glyoxylate aminotransferase (AGT) aggregate amorphously in the cytoplasm [Danpure *et al*., 1993] and sickle cell anemia, where a mutant of haemoglobin aggregates to form native-like fibrils of haemoglobin in the red blood cells [Wishner *et al*., 1975; Dykes *et al*., 1978]. Interestingly, immunoglobulins or their subunits are found in all the different types of protein aggregates, including amyloid (as in light chain amyloidosis), amorphous (as in light chain deposition disease) and native-like (as in Berger's disease), thus representing a remarkable manifestation of the multiplicity of pathways existing in portein aggregation and of structures/morphologies that can be generated [Berger and Hinglais, 1968; Glenner *et al*., 1971; Jimenez-Zepeda, 2012].

1.1.8 Characteristics of amyloid fibrils

It is well known that peptides and proteins associated with amyloid diseases which do not show similarities in size, amino acid composition, sequence and structure, convert in amyloid fibrils which share many common features [Dobson, 2003; Chiti and Dobson, 2006]. Moreover, many studies suggest that proteins that do not show an amyloidogenic propensity *in vivo* can be able to form structures indistinguishable from the amyloid fibrils produced by disease-related peptides and proteins when appropriate solution conditions are provided [Guijarro *et al*., 1998; Chiti *et al*., 1999; Pedersen *et al*., 2006b; Ramakrishna *et al*., 2012]. This even includes proteins having different secondary and tertiary structure moieties, different biological functions and belonging to different organisms, for example some plant proteins [Konno *et al*., 1999; Pertinhez *et al*., 2001; Fändrich *et al*., 2003]. Hence, it is widely accepted that fibril formation could be a generic property of almost all the proteins, independently of their sequence and native structure. This common mechanism of fibrillogenesis further suggests that organisms might have adapted protein fibril formation through evolution. Indeed, amyloid fibrils are found to perform important functions in the cellular physiology of many organisms, including humans. For this reason they are referred as "functional amyloids" [Chiti and Dobson, 2006; Fowler *et al*., 2006; Maji *et al*., 2009; Li *et al*., 2012; Usmani *et al*., 2014]. For instance, Orb2, that is a neuronal RNA-binding protein that participates in memory consolidation in *D. melanogaster*, is functional when acquires an amyloid-like structure [Hervás *et al*., 2016], and the fibrillar protein Pmel17 contributes to the melanosomal maturation [Kelly and Balch, 2003]. Other examples of proteins able to form functional amyloids are: the intralumenal domain of melanocyte protein PMEL, that forms fibrious striations inside

melanosomes upon which melanin granules form [Fowler *et al*., 2006]; various peptide hormones that act as a natural storage in pituitary secretory granules [Maji *et al*., 2009]; receptor-interacting serine/threonine-protein kinase 1/3 (RIP1/RIP3) that mediates the TNF-induced programmed cell necrosis [Li *et al*., 2012]; fragments of prostatic acid phosphatase and semenogelins, whose function is still unknown for humans, but it was found to be exploited by the HIV virus for infection [Usmani *et al*., 2014].

From a structural point of view, amyloid fibrils formed by homotypic polymerization of monomers of size ranging from 3 to 30 kDa, present a typic long, unbranched filamentous structure with a diameter of 5-15 nm and a length of several micrometers [Sunde *et al*., 1997; Serpell, 2000a; Nelson and Eisenberg, 2006; Toyama and Weissman, 2011]. X-ray fiber diffraction patterns obtained from different *ex vivo* and synthetic amyloid fibrils show intense meridional reflections of ~ 4.8 Å and broad equatorial reflections of ~ 10 Å, suggesting a regularly repeating and an ordered structural form, characteristic of the cross-β motif [Eanes and Glenner, 1968; Sunde *et al*., 1997; Sunde and Blake, 1997]. The fibrils consist of multiple thin fibers, called "protofilaments", which are intertwined with each other. The protofilament consists of multiple β-sheets running parallel to the fiber axis, with individual β-strands perpendicular to the fiber axis. In most of the cases β-sheets show a parallel orientation, but they can also be found in an antiparallel arrangement [Chiti and Dobson, 2006; Toyama and Weissman, 2011].

The morphological characterization of the amyloid fibrils can be carried out using microscopic techniques. Transmission electron microscopy (TEM) and atomic force microscopy (AFM) have shown that fibrils are usually formed by 2-6 protofilaments, each of 2-5 nm in diameter [Serpell *et al*., 2000b]. Protofilaments twist together and form supercoiled rope-like fibrils of 7-13 nm wide [Sunde and Blake, 1997; Serpell *et al*., 2000b] or associate laterally forming ribbons that are 2-5 nm thick and up to 30 nm wide [Bauer *et al*., 1995; Saiki *et al*., 2005; Pedersen *et al*., 2006a].

Amyloid fibrils can be identified using their ability to bind specific dyes, such as Congo red (CR) and Thioflavin T (ThT) [Klunk *et al*., 1989; LeVine, 1995; Nilsson, 2004]. CR is the most commonly accepted dye, since the molecular mechanism of interaction between CR and amyloids is clearly established [Nilsson, 2004; Lindgren and Hammarström, 2010]. Fibrillar aggregates stained with CR show a distinctive yellow-green birefringence when viewed under polarized light [Missmahl and Hartwig, 1953]. The change in the maximum absorption wavelength of CR in the visible region,

particularly the red-shift from 490 nm to 540 nm, is also used to characterize the fibrils [Klunk *et al*., 1989]. The binding of ThT to fibrils determines a red-shift of its maximum absorption wavelength from 336 nm to ~ 450 nm, and, consequently, the appearance of a peak in the emission spectrum centred at ~ 485 nm, with an intensity that is proportional to the quantity of amyloid aggregates [LeVine, 1995]. The wide employment of ThT to follow the kinetics of amyloid formation is due to its property of showing no significant increase in fluorescence upon interaction with amorphous aggregates [LeVine, 1993; Nilsson, 2004].

Spectroscopic techniques, such as circular dichroism (CD) and Fourier transform infrared spectroscopy (FTIR) spectroscopies, can be used to measure the secondary structural changes of amyloid fibrils, even those occurring during the aggregation process. The growth of β-sheet motifs can be detected using CD signal in the far-UV region of light. FTIR is also useful to detect the growth of β-sheet structure during amyloid fibril formation, quantifying the increase in the ratio of absorptions at 1626/1645 cm^{-1} or 1695/1630 cm^{-1} [Nilsson, 2004].

The recent progress in the application of solid-state NMR (ssNMR) spectroscopy to amyloid fibrils and the innovative nano- or micro-crystals of small peptide fragments with amyloid characteristics, have allowed to obtain structures of amyloid fibrils at molecular or even atomic level (Figure 1.2) [Jaroniec *et al*., 2002; Petkova *et al*., 2002; Makin *et al*., 2005; Nelson *et al*., 2005; Ritter *et al*., 2005]. By comparing the information obtained by the high-resolution structures of various fibrils, it was evident that different amyloid fibrils share a cross-β structure with the presence of repetitive hydrophobic or polar interactions along the fibrillar axis. Moreover, it was suggested that the core region is composed of two to four sheets that interact closely with each other. However, there are also significant differences attributable to the influence of the side chains, such as the lengths of the β-strands, the arrangement in a parallel or antiparallel orientation within each sheet, the lengths and the structural properties of regions that are not part of the amyloid core, the number of β-sheets in each protofilament, and even the space between the β-sheets [Fändrich and Dobson, 2002]. Hence, slight variations within the common fibrillar core may be introduced by specific interactions among the side chain of a given sequence.

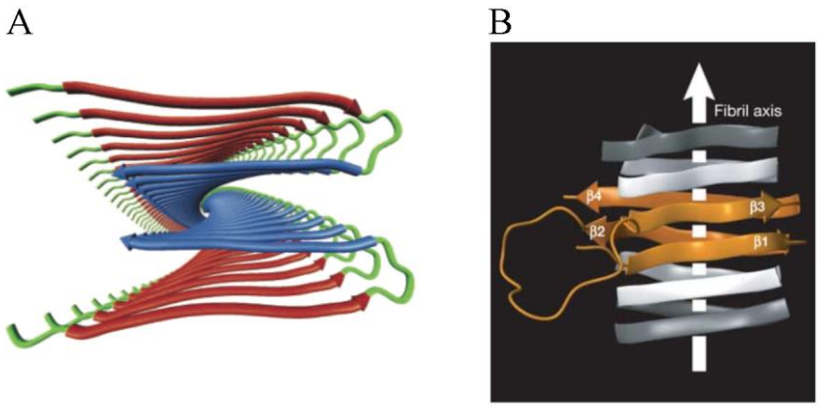

Figure 1.2. Molecular model of an amyloid fibril. (A) The protofilament of Aβ viewed down the long axis of the fibril. The segments 12-24 (red) and 30-40 (blue) are shown. Figure taken from Tycko, 2003. (B) The fibril from the C-terminal domain 218-289 of the fungal prion protein HET-s. The ribbon diagram shows the four β-strands (orange) (residues 226-234, 237-245, 262-270 and 273-282) and the long loop between β2 and β3 from one molecule. Flanking molecules along the fibril axis (gray) are shown. Figure taken from Ritter *et al*., 2005.

1.2 Misfolded protein oligomers

1.2.1 Oligomeropathies

The final product of the protein aggregation process occurring in pathology is normally represented by extracellular amyloid fibrils or intracellular inclusions (structurally equivalent), which can associate further to form larger assemblies. However, the possibility that low-molecular-weight oligomers and structured protofibrils can be the real pathogenic species rather than the mature fibrils, has acquired increasing relevance over the past 15-20 years, particularly for protein deposition diseases involving the central nervous system [Bucciantini *et al*., 2002; Billings *et al*., 2005; Cleary *et al*., 2005; Lesné *et al*., 2006; Koffie *et al*., 2009; Winner *et al*., 2011]. The term "oligomeropathies" is then used to define the neurodegenerative diseases associated with protein misfolding, where oligomers are the cause of neuronal dysfunction and are responsible for spreading the pathology. As an example, the severity of cognitive impairment in Alzheimer's disease correlates with the levels of small species of the Aβ peptide rather than with the amount of amyloid fibrils formed by the same peptide [Lue *et al*., 1999; McLean *et al*., 1999; Wang *et al*., 1999]. In particular, soluble Aβ oligomers were found to be both necessary and sufficient to disrupt learned behaviour [Cleary *et al*., 2005]. Another evidence of the importance of oligomers in the pathogenesis of Alzheimer's disease is that transgenic mice show deficits in cognitive learning before the accumulation of significant amount of amyloid plaques [Larson *et al*., 1999; Moechars *et al*., 1999;

Billings *et al*., 2005; Lesné *et al*., 2006]. Yet, in mice models of Alzheimer's disease synapse loss was found to be higher near senile plaques from which oligomers are released [Koffie *et al*., 2009].

Genetic mutations provide further support to the toxicity of the oligomers; the "Arctic" (E693G) mutation of the amyloid precursor protein (APP) gene, associated with a heritable early-onset manifestation of Alzheimer's disease, has been found specifically favor the formation of Aβ oligomers [Nilsberth *et al*., 2001; Tomiyama *et al*., 2008].

A number of experimental data have demonstrated that oligomers formed *in vitro* by proteins uncorrelated to any disease, such as the N-terminal domain of the procariotic protein HypF (HypF-N), which will be discussed extensively in the next section, the SH3 domain from bovine phosphatidylinositol 3' kinase (PI3-SH3) and apomyoglobin from sperm whale, can be strongly toxic to cultured cells, whereas the monomeric native forms and the amyloid-like fibrils formed *in vitro* display very little, if any, toxicity [Bucciantini *et al*., 2002; Sirangelo *et al*., 2004].

1.2.2 Oligomer structure and polymorphism

The structural characterization of oligomers has been hampered, relative to that of mature amyloid fibrils, mainly because these oligomers are heterogeneous in nature, form transiently, undergo interconversions and are often insoluble [Nelson and Eisenberg, 2006; Diaz-Espinoza and Soto, 2012; Eisenberg and Jucker, 2012; Tycko and Wickner, 2013]. In spite of these problems, several approaches and techniques have been introduced, allowing a deep molecular characterization of the oligomers structure.

When the aggregation process starts from fully or largely unfolded monomers, the initial oligomers show a large variety of conformations, with monomers still having a disordered structure (Figure 1.3). As an example, the early aggregates formed by $A\beta_{40}$ and $A\beta_{42}$ are dimers-tetramers and pentamers-hexamers, respectively, with a low level of structure; the acquisition of β-sheet occurs later on in the process, at the level of protofibrils [Bitan *et al*., 2003; Qi *et al*., 2008; Lee *et al*., 2011]. It was shown that also the initial aggregates formed by α-synuclein display unfolded monomers, that later interconvert into β-sheet containing oligomers which expose hydrophobic residues to the solvent [Cremades *et al*., 2012].

When aggregation initiates by native-like proteins, the beginning aggregates display monomers populating native-like states [Olofsson *et al*., 2004; Banci *et al*., 2005; Pagano *et al*., 2010], as in the case of the model protein Sso AcP, whose native structure

persists in its early aggregates [Pagano *et al*., 2010]. A mutational variant of SOD1 forms native dimers that interact to assemble larger oligomers which maintain monomers in a native-like fold [Banci *et al*., 2005]. Also transthyretin forms aggregates in which monomers maintain a native-like conformation (six β strands) with two misfolded edge strands [Olofsson *et al*., 2004]. Finally, initial oligomers from insulin are rich in α-helical motifs [Bouchard *et al*., 2000; Vestergaard *et al*., 2007].

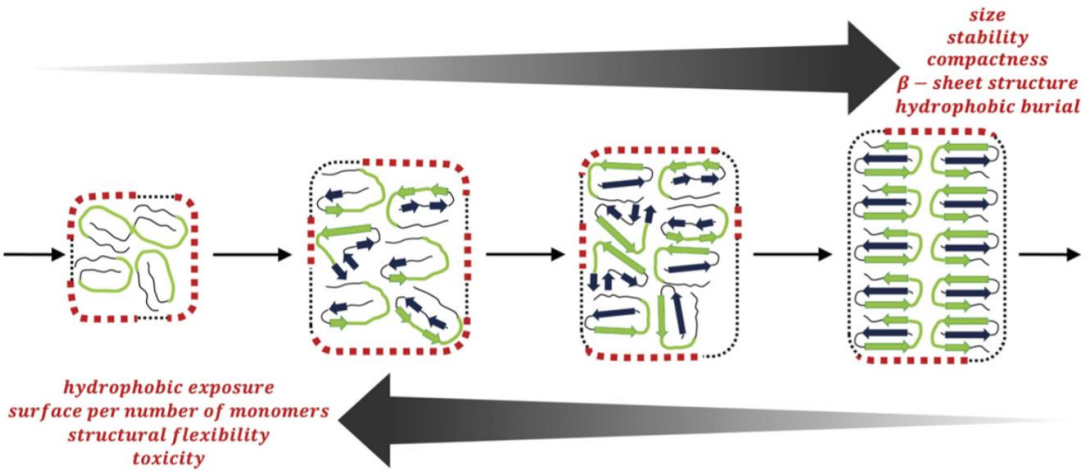

Figure 1.3. A schematic representation of the structural rearrangements occurring during oligomer formation. For simplicity, only aggregation starting from fully or largely unfolded monomers is considered. Amyloidogenic/hydrophobic segments are in green. The oligomer surface is drawn as a thin black when amyloidogenic/hydrophobic segments are buried and as a thick red dotted line when they are exposed to the solvent. While aggregation proceeds (left to right), a set of structural rearrangements takes place and leads to growth of thin filaments, which eventually originate amyloid fibrils: the top and bottom arrows show the parameters that increase and decrease, respectively. Image taken from Bemporad and Chiti, 2012.

The aforementioned examples of oligomers reveal that initial aggregates are far from the amyloid structure. Indeed, these aggregates do not bind amyloid specific dyes and do not show significant content of stable β-sheets [Plakoutsi *et al*., 2005; Lee *et al*., 2011]. As aggregation proceeds, oligomers reorganize their structure into species stabilized by β-sheet motifs, able to bind ThT and CR. Moreover, oligomers undergo an increase of their dimensions, compactness, stability and order, even still retaining a nonfibrillar morphology (Figure 1.3). During the aggregation process human muscle acylphosphatase (mAcP) oligomers turn into larger aggregates that exhibit a progressive increase of stability [Calamai *et al*., 2005]. The stable cross-β structure of the late aggregates is due to an internal reorganization of the early disordered oligomers, as confirmed by FRET studies carried out on α-synuclein oligomers, that determined a decrease in the distance between Tyr39 and Trp125 in the late oligomers relative to the early oligomers, suggesting an increased compactness [Kaylor *et al*., 2005; Cremades *et*

al., 2012]. Interestingly, the conversion into β-sheet containing amyloid-like aggregates was also observed for native-like aggregates with a significant level of α-helical structure, as in the case of α-helical native-like oligomers of insulin which convert into protofibrils with a high content of β-sheet [Bouchard *et al*., 2000; Vestergaard *et al*., 2007]. In addition, the β-sheet structure that form in the early aggregates, when present, is quite variable and unstable; solution NMR indicates that small globulomers of Aβ (38-48 kDa) contain both parallel and antiparallel β-sheet structure, while mature amyloid fibrils have only stable parallel β-sheet, as determined by solid-state NMR [Chimon *et al*., 2007; Yu *et al*., 2009].

In summary, as aggregation proceeds, oligomers undergo a continuous reorganization of their structure, which involves an increase in size, stability, compactness, regular β-sheet, and hydrophobic burial. Such a conversion can take place through many oligomeric states, or just in two states, each of which is an ensemble of oligomers with different size, structure, and so forth.

The fact that oligomers exist as a number of species with different morphologies and structures means that they exhibit polymorphism in terms of size, shape, compactness, stability and secondary/tertiary structure content [Calamai *et al*., 2005; Kaylor *et al*., 2005; Pountney *et al*., 2005; Mastrangelo *et al*., 2006; Bleiholder *et al*., 2011; Lee *et al*., 2011]. Different types of oligomers can be found in solution and *in vivo* at the same time [Goldsbury *et al*., 2005; Mastrangelo *et al*., 2006; Relini *et al*., 2010; Winner *et al*., 2011], but the predominance of some particular species can be influenced by a number of determinants. First, mutations can cause changes in the morphology/structure of the oligomers. An explicative example is represented by the Sso AcP oligomers, which can be β-structured when originated from a mutant variant of the protein, or native-like when formed by wild-type monomer [Soldi *et al*., 2008]. A second factor that can affect oligomer polymorphism is the solution conditions of the aggregation. For example, HypF-N is able to form oligomers under two different conditions that exhibit different cytotoxicities, attributed to differences in compactness and solvent exposure of hydrophobic regions [Campioni *et al*., 2010].

The importance of oligomer polymorphism is not restricted to the different structures and mechanisms of formation of oligomers, but it is also relevant for the biological activity of these oligomers. Indeed, it was shown that different mutants of Aβ in *D. melanogaster* led to different pathologies [Iijima *et al*., 2008] and that different oligomers of α-synuclein and Aβ induced cytotoxicity through different mechanisms

[Deshpande *et al*., 2006; Danzer *et al*., 2007]. Importantly, it is well established that polymorphism can help to explain the propagation of prion strain infectivity [Jones and Surewicz, 2005].

1.2.3 Structural determinants of oligomer toxicity

It has been observed that oligomers formed by different proteins are able to affect the cellular viability to the same extent, suggesting that the toxicity of these aggregates is due to their misfolded nature rather than to particular characteristics of their amino acid sequences. However, it has also been observed that different oligomers originated from the same protein show different levels of cytotoxicity. This hypothesis has induced many groups in the last years to study the structural elements that are responsible for the interaction between protein oligomers and cells and, then, that are the cause of the cell dysfunction.

A first important determinant of cytotoxicity was found to be the size of the oligomers: it was found that $A\beta_{42}$ pre-fibrillar aggregates having different sizes give rise to an inverse correlation between oligomer size and neuronal toxicity, with the smallest species having the highest ability to cause cell dysfunction [Cizas *et al*., 2010]. In addition, the same type of oligomers formed by two different Aβ peptides ($A\beta_{40}$ and $A\beta_{42}$) cause similar decreases of MTT reduction following their addition to the cells, wehereas MTT reduction increases with the size of the oligomers confirming the trend in which toxicity decreases with the increase of the oligomer size (Figure 1.4) [Bemporad and Chiti, 2012]. In addition, it was observed that three classes of small aromatic molecules can inhibit $A\beta_{42}$ oligomer toxicity by converting the small oligomers into large aggregates, fibrils, and monomers, respectively [Ladiwala *et al*., 2011]. Similarly, the formation of larger assemblies of toxic Aβ oligomers induced by other molecules, such as molecular chaperones, determined a suppression of their toxicity [Ojha *et al*., 2011], an observation confirmed by the chaperone-induced suppression of HypF-N oligomer toxicity [Mannini *et al*., 2012].

The higher ability of small soluble oligomers to cause cellular damage can be explained with their greater diffusion capability and higher hydrophobic surface per number of monomers compared to larger assemblies [Mannini *et al*., 2012]. This hypothesis suggests that fibrils formed at the end of the aggregation process have a lower toxicity with respect to their precursors, as they display hydrophobic burial and mass increase [Haass and Selkoe, 2007].

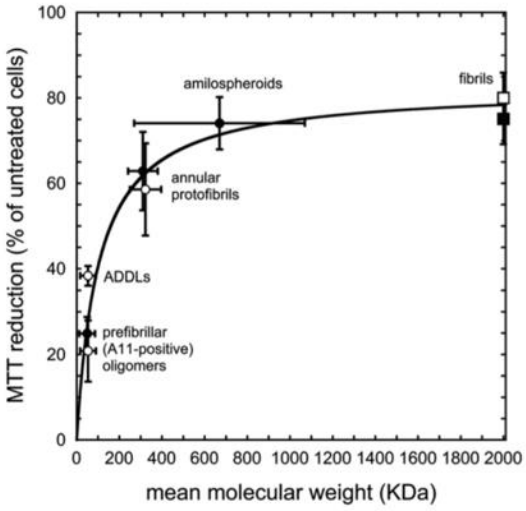

Figure 1.4. Toxicity versus size of $A\beta_{1-40}$ (filled circles) $A\beta_{1-42}$ (empty circles) aggregates. Toxicity is measured by determining MTT reduction by cultured cells following their exposure to oligomers added to the extracellular medium. Aggregate toxicity was expressed as percentage of MTT reduction relative to untreated cells, where 0% and 100% values are two extremes of full cell death and full viability, respectively. All data were obtained at a peptide concentration in the range of 2.0-2.7 mM and aggregate size was expressed as mean molecular weight. All data points were fitted to a hyperbolic function of the form y = a*x/(b+x). Image taken from Bemporad and Chiti, 2012.

Another important element of oligomer-mediated toxicity is the exposure of hydrophobic regions on the aggregates surface. For example, the two HypF-N oligomers formed under two different conditions, show similar morphology and size, but different toxicity, with one species found to be nontoxic altogheter [Campioni *et al*., 2010]. The reason of this different toxicity was found to be that the three most hydrophobic regions of the monomer sequence are structured and buried in the nontoxic oligomers, whereas in the toxic oligomers the same regions are more solvent exposed and flexible [Campioni *et al*., 2010]. Another study has demonstrated a strong correlation between toxicity of aggregates formed *in vitro* and added to the cell cultures medium and the solvent-exposure of the aggregates measured with ANS binding (Figure 1.5) [Bolognesi *et al*., 2010]. In addition, highly amyloidogenic proteins expressed in human embrionic kidney 293T cells present high levels of toxicity with the increase of the exposure of hydrophobic clusters on the aggregate surface [Olzscha *et al*., 2011]. In the latter study, the toxicity was attributed to the ability of the aggregates to interact with several cellular proteins, altering their biological functions [Olzscha *et al*., 2011], whereas toxicity of HypF-N oligomers was attributed to their interaction with the cell membrane that causes an uptake of calcium [Campioni *et al*., 2010; Zampagni *et al*., 2011]. Therefore, it is well established that hydrophobic exposure on oligomeric surface is an important determinant of toxicity, irrespective of the mechanism by which oligomers causes cell dysfunction.

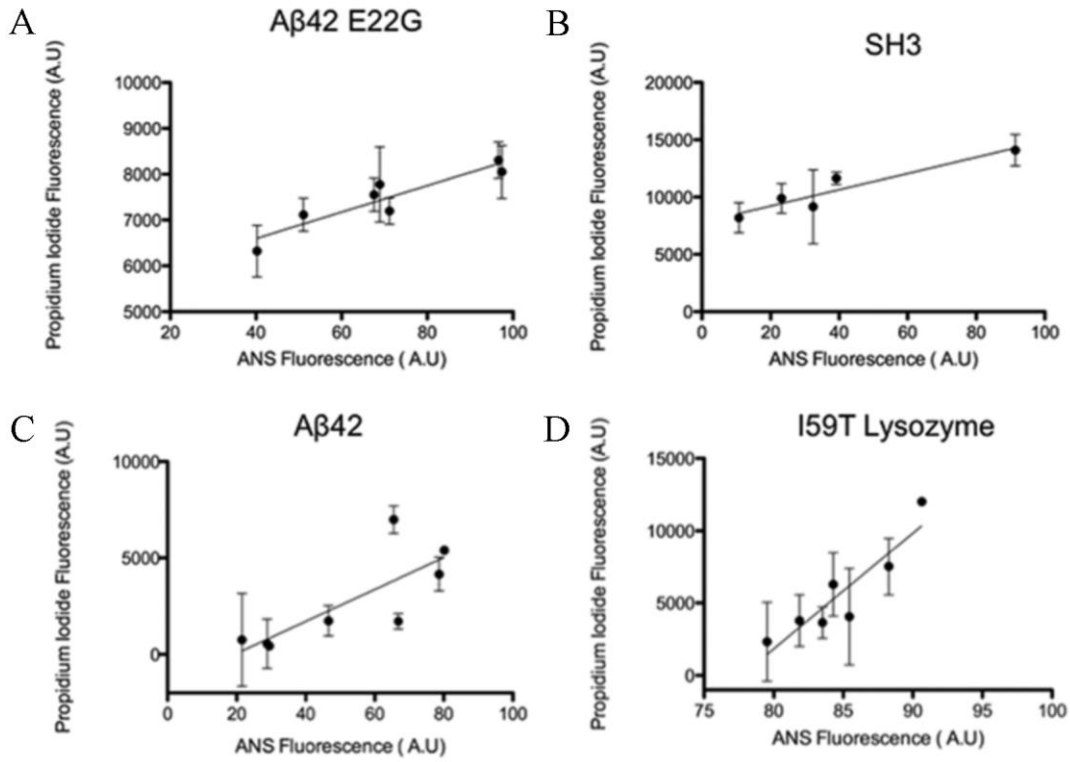

Figure 1.5. Correlation of ANS binding of aggregates with toxicity. Correlation graphs of the increment in ANS fluorescence signal and the corresponding increment in toxicity, as measured by PI incorporation, of the aggregates at different time points for (A) E22G $A\beta_{42}$, (B) PI3-SH3, (C) I59T lysozyme, and (D) WT $A\beta_{42}$. ANS data points are single measurements, while PI fluorescence data points are the mean of tree measurements. Error bars represent standard error of the mean. The results shown for E22G $A\beta_{42}$, SH3-PI3, I59T lysozyme, and $A\beta_{42}$ are representative of at least seven, three, three, and five independent experiments respectively. Image taken from Bolognesi *et al*., 2010.

As far as the degree of β-sheet structure is concerned, a detailed review of the literature shows that structured oligomers appear to be either more or less deleterious than unstructured ones depending on their size and solvent-exposed hydrophobicity, which again seem to be the most important factors in this regard. Nor does the shape of the oligomers appear to be very important: the interesting hypothesis that oligomers exert their toxicity by forming annular structures with a pore-like morphology does not appear to be supported by recent experimental data [Kayed *et al*., 2009; van Rooijen *et al*., 2010; Oropesa-Nuñez *et al*., 2016], and indeed the appearance of such structures may simply be a characteristic of the inherent architecture of the water-mediated face-to-face packing of pairs of β-sheet rather than a unique structural feature of the oligomers [Chen *et al*., 2015].

1.3 The model protein HypF-N

1.3.1 Function and structure of HypF-N

[NiFe]-hydrogenases are key enzymes involved in the prokaryotic hydrogen metabolism [Friedrich and Schwartz, 1993]. In their fully funtional states, the iron atoms of the active sites are stablized in the low oxidation state (Fe^{2+}) by binding to the carbon monoxide (CO) and cyanide (CN^-) ligands [Nicolet *et al*., 1999]. Both molecules have been shown to originate from the processing of carbamoylphosphate [Paschos *et al*., 2001]. In order to coordinate the assembly of the complex hydrogenase system, hydrogenase operons contain several genes, including a set of accessory genes (*hypA-F*) encoding maturation and regulatory proteins. One of these factors is HypF, which is essential for hydrogenase maturation [Colbeau *et al*., 1998]. HypF is a large multi-domain protein of *ca.* 82 kDa, constituted by three domains: a N-terminal "acylphosphatase" domain (residues 1-91), a sequence motif shared with enzymes catalysing O-carbamoylation reactions (residues 473-479), and two zinc-finger motifs similar to those found in the DnaJ chaperone (residues 109-134 and 159-184) [Casalot and Rousset, 2001]. Recent experiments shed light on the role of *E. coli* HypF in the conversion of carbamoylphosphate into CO and CN^-, and on the coordination of these ligands to the assembled hydrogenase metal cluster [Reissmann *et al*., 2003]. According to these observations, the N-terminal domain of HypF (HypF-N) acts as a carbamoyltransferase that transfers the carbamoyl moiety of carbamoyladenylate to the C-terminal cysteine of the partner protein HypE, forming an enzyme-thiocarbamate. HypE dehydrates the S-carbamoyl moiety in an ATP-dependent process to yield the enzyme thiocyanate. Finally, the cyano group can be nucleophically transferred to an iron complex [Reissmann *et al*., 2003].

HypF-N shares sequence and structure similarities to the acylphosphatase-like family (AcPs), that are small enzymes catalysing the hydrolysis of carboxyl-phosphate bonds in acylphosphates such as carbamoylphosphate, succinylphosphate and 1,3-bisphosphoglycerate [Stefani and Ramponi, 1995]. In addition, AcPs have been shown to possess nucleoside triphosphatase and nucleoside diphosphatase activities [Paoli *et al*., 2000] and catalyse also the hydrolysis of both DNA and RNA [Chiarugi *et al*., 1996]. However, in spite of sharing about 22% and 50% sequence identities with human and *E. coli* AcP, respectively, HypF-N does not show any catalytic activity characteristic of AcPs (Figure 1.6) [Chiti *et al*., 2001].

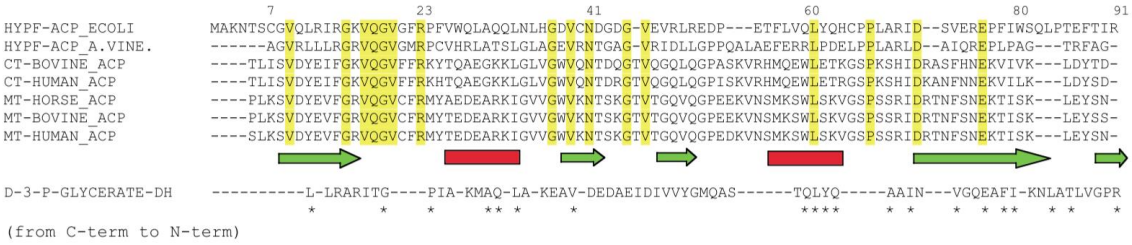

Figure 1.6. Multiple alignment of amino acid sequence of selected AcPs and HypF-N. The numbering on top refers to AcP. The positions of the secondary structure elements of HypF-N are reported on bottom. Conserved residues are enclosed in yellow boxes. Figure taken from Rosano *et al*., 2002.

The crystal structure of HypF-N was determined and, according to expectations on the basis of sequence homology, displays a ferredoxin-like fold with a α/β topology, consisting of a βαββαβ secondary structure (Figure 1.7) [Rosano *et al*., 2002]. More specifically, a five-stranded, slightly twisted, antiparallel β-sheet faces on one side two antiparallel amphipatic α-helices, with the sheet arrangement following a 4-1-3-2-5 β-strand topology. The domain covers a volume of about 43x28x27 Å [Rosano *et al*., 2002]. The compact, globular structure of HypF-N is stabilized by intramolecular contacts of the two α-helices, which turn their hydrophobic residues against the inner face of the β-sheet, leaving no core cavities in the protein structure. In order to disfavour intermolecular interactions and aggregation processes, the protein presents very short or highly twisted edge β-strands, a β-bulge (residues 71-72), a proline residue (Pro78) and a cluster of charged residues (Asp72, Glu75, Arg76, Glu77) [Rosano *et al*., 2002].

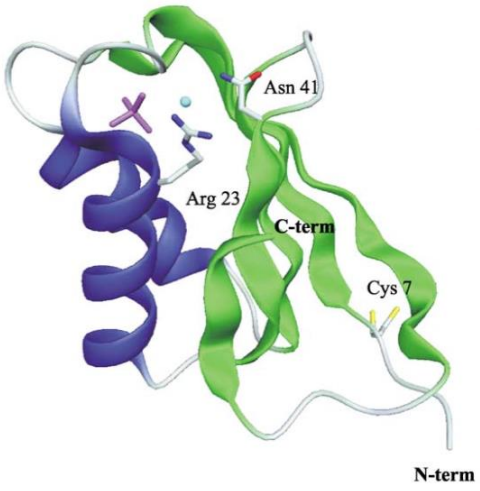

Figure 1.7. Ribbon representation of HypF-N structure. The secondary structure elements are displayed in blue (α-helices) and green (β-strands) colours. The putative active site is also shown with the conserved residues Arg23 and Asn41, the bound phosphate (purple sticks) and the bound chloride ion (light blue sphere). The Cys7 residue shown in figure was found to adopt two alternative conformations both able to form right-handed disulfides with a neighbouring molecule in the crystal. Figure taken from Rosano *et al*., 2002.

1.3.2 Folding of HypF-N

The folding process of HypF-N has been studied in detail by following changes in the intrinsic and extrinsic (dye derived) fluorescence of the protein upon refolding at different final concentrations of denaturant [Calloni *et al*., 2003]. The results have highlighted three major phases: very fast, fast and slow. Moreover, a molten intermediate forms in the submillisecond time-scale and is able to bind the hydrophobic probe 8-anilino-1-naphthalenesulphonic acid (ANS) [Calloni *et al*., 2003]. Experiments of refolding and unfolding kinetics have shown that the very fast phase corresponds to the folding process of the majority of molecules populating the intermediate state. By contrast, the folding kinetic traces acquired for the Pro78Ala HypF-N mutant indicate that the slow phase is due to the refolding of molecules having the Glu77-Pro78 peptide bond in a non-native *cis* configuration, and for this reason the slow *cis* to *trans* isomerisation step determines the rate of the process [Calloni *et al*., 2003]. In addition, double-jump experiments have shown that the intermediate fast phase could represent the folding process of a restricted group of molecules (10% of the unfolded ensemble) having one or more X-Pro peptide bonds in the *cis* configuration. These molecules are able to fold to a native-like form with the incorrect *cis* proline configuration(s) and, subsequently, reach the *trans* configuration(s) through a spectroscopically silent conversion [Calloni *et al*., 2003].

The folding process of HypF-N appeared faster than that of muscle-type and common-type AcP, even if these two latter proteins do not populate intermediate states having a non-native X-Pro peptide bond. This higher rate of folding is due to the fact that HypF-N, with respect to the AcP proteins, has a higher overall hydrophobicity [Calloni *et al*., 2003].

1.3.3 Aggregation of HypF-N *in vitro*

Aggregation of HypF-N can be induced *in vitro* by incubating the protein under conditions that destabilize its native globular fold. These conditions encompass low and high pH, mutations and the presence of moderate amount of trifluoroethanol (TFE) [Chiti *et al*., 2001; Relini *et al*., 2004; Marcon *et al*., 2005; Calloni *et al*., 2008; Campioni *et al*., 2008; Ahmad *et al*., 2010]. In a first work it was reported the formation of amyloid-like fibrils by incubating the protein in citrate buffer at pH 3.0 or in acetate buffer at pH 5.5 with 30% (v/v) TFE [Chiti *et al*., 2001]. Electron microscopy images showed the presence of 7-9 and 12-20 nm wide fibrils in the samples incubated at pH 3.0 for 1 month, whereas

the fibrils formed in TFE were mostly 3-5 and 7-9 nm in width [Chiti *et al*., 2001]. In addition to the fibrillar morphology, these aggregates were able to bind to ThT and CR, resembling the amyloid-like properties [Chiti *et al*., 2001]. The aggregation process in 30% (v/v) TFE was further investigated using AFM (Figure 1.8) and resulted to be a hierarchical path [Relini *et al*., 2004]. In the early stages of aggregation globular structures with a height of 2-3 nm are present, consistent with that of small oligomers. After 3 days upon the aggregating conditions, the globules self-assemble into beaded chains with crescent-like appearance. These latter form large rings 5 days later, that convert into ribbon-like fibers by opening and reorganizing their constituent globular units. After 8 days, supercoiled fibrils originated by a different number of protofilaments are present in the sample, and, after 11 days, the large majority of the structures observed are tangles of fibrils, that in most cases have a width of 3.5, 5.0 and 8.5 nm [Relini *et al*., 2004], in agreement with the previously reported TEM observations [Chiti *et al*., 2001]. Such fibrils show a cross-β structure in the X-ray diffraction pattern, characteristic of amyloid fibrils [Relini *et al*., 2004].

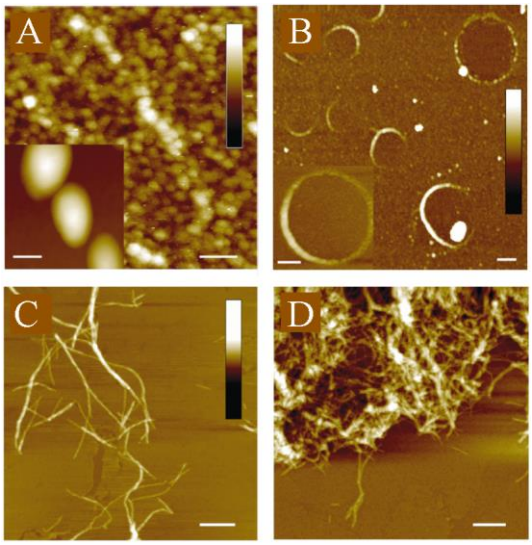

Figure 1.8. TM-AFM images of HypF-N aggregates formed in the presence of 30% (v/v) TFE at pH 5.5. (A) After few hours of incubation, globular aggregates are observed, The scale bar represents 100 nm. Inset: STM image of globular aggregates. The scale bar represents 10 nm. (B) After three days of incubation, crescents and rings are observed. Inset: observation of a ring at higher resolution. The scale bars represent 400 nm. (C) Supercoiled fibrils observed after 8 days of incubation. (D) Tangles of the mature fibrils that represent the large majority of the structures observed after 11 days of incubation. Scale bars represent 500 nm (C-D). Figure adapted from Relini *et al*., 2004.

The mechanism of HypF-N aggregation was studied in more detail in 6-12% (v/v) TFE [Marcon *et al*., 2005]. In these mildly denaturing conditions, HypF-N is initially in a predominantly native-like state, with the partially folded conformation being poorly populated. Kinetic analysis revealed that molecules accessing such a partially folded state were able to start the aggregation process. Considering the context of a physiological environment, this finding is relevant, since it underlines the need of the cells to constantly fight the propensity to aggregate for even the most stable proteins [Marcon *et al*., 2005].

The process of aggregation was studied in detail also at the low pH of 1.7, in which HypF-N was found to be largely unfolded, though still containing significant secondary structure elements and hydrophobic clusters [Campioni *et al*., 2008]. By increasing the ionic strength of the solution, the aggregation of this precursor state was induced and amyloid-like protofibrils were detected in the samples, as revealed by ThT fluorescence and AFM [Calloni *et al*., 2008; Campioni *et al*., 2008; Campioni *et al*., 2012]. The NMR analysis of the pH-denatured precursor state allowed to identify the regions of the primary sequence that form hydrophobic interactions and adopt secondary structure. The regions spanning residues 23-34, 56-64 and 81-82 were found to form hydrophobic clusters, whereas the regions spanning residues 26-30, 56-61 and 46-49 form α-helical structure [Calloni *et al*., 2008]. Moreover, the regions of the sequence that show an important role in the conversion of the pH-denatured state of HypF-N into ThT-binding and β-sheet containing protofibrillar species were also identified as corresponding to the residues 9-15, 27-35, 46-48 and 58-60. These groups of residues correspond to the regions of the sequence having the highest intrinsic aggregation propensity [Calloni *et al*., 2008].

The formation of HypF-N amyloid-like oligomers under conditions of acidic pH has been recently studied under the influence of different salts [Campioni *et al*., 2012]. The AFM images reveal that, irrespective of the salt used, the aggregation process leads to the formation of bead-like oligomers with similar morphologies and heights. However, it was observed that salts differing for the cation and having the Cl^- ion as counteranion induced similar accelerations to the conversion of acid-denatured HypF-N into spherical and chain-like protofibrils, whereas salts differing for the anion and having the Na^+ ion as countercation produced accelerations at very different concentrations. This difference indicated that salts exert their effect through the anions rather than their cations [Campioni *et al*., 2012]. Moreover, the scale of efficiency of the various anions tested in accelerating HypF-N aggregation under acidic conditions followed the electroselectivity series, indicating that they act via a mechanism of preferential binding to the protein chain, most likely to positively charged residues [Campioni *et al*., 2012].

It was also observed that HypF-N oligomers formed in condition of alkaline pH and low concentrations of TFE are able to bind to ThT and CR, contain extensive β-sheet structure and have a morphology similar to the HypF-N oligomers formed at low and nearly neutral pH [Ahmad *et al*., 2010].

1.3.4 Aggregation of HypF-N *in vivo*

The aggregation behaviour of wild-type HypF-N and of different variants was also investigated in its natural environment, where several additional factors may affect the aggregation process. In *E. coli* cells, wild-type HypF-N does not precipitate in inclusion bodies after expression, probably because its rapid folding rate and high native state stability prevent any protein molecules in partially folded states to be populated at any significantly high concentration [Calloni *et al*., 2005]. Conversely, HypF-N variants produced in order to destabilize the native state accumulate into inclusion bodies after expression [Calloni *et al*., 2005]. The aggregation of unstable mutants can be inhibited by incorporating additional mutations that increase the net charge and, therefore, reduce the polypeptide chain propensity to aggregate [Calloni *et al*., 2005]. Interestingly, the aggregating variants were found to be less stable than the soluble variants, suggesting that the HypF-N aggregation process *in vivo* also requires partial unfolding of the native state [Calloni *et al*., 2005].

In a later study, in which wild-type HypF-N and 21 folding-incompetent mutants in *E. coli* were produced, a significant inverse correlation was observed between the solubility of the variants and their intrinsic propensity to originate amyloid fibrils, indicating that the physicochemical parameters recognized to affect amyloid formation by fully or partially unfolded proteins *in vitro*, such as hydrophobicity, β-sheet propensity, and charge, are generally valid for situations *in vivo* [Winkelmann *et al*., 2010].

1.3.5 Cytotoxicity of prefibrillar aggregates formed by HypF-N

As mentioned above, the HypF-N oligomers formed during the aggregation process share structural features with those related to disease [Chiti *et al*., 2001; Relini *et al*., 2004; Marcon *et al*., 2005; Campioni *et al*., 2008]. In addition, they have a cytotoxic effect when added to cultured cells and injected in rat brains, in a manner similar to the pathology-related pre-fibrillar aggregates [Bucciantini *et al*., 2002; Bucciantini *et al*., 2004; Cecchi *et al*., 2005; Baglioni *et al*., 2006; Pellistri *et al*., 2008; Campioni *et al*., 2010; Zampagni *et al*., 2011; Tatini *et al*., 2013].

As an initial observation, pre-fibrillar HypF-N aggregates grown in the presence of 30% (v/v) TFE have been found to reduce the viability of cell cultures, as observed by using the 3-(4,5-dimethylthiazol-2-yl)-2,5-diphenyltetrazolium bromide (MTT) reduction inhibition assay (Figure 1.9), a common indicator of cellular stress, and the

trypan blue internalization assay [Bucciantini *et al.*, 2002]. Interestingly, the levels of cell impairment determined by HypF-N pre-fibrillar aggregates were comparable to those reported for the disease-associated proteins, such as α-synuclein, $A\beta_{1-42}$ and transthyretin [Bucciantini *et al.*, 2002]. Moreover, the cytotoxic effects were not detected in cells treated with the same mass concentration of HypF-N aggregates incubated for several days in the aggregating conditions and containing fibrillar structures [Bucciantini *et al.*, 2002].

It has later been observed that HypF-N oligomers cause an increase of reactive oxygen species (ROS) and free Ca^{2+} levels into the cells, phenomena that can be responsible of apoptosis or necrosis [Bucciantini *et al.*, 2004; Bucciantini *et al.*, 2005; Cecchi *et al.*, 2005]. These events are triggered by the ability of oligomers to interact and disrupt the cell membranes, and even penetrate them until they reach the cytosol. Indeed, HypF-N oligomers produced in 30% (v/v) TFE were able to permeabilize synthetic membranes formed by phospholipids and devoid of proteins [Relini *et al.*, 2004; Canale *et al.*, 2006] and also plasma membranes of cultured cells [Bucciantini *et al.*, 2004; Bucciantini *et al.*, 2005; Cecchi *et al.*, 2005], allowing an influx of Ca^{2+} ions from the extracellular medium to the cytosol. The activation of the glutamatergic channels, NMDA and AMPA receptors, following their interaction with HypF-N oligomers, is considered an important mechanism in causing membrane permeabilization and Ca^{2+} influx, in addition to a non specific interaction of the aggregates with the phospholipid component of the cell membrane [Pellistri *et al.*, 2008].

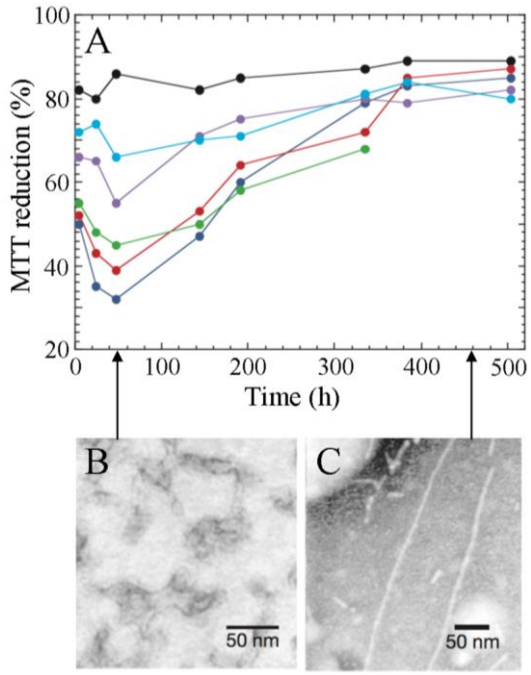

Figure 1.9. Differential cytotoxicity of prefibrillar and fibrillar HypF-N aggregates. (A) Cell viability was checked by MTT inhibition reduction test, after addition to the cell medium of either 20 μM native protein (•), or different concentration of aggregates formed at different times of incubation at pH 5.5 in the presence of 30% (v/v) TFE: 20 μM (•), 5 μM (•), 1 μM (•), 0.2 μM (•), and 0.04 μM (•). Values are relative to untreated cells. (B) Electron micrograph of prefibrillar aggregates formed after 48 h incubation. (C) Electron micrograph of mature amyloid fibrils formed after 20 days incubation. Figure adapted from Bucciantini *et al.*, 2002.

It is well known that two different types of HypF-N oligomers show different abilities to determine cellular impairment, with one species being nontoxic [Campioni *et al*., 2010]. This finding has provided a chance to investigate the structure and activity of toxic and nontoxic oligomers by comparing them [Campioni *et al*., 2010]. The toxic HypF-N oligomeric aggregates, named also type A oligomers, were formed in 12% (v/v) TFE, whereas the nontoxic, or type B, oligomers were produced at pH 1.7. Type A oligomers were able to reduce cell viability in human neuroblastoma cells (SH-SY5Y) and mouse endothelial cells (Hend), as demonstrated by the MTT reduction assay and the Hoechst 33342 staining test; by contrast, type B oligomers had no effect on the cell viability [Campioni *et al*., 2010]. In addition, type A oligomers were found to penetrate the plasma membrane, induce Ca^{2+} influx into the cytosol, increase intracellular ROS production and lipid peroxidation with consequent activation of the apoptotic pathway, as indicated by the increase of caspase-3 level [Campioni *et al*., 2010; Zampagni *et al*., 2011]. Vice versa, type B oligomers were not able to induce these effects [Campioni *et al*., 2010; Zampagni *et al*., 2011]. At a later time, it was also observed that type A oligomers, but not type B oligomers, colocalized with post-synaptic densities in primary rat hippocampal neurons, inhibited long term potentiation (LTP) in rat hippocampal slices, and impaired spatial learning of rats in the Morris Water Maze test, mimicking the effects of the synaptotoxicity of Aβ aggregates [Tatini *et al*., 2013].

Hence, the interaction of the oligomers with cell membranes is established to be the primary event causing cytotoxicity. For this reason, the prevention of such interaction mediated by the competitive binding of glycosaminoglycans to cell membranes with their resulting shielding results in a loss of toxicity of type A oligomers [Saridaki *et al*., 2012]. Further investigations revealed that oligomer toxicity depends on the contributions of the physicochemical properties of both the aggregates and the cell membrane with which they interact [Evangelisti *et al*., 2012]. In fact, by increasing the content of cholesterol and decreasing the content of the ganglioside GM1 in the cell membrane, type A oligomers become benign, whereas, by decreasing the content of cholesterol and increasing that of the ganglioside GM1, type B oligomers acquired toxic function [Evangelisti *et al*., 2012]. Moreover, it was observed that the two pairs of toxic and nontoxic oligomers obtained from the different protein systems HypF-N and $A\beta_{42}$, behave with close similarity under the same conditions [Evangelisti *et al*., 2016]. In particular, similar quantitative relationships were found between the GM1 content of the cell membrane and the ability of the membrane to bind oligomers from different peptides/proteins (HypF-N and $A\beta_{42}$),

but with the same level of toxicity. However, the relationship appeared different for toxic type A and nontoxic type B HypF-N oligomers, as well as for toxic A^+ and nontoxic A^- $A\beta_{42}$ oligomers. In fact, HypF-N type A or $A\beta_{42}$ A^+ oligomers binding to the cell membrane occurs with high affnity and saturation at high GM1 levels, whereas the GM1-dependence of HypF-N type B or $A\beta_{42}$ A^- oligomers binding showed lower affinity [Evangelisti *et al*., 2016]. Recently, it was found that the importance of GM1 in mediating the cytotoxicity of HypF-N oligomers can be traced back to its ability to recruit protein aggregates to lipid raft domains of the cell membrane, a behaviour that appears mainly due to the negative charge of GM1 and does not require the participation of protein components or the adoption of a well defined annular morphology [Oropesa-Nuñez *et al*., 2016].

It has also been found that further assembly of type A oligomers into large aggregates could be mediated by molecular chaperones, resulting in suppression of the toxicity of the oligomeric species [Mannini *et al*., 2012; Cascella *et al*., 2013]. To this regard, in a recent study, the effects of different concentrations of three molecular chaperones, named αB-crystallin (αBc), clusterin (Clu), and an engineered monomeric variant of transthyretin (M-TTR), were tested on the toxicity of type A HypF-N oligomers in N2a (murine neuroblastoma) cells [Cappelli *et al*., 2016]. In the absence of chaperones, the viability of cells treated with toxic oligomers, tested using the MTT assay, was found to be reduced with respect to the untreated cells (45% and 100% of cell viability, respectively). By contrast, in the presence of HypF-N oligomers preincubated with progressively high concentrations of αBc, Clu, or M-TTR (0.25, 0.5, 1.0, 2.0, 4.0 μM), cell viability was increasingly greater, reaching about 80-85% of the untreated cells, indicating that these chaperones inhibit HypF-N oligomers toxicity over the range of the concentrations used [Cappelli *et al*., 2016].

1.3.6 Determinants for HypF-N cytotoxicity

The different biological behaviour of HypF-N type A and type B oligomers previously described was found to arise from structural differences between the two types of oligomers [Campioni *et al*., 2010]. Type A and type B oligomers were produced by incubating 48 μM HypF-N for 4 h in 50 mM acetate buffer, 12% (v/v) TFE, 2 mM DTT, pH 5.5 (condition A), and in 20 mM trifluoroacetic acid (TFA), 330 mM NaCl, pH 1.7 (condition B), respectively [Campioni *et al*., 2010].

The two types of oligomers showed similar abilities to bind to ThT and appeared to be indistinguishable by analysing their morphology by using AFM [Campioni *et al*., 2010]. In order to identify the structural characteristics responsible for the different biological properties of the oligomers, 18 HypF-N variants, each carrying a single cysteine residue located at different positions along the polypeptide chain, were purified and labelled with the fluorescent probe N-(1-pyrene)maleimide (PM). PM is a probe of proximity that can be used to obtain information about the distance between two labelled residues located on adjacent protein molecules, because of its ability to form excited-state dimers, or excimers [Betcher-Lange and Lehrer, 1978; Hammarström *et al*., 1997; Hammarström *et al*., 1999; Krishnan and Lindquist, 2005]. Excimers originate when the distance between two PM moieties is lower than 10 Å; consequently, the fluorescence emission spectrum shows a broad band in the region 440-470 nm. By contrast, when the two PM molecules are distant, that means higher than 10 Å, the excimer band is absent [Betcher-Lange and Lehrer, 1978; Hammarström *et al*., 1997; Hammarström *et al*., 1999; Krishnan and Lindquist, 2005].

Each labelled variant was then allowed to aggregate both in condition A and B and the PM fluorescence emission spectra of the resulting samples were acquired. From the spectra obtained for each labelled position, the ratio of the excimer to monomer fluorescence intensities (FI_{440}/FI_{375}) was determined (Figure 1.10). By using this approach it was revealed that the regions involved in the formation of the structural core of the aggregates are the same in the two types of oligomers and, interestingly, correspond to the three major hydrophobic regions of the HypF-N primary sequence (Figure 1.10). However, structural differences between the two types of oligomers emerged from the excimer ratio profile; indeed, the three major hydrophobic regions of the protein were characterized by higher values in the case of type B oligomers with respect to type A oligomers, suggesting that such regions are tightly packed within the structural core of type B oligomers, whereas are more solvent-exposed and less packed in the interior of type A oligomers [Campioni *et al*., 2010].

In addition, type A oligomers were found to strongly bind to the fluorescent probe ANS than the type B oligomers, indicating that the exposure to the solvent of hydrophobic surface is greater in the toxic aggregates [Campioni *et al*., 2010]. Taken together, these results indicate that the ability of the oligomers to cause cell dysfunction is linked to the level of structural flexibility and solvent-exposure of the hydrophobic portions of the

aggregate. Due to these properties, the oligomeric species can interact and damage the cell membranes, leading ultimately to cell death [Campioni *et al*., 2010].

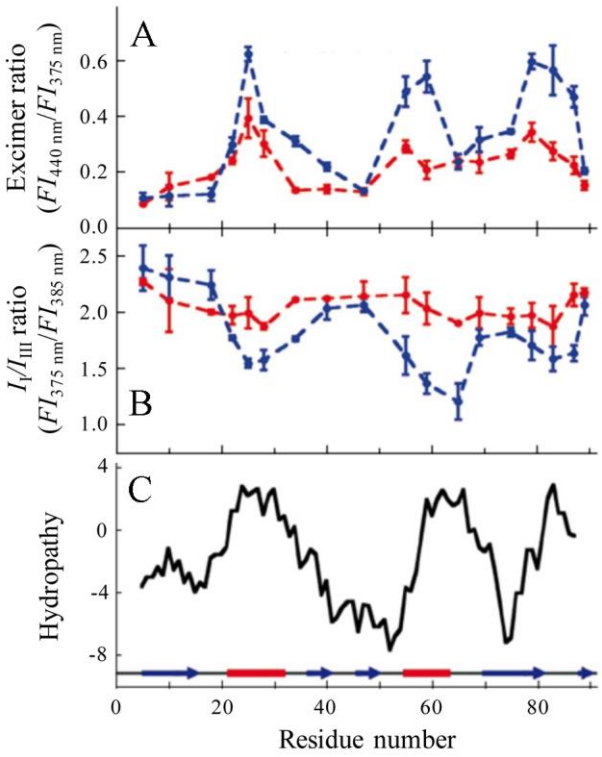

Figure 1.10. Structural differences between toxic and nontoxic oligomeric aggregates of HypF-N. (A) Excimer ratio of PM (related to the degree of structure formation) versus a number of labelled residue for toxic (red lines) and nontoxic (blue lines) HypF-N oligomers. (B) I_I/I_{III} ratio of PM (a correlate of the degree of solvent exposure) versus a number of labelled residue for toxic (red lines) and nontoxic (blue lines) HypF-N oligomers. (C) Hydropathy profile of the HypF-N sequence. The three panels show that in nontoxic aggregates, unlike the toxic aggregates, the three hydrophobic regions of the primary sequence are structured and buried inside the oligomers. Figure adapted from Campioni *et al*., 2010.

As mentioned above, it was found that the chaperones αBc, Clu, and and M-TTR are able to inhibit the cellular toxicity of extracellular protein oligomers formed by $A\beta_{42}$, IAPP, and HypF-N, through binding to oligomers and promoting their further assembly into larger species, in the absence of any significant reorganization of their internal molecular structure [Mannini *et al*., 2012]. Such results suggest that the size of extracellular protein aggregates is an inverse correlate of their toxicity. Indeed, the chaperone-induced oligomer clusters are characterized by a reduction in their exposed hydrophobic surface and diffusional mobility, both of which are expected to reduce their citotoxicity [Mannini *et al*., 2012]. Interestingly, the oligomers were formed before adding the chaperones, showing that the protective action of the latter also includes the neutralization of toxic oligomers after they have formed [Mannini *et al*., 2012].

In a recent study, HypF-N mutants were produced in order to increase the hydrophobicity of the three main hydrophobic regions of the sequence [Mannini *et al*., 2014]. The results showed that SH-SY5Y cells exposed to the mutant type A oligomers generally determined higher levels of viability than cells treated with wild-type type A oligomers and that mutant type B oligomers appeared toxic in some cases. To shed light on the link between the oligomer toxicity and their structural properties, the extent of exposed hydrophobic surface areas of the various mutant oligomers was tested by using ANS and their size was tested by using light scattering [Mannini *et al*., 2014]. Although toxicity did not correlate with either oligomers surface hydrophobicity or with oligomer size when considered individually, oligomer toxicity was found to correlate, in a three-dimensional plot, with both solvent-exposed hydrophobicity and size, indicating that both parameters play an important role in determining the deleterious effects of HypF-N misfolded oligomers (Figure 1.11) [Mannini *et al*., 2014].

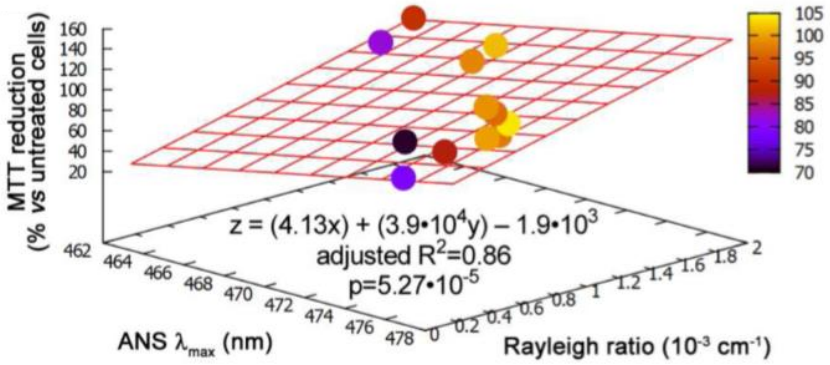

Figure 1.11. Correlation of properties of the oligomeric species of wild-type and mutated HypF-N. 3D graph showing ANS λ_{max} (x-axis), Rayleigh ratio (y-axis) and MTT reduction values (z-axis) of the oligomeric species studied, which are highlighted again using the color scale corresponding to MTT reduction values and reported on the right. The red grid represents the plane of best fit to all the data points and corresponds to the equation $R_{MTT} = (4.13\lambda_{max})+(3.9\times10^4 R_\theta)-1.9\times10^3$. Figure adapted from Mannini *et al*., 2014.

1.4 Aim of the thesis

The description of HypF-N reported in the previous section shows how this protein can be considered a valid model system for the study of the principles underlying protein aggregation, since its behaviour resembles that of many disease-related peptides and proteins. The ability of HypF-N to produce oligomers with different biological properties

when incubated in solution conditions with different pH values, salt concentrations, presence of mild denaturing agents, etc, allowed to focus the attention on the parameters that determine a higher or a lower capacity of the oligomers to cause cellular dysfunction. In particular, previous data revealed that toxic HypF-N oligomers present a high degree of solvent-exposure and flexibility of the hydrophobic cores, necessary to interact and permeabilize the cellular membrane and, subsequently, determine an increase of Ca^{2+} influx, production of ROS, activation of caspase-3, and, finally, cellular death.

This thesis work aims at contributing to elucidate the structural differences between toxic type A and nontoxic type B HypF-N oligomers with a level of detail higher than that obtained in previous studies. A first set of experiments was carried out to investigate the differences between the two types of oligomers on the solvent-exposure of the three major hydrophobic regions of HypF-N; 12 mutational variants of HypF-N carrying a single cysteine residue located at different positions along the polypeptide chain were labelled with the fluorescent dye 1,5-IAEDANS and, then, were allowed to form oligomers under conditions A and B. The maximum fluorescence emission (λ_{max}) of this dye is influenced by the dielectric constant of the medium in which it is located. Thus, it is indicative of the hydrophilic/hydrophobic environment around the labelled residue in the oligomer. The results show that the hydrophobic core in type A oligomers are more solvent-exposed than in type B oligomers, in agreement with the PM excimer ratio analysis previously performed [Campioni *et al*., 2010].

As a second set of experiments, a structural investigation of such toxic and nontoxic HypF-N oligomers was carried out using Förster Resonance Energy Transfer (FRET). The mechanism of FRET involves a donor fluorophore in an excited electronic state, which may transfer its excitation energy to a nearby acceptor chromophore in a non-radiative fashion through long-range dipole-dipole interactions. The dyes 1,5-IAEDANS and 6-IAF have the necessary prerequisites to be considered a suitable pair of donor/acceptor probes and were used for the present analysis. Thus, all the single cysteine variants previously labelled with the donor 1,5-IAEDANS, were also labelled with the acceptor 6-IAF. By combining each donor-labelled variant with each acceptor-labelled variant in a 1:1 molar ratio to form toxic and nontoxic oligomers, and by calculating the FRET efficiency from the donor to the acceptor, it was possible to determine the intermolecular interactions between various residues in the oligomers. The results show that FRET efficiency values are generally higher in the toxic oligomers formed under condition A than in the nontoxic oligomers produced under condition B. This means that

the intermolecular distances between pairs of labelled residues in adjacent protein molecules in the oligomer are lower in the case of type A oligomers, indicating that these aggregates are more compact and structured than the oligomers B. However, a number of hydrophobic interactions appear to be less structured in the toxic type A oligomers, allowing the key solvent-exposed residues to be identified in the toxic assemblies.

Chapter 2

Materials and Methods

2.1 HypF-N expression and purification

The gene coding for HypF-N was previously cloned by Dr. Giulia Calloni in a modified pQE30-Xa plasmid (Qiagen S.p.A., Milan, Italy), in which the DNA stretch coding for the factor Xa cleavage site was substituted by a sequence coding for the thrombin cleavage site (pQE30-Th). As a result of this change, the purified protein has the N-terminal Met residue substituted by a Gly-Ser dipeptide attributed to positions 0 and 1, respectively.

Cultures of *E. coli* XL1 Blue cells harbouring the pQE30-Th/HypF-N plasmid were grown overnight at 37 °C in LB medium with 100 μg/mL ampicillin (Sigma-Aldrich, St. Louis, MO, USA) under shaking. The cells were then diluted 1:10 in fresh medium and grown at 25 °C until the optical density at 600 nm (OD_{600}) reached ~ 0.6. Protein expression was induced overnight at 25 °C by means of 1 mM isopropyl β-D-thiogalactoside (IPTG; Inalco, Milan, Italy). Cells were harvested by centrifugation, resuspended in 40 mL of lysis buffer (50 mM sodium phosphate, 300 mM NaCl, 10 mM imidazole at pH 8.0) and then lysed by 1 h incubation with 1 mg/mL lysozyme in ice, followed by sonication at 40 kHz (five cycles of 30 s each spaced by 30 s in ice). The cell lysate was applied at 4 °C to an affinity chromatography column packed with the HIS-Select Nickel Affinity Gel (Sigma-Aldrich, St. Louis, MO, USA) previously equilibrated with lysis buffer at 4 °C. The column was washed with 50 mM phosphate buffer, 300 mM NaCl, 20 mM imidazole, pH 8.0, 4 °C, equilibrated in 50 mM phosphate buffer, 50 mM NaCl, pH 8.0, and then incubated overnight at 4 °C with 50 units of human thrombin (Sigma-Aldrich, St. Louis, MO, USA). Fractions containing pure HypF-N separated from the His-tag were eluted at 4 °C with 50 mM phosphate buffer, 50 mM NaCl, 10 mM imidazole, pH 8.0 and checked by SDS-PAGE. The purest fractions were buffer-exchanged with 5 mM acetate buffer, 2 mM dithiothreitol (DTT), pH 5.5 and concentrated at 4 °C using an ultrafiltration cell with a 3000 Da cut-off cellulose membrane (Millipore, Billerica, MA, USA). Protein concentration was assessed by optical absorption (ε_{280} =

12,490 $M^{-1}cm^{-1}$) and stock solutions were stored at –80 °C in 20 mM potassium phosphate buffer, pH 7.0, with 2 mM DTT.

2.2 Site-directed mutagenesis

Mutations in the HypF-N gene were previously generated by Dr. Silvia Campioni using the QuikChange site-directed mutagenesis kit (Stratagene, La Jolla, CA, USA). Briefly, the sequence of wild-type HypF-N contains three cysteine residues located at positions 7, 40 and 65. Two double mutants of HypF-N (C7S/C40S and C7S/C65A) were produced to obtain two variants with one single cysteine residue at positions 65 and 40, respectively. A triple mutant of HypF-N (C7S/C40S/C65A) lacking all the cysteine residues was then produced (ΔCys). Finally, 10 different quadruple mutants carrying a single cysteine residue located at different positions along the protein chain were produced: ΔCys/T5C, ΔCys/Q10C, ΔCys/Q18C, ΔCys/F25C, ΔCys/N34C, ΔCys/E55C, ΔCys/V59C, ΔCys/E75C, ΔCys/Q83C, ΔCys/T89C. 12 mutants of HypF-N, each carrying a single cysteine residue, were therefore produced. The entire genes were sequenced to ensure the presence of the desired mutation. The expression and purification protocols of these mutants were the same as the ones described for the wild-type protein in section 2.1. After purification, these variants were buffer-exchanged by ultrafiltration (membrane cut-off 3000 Da) in 100 mM potassium phosphate buffer, pH 7.0, with 2 mM tris(2-carboxyethyl)phosphine hydrochloride (TCEP) and stored at –80 °C.

2.3 Labelling of HypF-N variants with 1,5-IAEDANS and 6-IAF

Each of the 12 single cysteine variants of HypF-N was diluted to reach a final protein concentration of 180 µM in 100 mM potassium phosphate buffer, pH 7.0, 3 M guanidine hydrochloride (GdnHCl). 45 µL of a 30 mM stock solution of 5-((((2-Iodoacetyl)amino)ethyl)amino)Naphthalene-1-Sulfonic Acid (1,5-IAEDANS) dye (Figure 2.1A) or 30 µL of a 30 mM stock solution of 6-iodoacetamidofluorescein (6-IAF) dye (Figure 2.1B) (Thermo Fisher Scientific, Waltham, MA, USA) dissolved in dimethylformamide (DMF) was added to a final sample volume of 500 µL, in order to obtain a 15- and 10-fold molar excess of 1,5-IAEDANS and 6-IAF, respectively. Final conditions were 180 µM protein, 2.7 mM 1,5-IAEDANS, 3 M GdnHCl, 100 mM potassium phosphate buffer, pH 7.0 for the labelling with 1,5-IAEDANS and 180 µM protein, 1.8 mM 6-IAF, 3 M GdnHCl, 100 mM potassium phosphate buffer, pH 7.0 for

the labelling with 6-IAF. The mechanism of reaction with iodoacetamide occurs by the thiolate anion attacking and displacing the iodine atom in a nucleophilic reaction (Figure 2.1C). Both types of reaction mixtures (one containing 1,5-IAEDANS and one containing 6-IAF) were left in the dark on a mechanical shaker for 2 h at 30 °C, then overnight in the dark under shaking at 4 °C. The labelled samples were dialysed (membrane cut-off of 3000 Da) in the dark against (i) 0.25 L of 100 mM potassium phosphate buffer, pH 7.0, with 1.5 M GdnHCl for 4 h, (ii) 0.25 L of 100 mM potassium phosphate buffer, pH 7.0 for 4 h, (iii) 0.5 L of 50 mM potassium phosphate buffer, pH 7.0, overnight, (iiii) 1.0 L of 20 mM or 5 mM potassium phosphate buffer (depending on whether the labelled mutants were used to produce oligomers A or oligomers B, respectively), pH 7.0, for 6 h. The samples were then centrifuged to remove any precipitate.

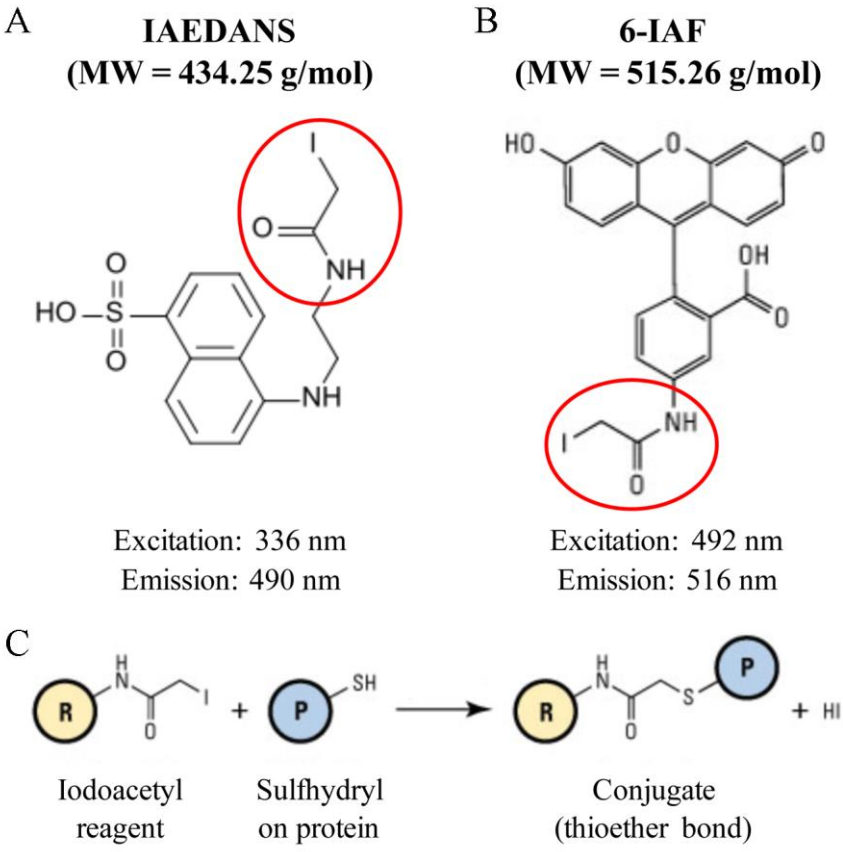

Figure 2.1. Molecular structure of the iodoacetamide dyes (A) 1,5-IAEDANS and (B) 6-IAF. Other information is reported, such as the molecular weight (434.25 g/mol and 515.26 g/mol for 1,5-IAEDANS and 6-IAF, respectively) and the excitation/emission wavelengths (336/490 nm and 492/516 nm for 1,5-IAEDANS and 6-IAF, respectively). The red circles indicate the iodoacetamide group present in each dye that is responsible for the reaction with a thiol group of a protein. (C) Iodoacetyl reaction scheme for chemical conjugation to a sulfhydryl. R represents a labelling reagent having the iodoacetyl reactive group, P represents a protein or other molecule that contains the target functional sulfhydryl group.

The concentration of the dye in each 1,5-IAEDANS-labelled variant and in each 6-IAF-labelled variant was determined spectrophotometrically, using ε_{336} = 5700 $M^{-1}cm^{-1}$ and ε_{491} = 8200 $M^{-1}cm^{-1}$, respectively. The protein concentration was determined spectrophotometrically using ε_{336} = 12490 $M^{-1}cm^{-1}$ after subtraction of the absorbance contribution of the 1,5-IAEDANS/6-IAF probe at the same wavelength of 280 nm. To estimate this contribution, the following equations were used:

$$y = 0.00247 + 0.00012436x; \text{ for the 1,5-IAEDANS-labelled variant} \quad (2.1)$$

$$y = -0.017948 + 0.0037404x; \text{ for the 6-IAF-labelled variant} \quad (2.2)$$

where "x" represents the molar concentration of the dye, and "y" is the absorbance value of the dye at 280 nm. The degree of labelling of the sample was then estimated by determining the ratio between the two measured dye and protein concentrations.

In FRET experiments described below 1,5-IAEDANS and 6-IAF act as donor and acceptor, respectively.

2.4 Preparation of HypF-N oligomers

Oligomeric aggregates of HypF-N were prepared by incubating the protein for 4 h at 25 °C without agitation and at a concentration of 48 μM in two different experimental conditions: (i) 50 mM acetate buffer, 12% (v/v) trifluoroethanol (TFE), 2 mM DTT, pH 5.5 (condition A) and (ii) 20 mM trifluoroacetic acid (TFA), 330 mM NaCl, pH 1.7 (condition B). For the FRET experiments, type A and type B oligomers formed by each 1,5-IAEDANS-labelled variant and each 6-IAF-labelled variant ("xD_yA") were produced, maintaining a constant molar ratio between donor-labelled variant and acceptor-labelled variant of 1:1 (24 μM of "xD" and 24 μM of "yA"). Oligomers "xD_wt" (lacking acceptor-labelled variant replaced with wild-type HypF-N) and "wt_yA" (lacking donor-labelled variant replaced with wild-type HypF-N), where labelled and unlabelled wild-type HypF-N were also in a 1:1 molar ratio, were also produced.

2.5 1,5-IAEDANS and 6-IAF emission spectra

The oligomers "xD_yA", "xD_wt" and "wt_yA", formed at a total monomer concentration of 48 μM, were then diluted in 20 mM and 5 mM photassium phosphate

buffer (for type A and type B oligomers, respectively), pH 7.0, in order to obtain a final HypF-N monomer concentration of 2 μM. Fluorescence emission spectra were recorded on a Perkin-Elmer LS 55 spectrofluorimeter (Wellesley, MA, USA) equipped with a thermostated cell-holder attached to a Haake F8 water-bath (Karlsruhe, Germany). The measurements were performed using a 2×10 mm quartz cell at 25 °C and exciting the sample at 336 nm. Emission spectra of type A and type B oligomers formed under the same conditions using 48 μM wild-type protein, as well as emission spectra of 48 μM native, unaggregated, 1,5-IAEDANS- and 6-IAF-labelled HypF-N variants, and 48 μM 1,5-IAEDANS- and 6-IAF-labelled L-glutathione (GSH), were also acquired.

2.6 FRET determination

In order to determine the FRET efficiency between a donor-labelled residue (1,5-IAEDANS-labelled residue) and an acceptor-labelled residue (6-IAF-labelled residue) in type A and B oligomers, some calculations were carried out on the three fluorescence emission spectra obtained in the presence of the oligomers "xD_yA", "xD_wt" and "wt_yA". As an example, figure 2.2 reports the case of the pair of mutants with the cysteine residue at positions 59 and 25 used to form nontoxic oligomers in a 1:1 molar ratio and labelled with donor and acceptor, respectively (Figure 2.2). The gross spectra of "59D_25A", "59D_wt" and "wt_25A" are shown in Figure 2.2A. As a first correction, the background spectrum was subtracted from the three gross spectra, determined as the fluorescence emission value at 480 nm of the spectrum obtained in the presence of the sample "wt_25A" (Figure 2.2B). The choice of the 480 nm wavelength resides on the fact that at this wavelength the acceptor emission is still constant and close to zero (Figure 2.2A). In order to determine the contribution of the donor to the fluorescence emission in the spectrum "59D_25A", a further corrrection was carried out. The ratio between "59D_25A" and "59D_wt", at 475 nm emission (wavelength at which the acceptor is not able to emit its fluorescence), has been multiplied by the spectrum "59D_wt" (Figure 2.2C, red dashed line) to the donor contribution (Figure 2.2C, red solid line). Additionally, the spectra related to the contribution of the donor (Figure 2.2C, red solid line) and the acceptor (Figure 2.2C, green solid line) were subtracted from the "59D_25A" spectrum (Figure 2.2C, blue solid line). The corrected spectrum is shown in Figure 2.1D as orange solid line and it has been further normalized taking account of the degree of donor-variant labelling, which is 98% in this case, as shown in Figure 2.2E (orange dashed line). The last correction is shown in Figure 2.2E, obtained by summing

the labelling degree-corrected spectrum (orange dashed line) and the "wt_25A" spectrum (green dashed line), resulting in the "59D_25A" spectrum, diplayed as a blue solid line.

To calculate the FRET efficiency, the following formula was used:

$$E = \frac{I_{AD}A_A - I_A A_A}{I_A A_D} \tag{2.3}$$

where E is the FRET efficiency, A_A and A_D represent the absorbance values at 336 nm of acceptor (A_A = 0.05) and donor (A_D = 0.07), respectively, obtained in the presence of a concentration of dye of 120 µM; I_{AD} and I_A represent the acceptor fluorescence emission at 1 mM (excitation 336 nm) obtained in the presence and in the absence of donor, respectively, determined from the area between 490 nm and 600 nm below the corresponding curves (Figure 2.2E, blue solid line spectrum for I_{AD} and green dashed line for I_A).

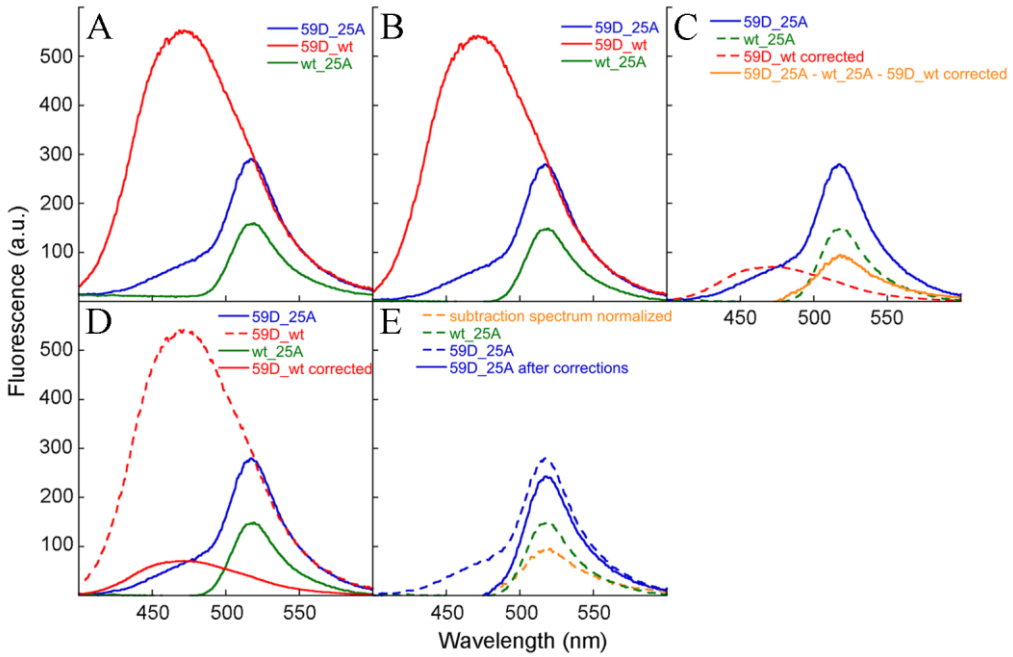

Figure 2.2. Correction of the spectra obtained for the nontoxic oligomers "59D_25A", "59D_wt" and "wt_25A". (A) Gross spectra acquired at the fluorimeter using a 2 µM concentration of oligomer (oligomer "59D_25A" = blue line; oligomer "59D_wt" = red line; oligomer "wt_25A" = green line). (B) Spectra after the subtraction of the background, determined as the fluorescence emission value at 480 nm of the spectrum obtained in the presence of the sample "wt_25A". (C) The ratio between "59D_25A" (blue solid line) and "59D_wt" (red dashed line), at 475 nm emission (wavelength at which the acceptor is not able to emit its fluorescence), has been multiplied by the spectrum "59D_wt" to determine the contribution of the donor (red solid line) to the fluorescence emission of the acceptor in the spectrum "59D_25A". (D) The spectra related to the contribution of the donor (red dashed line) and the acceptor (dashed green line) were subtracted from the "59D_25A" spectrum (blue solid line). The difference spectrum is represented in orange. (E) The difference spectrum was then normalized taking account of the degree of donor-variant labelling, which is 98% in this case, (orange dashed line). The last correction was obtained by summing the labelling degree-corrected spectrum (orange dashed line) and the "wt_25A" spectrum (green dashed line), resulting in the "59D_25A" spectrum (blue solid line).

2.7 ThT assay

Tinctorial properties of HypF-N oligomers in conditions A and B, formed by each 1,5-IAEDANS-labelled variant and the unlabelled wild-type protein in a 1:1 molar ratio ("xD_wt"), were investigated. After the aggregation process, the oligomer samples containing 48 µM total protein were centrifuged for 10 min at 16100 rcf and the pellets were resuspended in 5 mM potassium phosphate buffer, pH 7.0. Aliquots (60 µL) of HypF-N aggregates were then added to 440 µL of a solution of 25 µM ThT in 25 mM phosphate buffer at pH 6.0, in order to keep a 3.7-fold molar excess of dye. The intensity of ThT fluorescence emission at 485 nm (excitation at 440 nm) was recorded at 25 °C by using a Perkin-Elmer LS 55 spectrofluorimeter (Wellesley, MA, USA) equipped with a thermostated cell-holder attached to a Haake F8 water-bath (Karlsruhe, Germany), and a 2×10 mm quartz cell. The ratio between the ThT emission in the presence (F) and absence (F_0) of HypF-N oligomers were determined. As a control the experiment was repeated using HypF-N oligomers formed in condition A and B using only wild-type unlabelled HypF-N at the same protein concentration.

Chapter 3

Results

3.1 ThT binding to labelled-HypF-N oligomers

The two types of HypF-N oligomers formed in conditions A and B display similar morphology and tinctorial properties, but show different abilities to impair cell viability when added to cultered cells [Campioni *et al*., 2010]. In order to identify structural differences between toxic type A and nontoxic type B oligomers, Campioni and co-workers reported a comparative analysis of the structure of the two types of HypF-N oligomers using PM labelling, which showed that the three highest hydrophobic regions of the HypF-N primary sequence are tightly packed within the structural core of the oligomers B, whereas are less packed in the interior of the oligomers A [Campioni *et al*., 2010].

To gain further insight into the structural differences between toxic type A and nontoxic type B oligomers, here we present a comparative analysis between the two types of oligomers. To this aim, we expressed 12 variants of HypF-N carrying a single cysteine residue located at different positions along the polypeptide chain, and, then, we labelled each variant with donor and acceptor dyes suitable for the FRET technique, which are 1,5-IAEDANS and 6-IAF, respectively. Considering that the structural analysis was carried out by using oligomers formed by labelled variants, it was first necessary to ensure that the labelling had no effects on the structure of type A and type B oligomers. In particular, it was assessed whether the 12 oligomers "xD_wt", *i.e.* formed by each 1,5-IAEDANS-labelled variant and the unlabelled wild-type HypF-N in a 1:1 molar ratio, formed under conditions A and B, maintained the ability to bind the amyloid specific dye ThT. The various type A oligomers tested were found to increase the ThT emission intensity by *ca.* 6-10 times to an extent similar to the type A oligomers formed by the wild-type protein only (Figure 3.1A,C). The various type B oligomers were found to increase the ThT emission intensity by *ca.* 3-4.5 times similarly to the type B oligomers formed by the wild-type protein only (Figure 3.1B,C). This suggests that the intermolecular β-sheet structure of the oligomers is maintained after labelling in both

conditions. This assay was not performed on oligomers "wt_xA", *i.e.* formed by the unlabelled wild-type HypF-N and each 6-IAF-labelled variant, because the acceptor 6-IAF can be partially excited at the absorption wavelength of ThT, and, consequently, can interfere with the fluorescence emission of the amyloid dye. As expected, no ThT fluorescence increase was observed in the presence of soluble donor-labelled GSH (Figure 3.1).

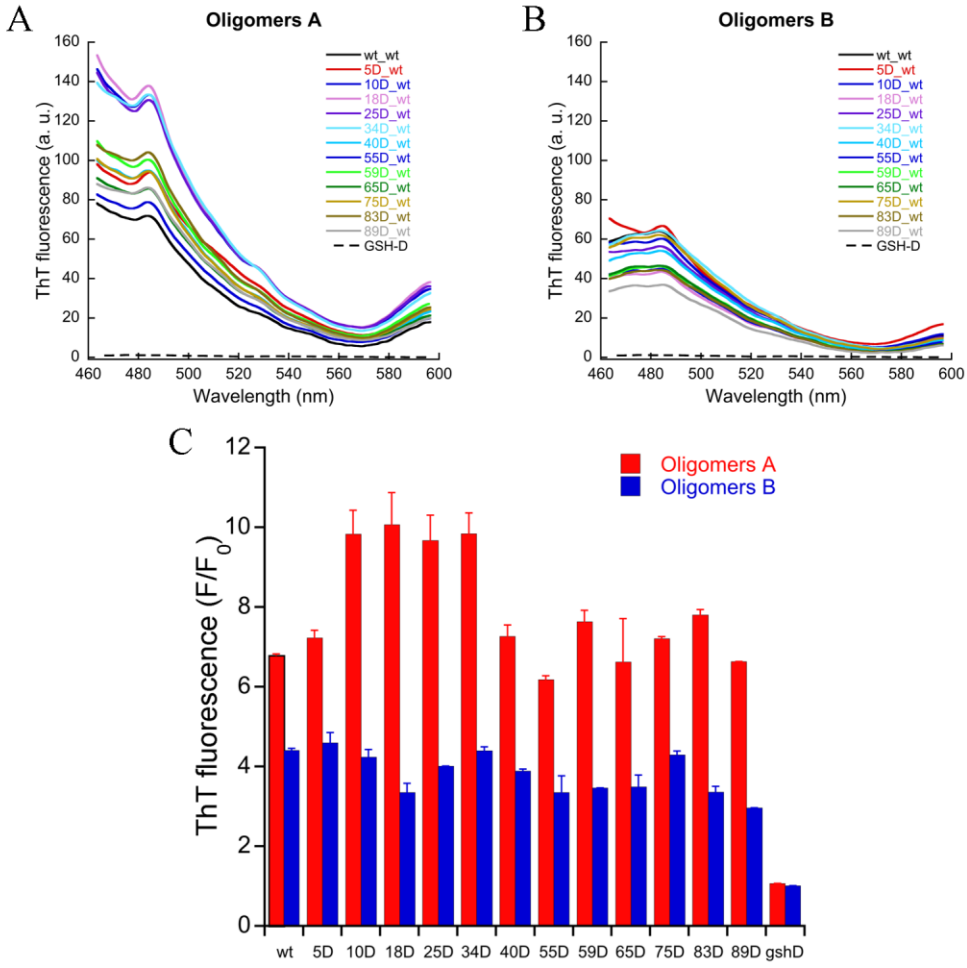

Figure 3.1. ThT fluorescence emission spectra (excitation 440 nm) in the presence of type A (A) and type B (B) HypF-N oligomers formed by only wild-type ("wt_wt"), and each donor-labelled variant and wild-type in a 1:1 molar ratio ("xD_wt"). ThT fluorescence emission spectra of soluble donor-labelled GSH are also reported as a negative control. (C) The ThT fluorescence emission values at the wavelength of 485 nm are also reported as the ratio between the ThT fluorescence in the presence (F) and absence (F_0) of samples. Data are means ± SD of three independent experiments.

3.2 Hydrophobicity profile of HypF-N oligomers

To gain information into the solvent-exposure of the hydrophobic regions in type A and type B oligomers, we produced 12 "xD_wt" oligomers, where the variant labelled with 1,5-IAEDANS and the unlabelled wild-type HypF-N are mixed in a 1:1 molar ratio, under

conditions A and B. Since 1,5-IAEDANS is substantially more hydrophilic than PM, the comparison between the analysis carried out with 1,5-IAEDANS-labelled oligomers and PM-labelled oligomers allow to establish whether the results depend on the hydrophobicity of the probe used or are rather indipendent on whether a hydrophobic or hydrophilic probe is used to label type A and type B HypF-N oligomers.

In a previous report, the influence of the medium dielectric constant (ε_r) on the wavelength of maximum fluorescence emission (λ_{max}) of the model 1,5-IAEDANS-mercaptoethanol was determined [Hammarström *et al.*, 2001]. Such analysis was obtained dissolving 1,5-IAEDANS-mercaptoethanol in water and in several primary alcohols and determining the λ_{max} value for each solvent. The results showed that the λ_{max} of 1,5-IAEDANS was most blue-shifted using 1-butanol, but, interestingly, it was red-shifted when using both more hydrophobic (1-pentanol, 1-hexanol, 1-heptanol, 1-octanol, 1-nonanol) and hydrophilic (water, methanol, ethanol, 1-propanol) solvents [Hammarström *et al.*, 2001]. The graph reported in Figure 3.2 replots this result using the previously published data and due to this characteristic behaviour of 1,5-IAEDANS, it was possible to divide the plot in two parts with dielectric constants lower and higher than that of 1-butanol (green and red points in Figure 3.2, respectively) and fit the data separately with linear functions (green and red lines in Figure 3.2, respectively). In particular, the green function describes the dependence of λ_{max} on ε_r when 1,5-IAEDANS is mixed with hydrophobic solvents, whereas the red function is indicative of the dye behaviour when it is dissolved in hydrophilic solvents (Figure 3.2).

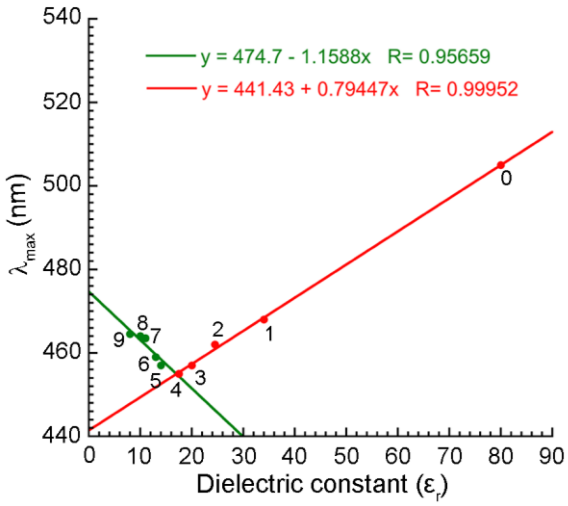

Figure 3.2. Influence of the dielectric constant on the wavelength of maximum fluorescence emission (λ_{max}) of the model 1,5-IAEDANS-mercaptoethanol. The numbers in the figure correspond to the solvents as follows: 0 = water; 1 = methanol; 2 = ethanol; 3 = 1-propanol; 4 = 1-butanol; 5 = 1-pentanol; 6 = 1-hexanol; 7 = 1-heptanol; 8 = 1-octanol; 9 = 1-nonanol. The green and red linear functions describe the λ_{max} trend when 1,5-IAEDANS is mixed with hydrophobic (green points) and hydrophilic (red points) solvents, rspectively. Figure modified from Hammarström *et al.*, 2001.

Considering that the dielectric constant of a folded protein interior is approximately 4 [Dwyer *et al*., 2000], it was possible to calculate the theoretical λ_{max} value of 1,5-IAEDANS in a highly structured hydrophobic core, using the green function reported in Figure 3.2. Such λ_{max} value was found to be ~ 470 nm. These observations led us to interpret the λ_{max} values obtained in the presence of type A and type B HypF-N oligomers formed by each of the 12 1,5-IAEDANS-labelled variants and the unlabelled wild-type HypF-N, in a 1:1 molar ratio (Figure 3.3). The threshold λ_{max} value of 470 nm, characteristic of a hydrophobic protein interior, allowed us to divide the resulting profiles for the two types of oligomers in hydrophobic (dark gray) and hydrophilic (light gray) regions versus residue number (Figure 3.3). In particular, values of λ_{max} > 470 nm can only be assigned to a hydrophilic environment, as such values are not obtainable in protein hydrophobic environments. Residues labelled with 1,5-IAEDANS featuring such values indicate a hydrophilic environment around the 1,5-IAEDANS moiety. Residues with values of λ_{max} < 470 nm have a less hydrophilic (or more hydrophobic) environment. Residues with small values of λ_{max} in Figure 3.3 indicate that such residues experience the most hydrophobic environment, whereas residues with high values of λ_{max} refer to that residues contained in the most hydrophilic environment. However, since the former are in the dark grey region, the observation that such residues have lower λ_{max} values in type A oligomers than type B oligomers indicate that the hydrophobic environment is lower for the toxic type A oligomers.

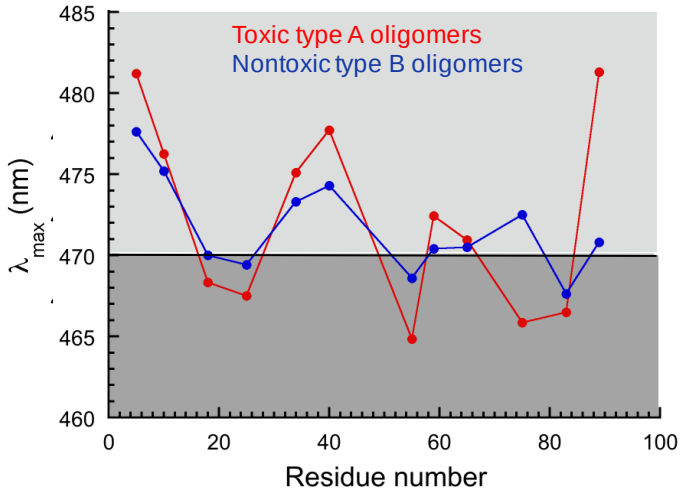

Figure 3.3. λ_{max} of 1,5-IAEDANS versus residue number obtained for the type A (red) and type B (blue) HypF-N oligomers. The black line indicates the λ_{max} value of 470 nm typical of the hydrophobic core of the oligomer. The treshold λ_{max} value of 470 nm divides the plot in hydrophobic and hydrophilic regions of the oligomer, represented by the dark and light grey areas, respectively.

We then compared the two λ_{max} profiles obtained with 1,5-IAEDANS for type A and type B HypF-N oligomers with the PM excimer ratio profiles for the same oligomers reported by Campioni *et al*., 2010, and with the hydropathy profile of the HypF-N sequence (Figure 3.4). PM is a probe of proximity between two labelled residues in the species under investigation, because of its ability to form excited-state dimers, or excimers, when the two PM moities are within a short distance [Hammarström *et al*., 1999; Krishnan and Lindquist, 2005; Campioni *et al*., 2010]. As mentioned above, the PM excimer ratio profile reveals that the three major hydrophobic regions of the protein, identified by the hydropathy profile, appear to be buried into a nonpolar environment and more highly organized in oligomers B compared to oligomers A (Figure 3.4). Interestingly, the 1,5-IAEDANS λ_{max} profiles are quite consistent with both the PM excimer ratio and the hydropathy profiles: the three most hydrophobic regions of the protein show a general blue-shift of fluorescence emission, indicating their burial, which appears to be less marked for oligomers A, due to the aforementioned hydrophobic solvent-dependent λ_{max} plot (green side in the graph reported in Figure 3.2). Vice versa, the more hydrophilic regions of the protein show a predominant red-shift, that is generally greater for the oligomers A (Figure 3.4).

Overall, the results obtained with 1,5-IAEDANS are superimposable with those obtained with PM, indicating that the aggregation process of HypF-N under both conditions A and B is not affected by the degree of hydrophobicity of the probe used to label them.

3.3 FRET analysis under native conditions

The results shown in section 3.2 provided information on the degree of solvent-exposure of the various labelled residues in both type A and type B oligomers. However, since these data did not help to sort out the structure of the oligomers, the FRET technique was used to further investigate the three-dimensional organization of the aggregates, by determining the intermolecular interactions between pairs of residues located at different positions in the polypeptide chain. FRET relies on the distance-dependent transfer of energy from a donor fluorophore in an excited electronic state to an acceptor chromophore, that leads to a reduction in the donor fluorescence intensity and excited-state lifetime, and an increase in the acceptor emission intensity [Van Der Meer *et al*., 1994; Lakowicz, 1999; Selvin, 2000].

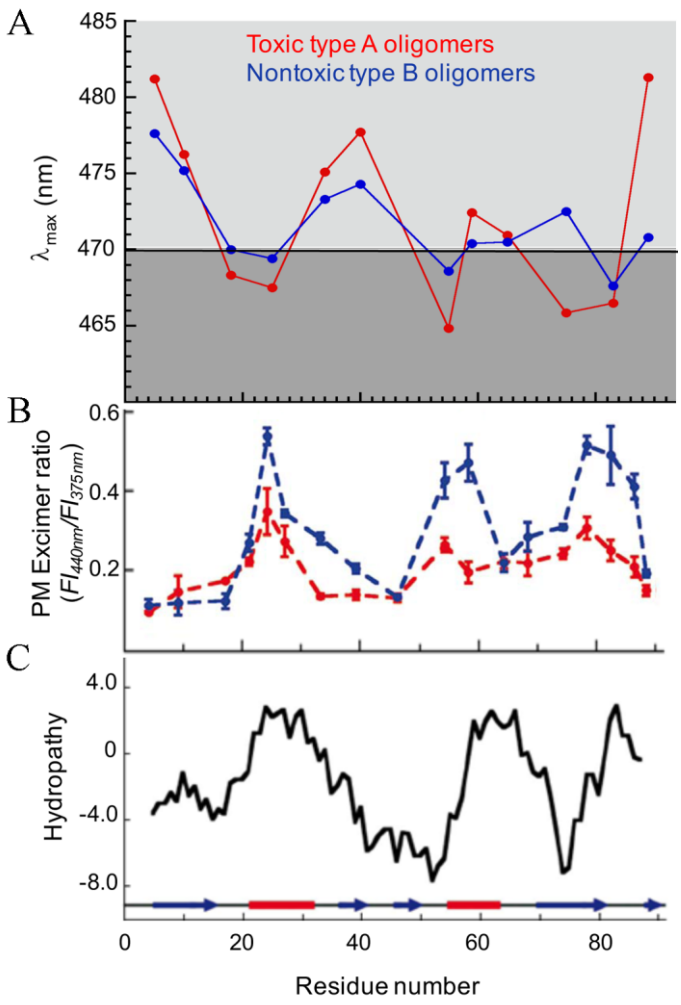

Figure 3.4. (A) λ_{max} of 1,5-IAEDANS versus residue number obtained for the type A (red) and type B (blue) HypF-N oligomers. The black line indicates the λ_{max} value of 472 nm typical of the hydrophobic core of the oligomer. (B) Ratio between the fluorescence intensities measured at 440 nm (excimer peak) and 375 nm (monomer peak) for all the PM-labelled positions along the HypF-N sequence for type A (red) and type B (blue) HypF-N oligomers. (C) Hydropathy profile of HypF-N calculated using the Roseman hydrophobicity scale. The positions of α-helices (red) and β-strands (blue) in the native structure (protein data bank entry 1GXU) are also indicated as determined by MOLMOL. Panels A and B were readapted from Campioni *et al.*, 2010.

A basic prerequisite of this technique is that the fluorescence emission spectrum of the donor widely overlaps with the absorption spectrum of the acceptor, in order to ensure that the energy transfer from donor to acceptor occurs. In this regard, the thiol reactive fluorescence dyes 1,5-IAEDANS and 6-IAF are considered a suitable pair of dyes for the FRET technique, in which the former is the donor and the latter is the acceptor [Palm *et al.*, 1999; Nyitrai *et al.*, 2000; Putilina *et al.*, 2003]. The absorption spectra obtained with 1,5-IAEDANS and 6-IAF conjugated to GSH at a concentration of 200 µM in 100 mM potassium phosphate buffer, pH 7.0, after a labelling time of 2 h at 30 °C, were typical of monomeric thiol-conjugated 1,5-IAEDANS and 6-IAF, with the characteristic absorbance peaks at 336 and 491 nm, respectively (Figure 3.5A). The fluorescence

emission spectra obtained in the presence of 1,5-IAEDANS-labelled GSH and 6-IAF-labelled GSH at a concentration of 1 μM in 20 mM potassium phosphate buffer, pH 7.0, at 25 °C, after exciting the samples at 336 nm and 491 nm, respectively, show the characteristic peaks at 480 nm and 516 nm, respectively (Figure 3.5B).

The following experiments were planned: (1) to label the 12 single cysteine variants of HypF-N, previously labelled with the 1,5-IAEDANS dye, also with the 6-IAF dye; (2) to combine each of the 12 1,5-IAEDANS (donor)-labelled variants and each of the 12 6-IAF (acceptor)-labelled variants in a 1:1 molar ratio; (3) to induce their aggregation under solution conditions A and B; (4) to determine the energy transfer from donor to acceptor, related to the proximity between the two specific labelled residues in the oligomer under investigation. Before approaching this analysis, we have carried out the same experiment

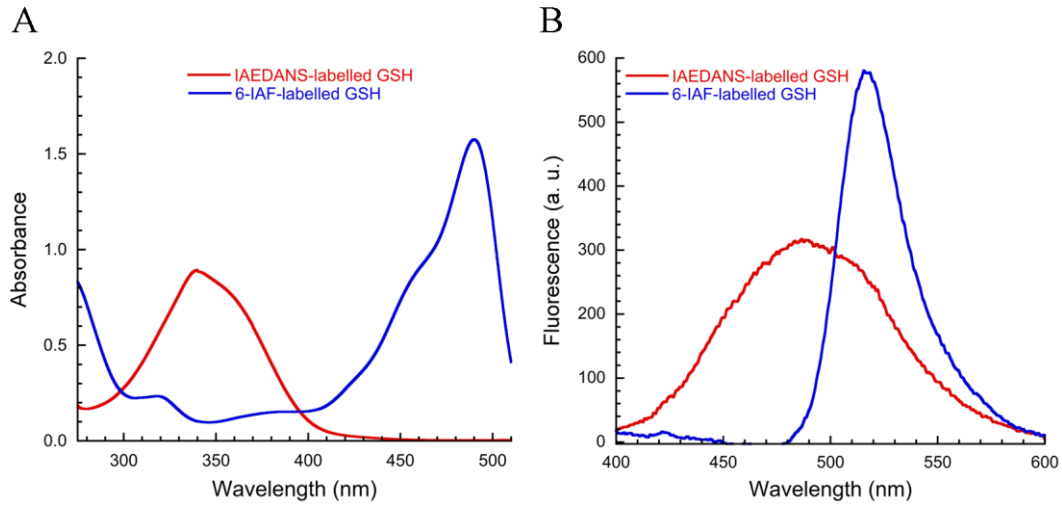

Figure 3.5. (A) Absorption spectra of 1,5-IAEDANS-labelled (red spectrum) and 6-IAF-labelled (blue spectrum) GSH. The red spectrum is typical of 1,5-IAEDANS, with the predominant absorption peak at 336 nm, whereas the blue spectrum is typical of 6-IAF, with the major absorption peak at 491 nm. (B) Fluorescence emisison spectra of 1,5-IAEDANS-labelled (red spectrum) and 6-IAF-labelled (blue spectrum) GSH, obtained exciting the samples at 336 nm and 491 nm, respectively. The fluorescence emission spectra show the characteristic peaks at 480 nm and 516 nm for 1,5-IAEDANS-labelled GSH and 6-IAF-labelled GSH samples, respectively.

under conditions in which the labelled proteins maintain their monomeric, folded state. Thus, we have replaced step 3 listed above with the following: (3) to maintain their folded conformations in 20 mM potassium phosphate buffer, pH 7.0, at 25 °C. This first set of experiments was intended to exclude that protein molecules labelled with either donor or acceptor may transfer energy when they are in native conditions in the same sample, thus far away from each other.

The absorption spectra obtained with variants of HypF-N in their native folded state labelled with the donor and the acceptor in 20 mM potassium phosphate buffer, pH 7.0, at 25 °C showed the typical protein peak at 280 nm in addition to the dye peak at either

336 or 491 nm. As an example, Figure 3.6 reports two mutants at a concentration of 1 µM with the cysteine residue at positions 40 and 65, respectively, each labelled separately with 1,5-IAEDANS (Figure 3.6A) and 6-IAF (Figure 3.6B). The HypF-N variant having the cysteine at position 65 was labelled with both donor and acceptor separately and the two labelled proteins were combined together at different concentrations, maintaining a constant molar ratio of 1:1 (0.5:0.5 µM, 1:1 µM, 2:2 µM, 4:4 µM) under solution conditions in which they maintain a monomeric foled state, that is 20 mM potassium phosphate buffer, pH 7.0, at 25 °C. The fluorescence emission spectrum of the resulting sample "65D_65A" upon excitation at 336 nm, *i.e.* the maximum absorption wavelength of the donor 1,5-IAEDANS, was acquired. We also acquired the fluorescence emission spectrum in the presence of the HypF-N chain labelled at position 65 with donor and the same unlabelled HypF-N chain ("65D_65"), still in a 1:1 molar ratio, as well as the fluorescence emission spectrum in the presence of the HypF-N chain labelled at position 65 with acceptor and the same unlabelled HypF-N chain ("65_65A") (Figure 3.7). The excitation and emission slits set up at the fluorimeter were properly modified in order to account for the different protein concentrations (Figure 3.7). The results indicate that in the presence of native proteins, the donor-labelled monomer is not able to transfer the energy to the acceptor-labelled monomer, for all the protein concentrations tested. Indeed, the fluorescence emission spectrum obtained in the presence of the sample "65D_65A" (blue spectrum) is quite similar to the mathematical sum (orange spectrum) between the fluorescence emission spectra obtained in the presence of the samples "65D_65" (red spectrum) and "65_65A" (green spectrum), suggesting that the distance between donor and acceptor molecules in solution is sufficiently high to avoid any energy transfer (Figure 3.7).

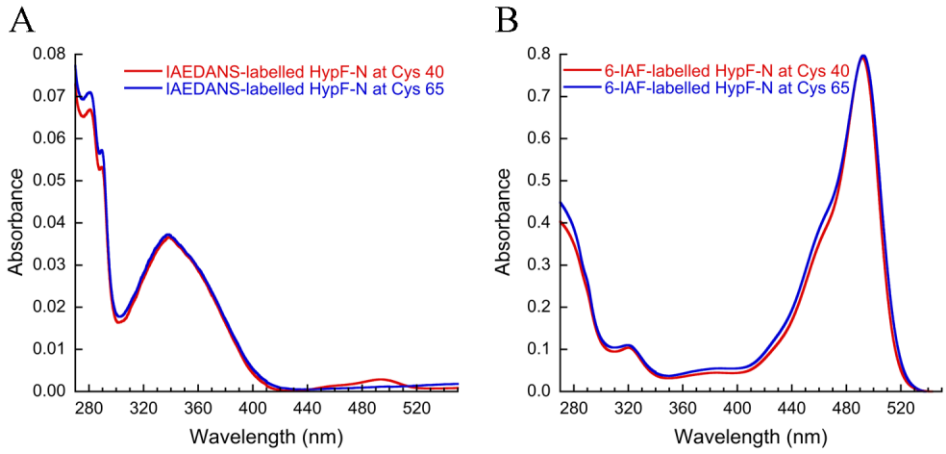

Figure 3.6. Absorption spectra of two HypF-N variants with the cysteine residue at positions 40 (red spectra) and 65 (blue spectra), respectively, each labelled with (A) 1,5-IAEDANS and (B) 6-IAF. All the absorption spectra show the characteristic protein peak at 280 nm in addition to the dye peak.

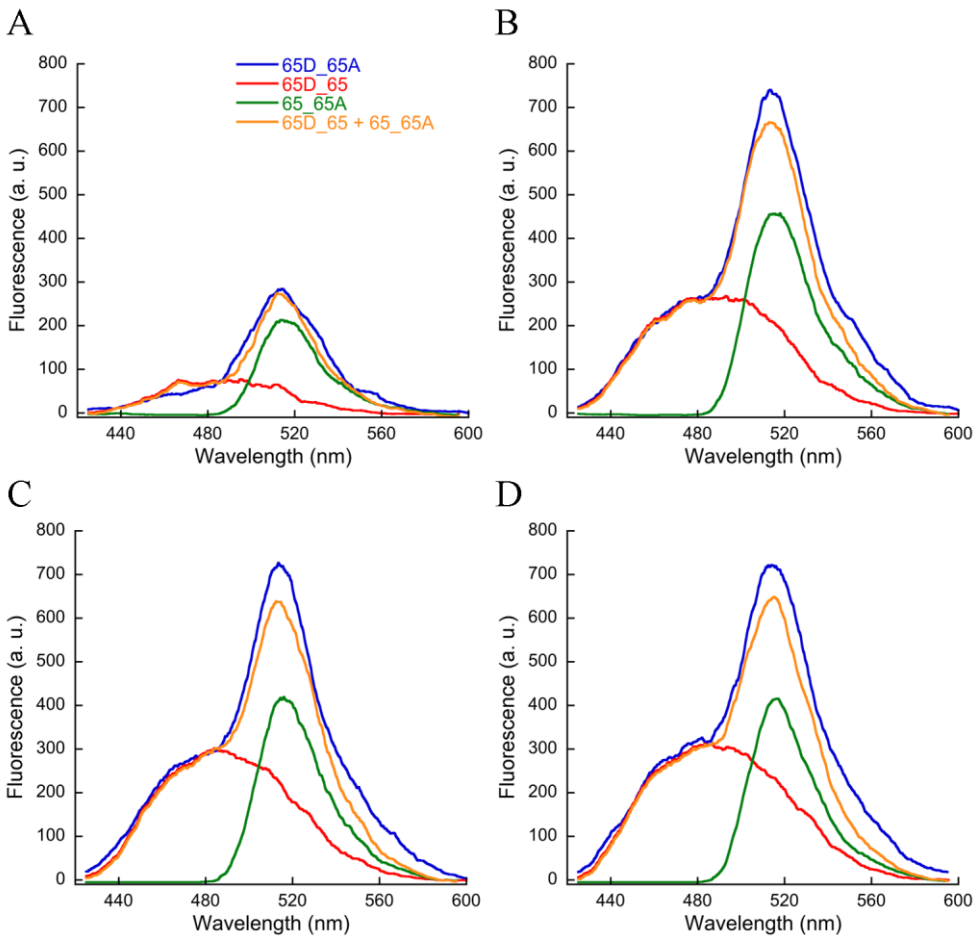

Figure 3.7. Fluorescence emission spectra of the native samples "65D_65A" (blue spectra), "65D_65" (red spectra), and "65_65A" (green spectra), where the two species in each sample are in a 1:1 molar ratio. The orange spectra represent the mathematical sum between the red and the green spectra, and are quite similar to the blue spectra, indicating that in native conditions, when both donor- and acceptor-labelled proteins are monomeric and folded, there is no energy transfer from donor to acceptor. The samples were prepared at different concentrations and the spectra acquisition was carried out after opportunately changing the excitation/emission (Ex/Em) slits: (A) 0.5:0.5 µM, Ex/Em = 2.5/3.5; (B) 1.0:1.0 µM, Ex/Em = 2.5/3.5; (C) 2.0:2.0 µM, Ex/Em = 2.5/2.5; (D) 4.0:4.0 µM, Ex/Em = 2.5/2.5 obscured.

3.4 FRET analysis under conditions A and B

The same analysis presented in the previous section was repeated by incubating the mixture of donor- and acceptor-labelled HypF-N variants in a 1:1 molar ratio. Figure 3.8 shows a comparison between the fluorescence emission spectra obtained in the presence of the samples "83D_59A", "83D_59" and "83_59A", in native conditions (Figure 3.8A), after allowing them to aggregates under condition A (Figure 3.8B) and after allowing them to aggregate under condition B (figure 3.8C). Whilst in the native conditions no energy transfer was detected, since the fluorescence emission spectrum of donor is similar in the presence (blue spectrum "83D_59A") and in the absence (red spectrum "83D_59")

of acceptor (Figure 3.8A), in the presence of the oligomeric species a partial energy transfer from donor to acceptor is observed (Figure 3.8B,C). In fact, the spectrum of the oligomeric sample "83D_59A" (blue spectrum) is characterized by a lower fluorescence emission of donor compared to the spectrum of the sample "83D_59" (red spectrum), and, at the same time, is characterized by a higher fluorescence emission of acceptor compared to the spectrum of the sample "83_59A" (green spectrum) (Figure 3.8B,C).

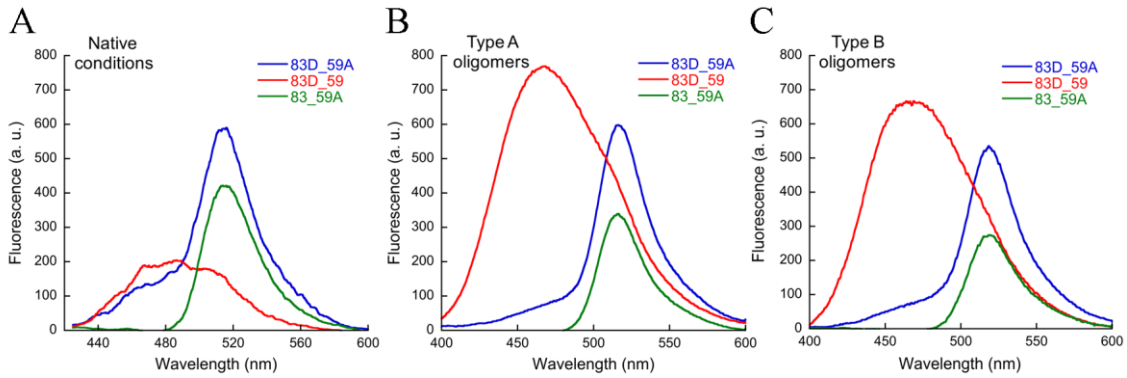

Figure 3.8. Comparison between the fluorescence emission spectra of the samples "83D_59A" (blue spectra), "83D_59" (red spectra), and "83_59A" (green spectra), in (A) native conditions, (B) aggregating condition A, and (C) aggregating condition B. In native conditions, the energy transfer from donor to acceptor is not detected, since the fluorescence emission spectrum of donor is similar in the presence (blue spectrum "83D_59A") and in the absence (red spectrum "83D_59") of acceptor. By contrast, in the presence of type A and type B oligomers, an energy transfer from donor to acceptor is observed; in fact, the spectrum "83D_59A" (blue spectrum) is characterized by a lower fluorescence emission of donor compared to the spectrum "83D_59" (red spectrum), and by a higher fluorescence emission of acceptor compared to the spectrum "83_59A" (green spectrum).

3.5 Toxic and nontoxic HypF-N oligomers structure

Once assured that the energy transfer from donor-labelled variant to acceptor-labelled variant can occur only when the protein is aggregated, each donor-labelled variant and each acceptor-labelled variant (1:1 molar ratio) were allowed to form toxic type A and nontoxic type B aggregates and the resulting oligomers were used to determine the FRET efficiency (*E*) by the fluorimeter, as reported in the *Materials and Methods* section. The availability of 12 donor-labelled variants and 12 acceptor-labelled variants allowed to form, potentially, 12^{12} = 144 type A oligomers and 12^{12} = 144 type B oligomers and obtain *E* values for various pairs of residues located in different protein molecules in the oligomer. However, some of the 144 oligomer types could not be obtained due to the difficulties in purifying enough quantity of each HypF-N single cysteine variant to permit its labelling with both donor and acceptor dyes and to allow the formation of the

oligomers between each donor-labelled variant and each acceptor-labelled variant, under both conditions A and B. Hence, our analysis was carried out with 115 labelled-type A oligomers and 97 labelled-type B oligomers. Importantly, for each pair of labelled-variants, two different oligomers were produced: the oligomer "xD_yA", but also the oligomer "yD_xA", where the donor- and the acceptor-labelled residues were swapped. This allowed us to compare the two *E* values obtained for each pair of mutants, and to eliminate from the analysis the pairs of mutants which produced distant *E* values. In addition to the oligomer "xD_yA", the oligomers "xD_wt" (lacking the acceptor dye) and "wt_yA" (lacking the donor dye) were also produced, since the resulting spectra were necessary for the *E* determination, as reported in *Materials and Methods* section. Figures 3.9 and 3.10 report the three spectra "xD_yA" (blue spectra), "xD_wt" (red spectra), and "wt_yA" (green spectra) obtained for each pair of mutants combined to form toxic type A (Figure 3.9) and nontoxic type B (Figure 3.10) oligomers.

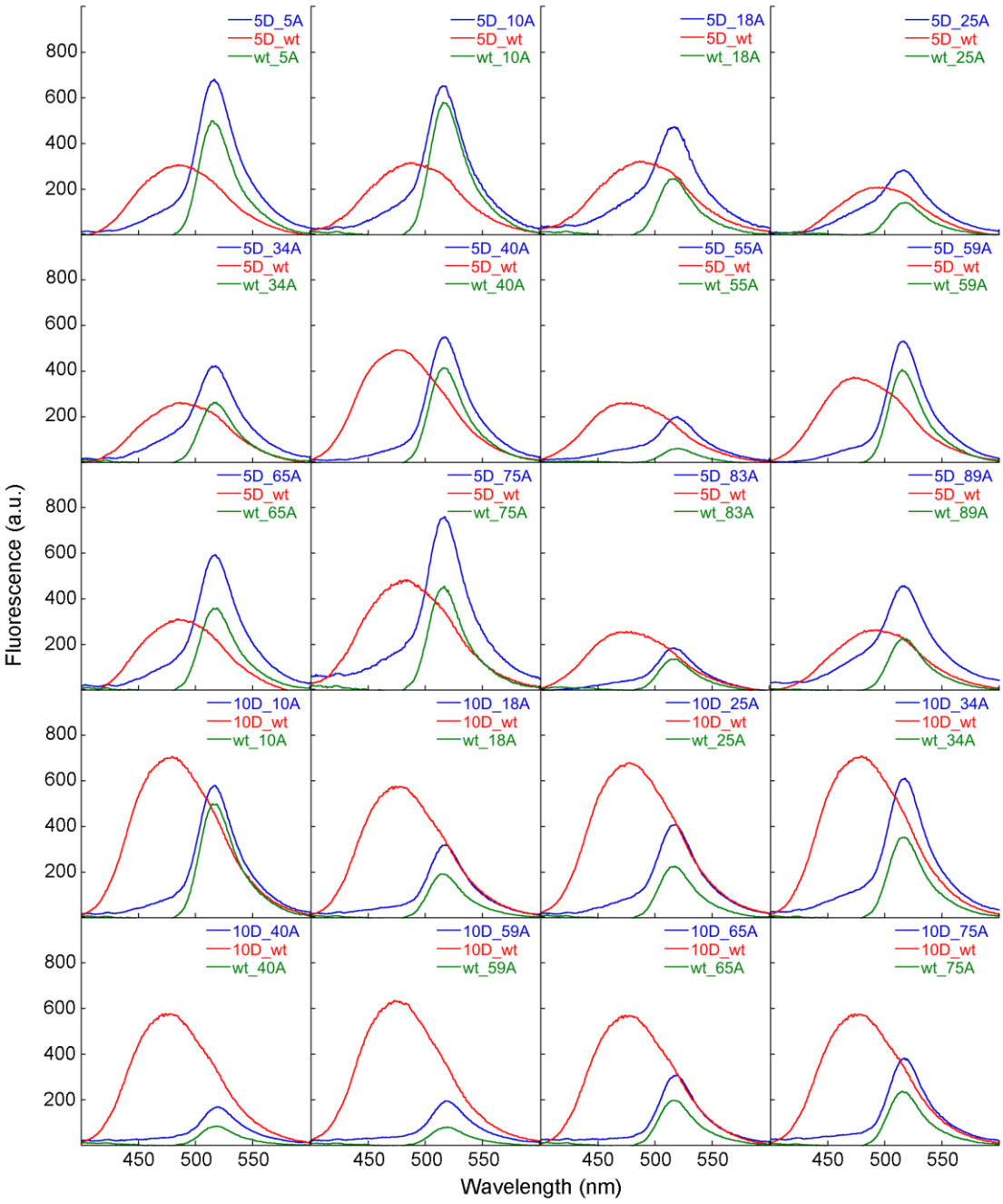

Figure 3.9. Fluorescence emission spectra obtained in the presence of type A HypF-N oligomers formed by pairs of donor-labelled variants and acceptor-labelled variants ("xD_yA") in a 1:1 molar ratio (blue spectra). Oligomers lacking the acceptor dye ("xD_wt") (red spectra) and oligomers lacking the donor dye ("wt_yA") (green spectra) are also acquired. The analysis is presented for 115 type A oligomers presenting various pairs of donor-labelled and acceptor-labelled variants and follows on the next pages.

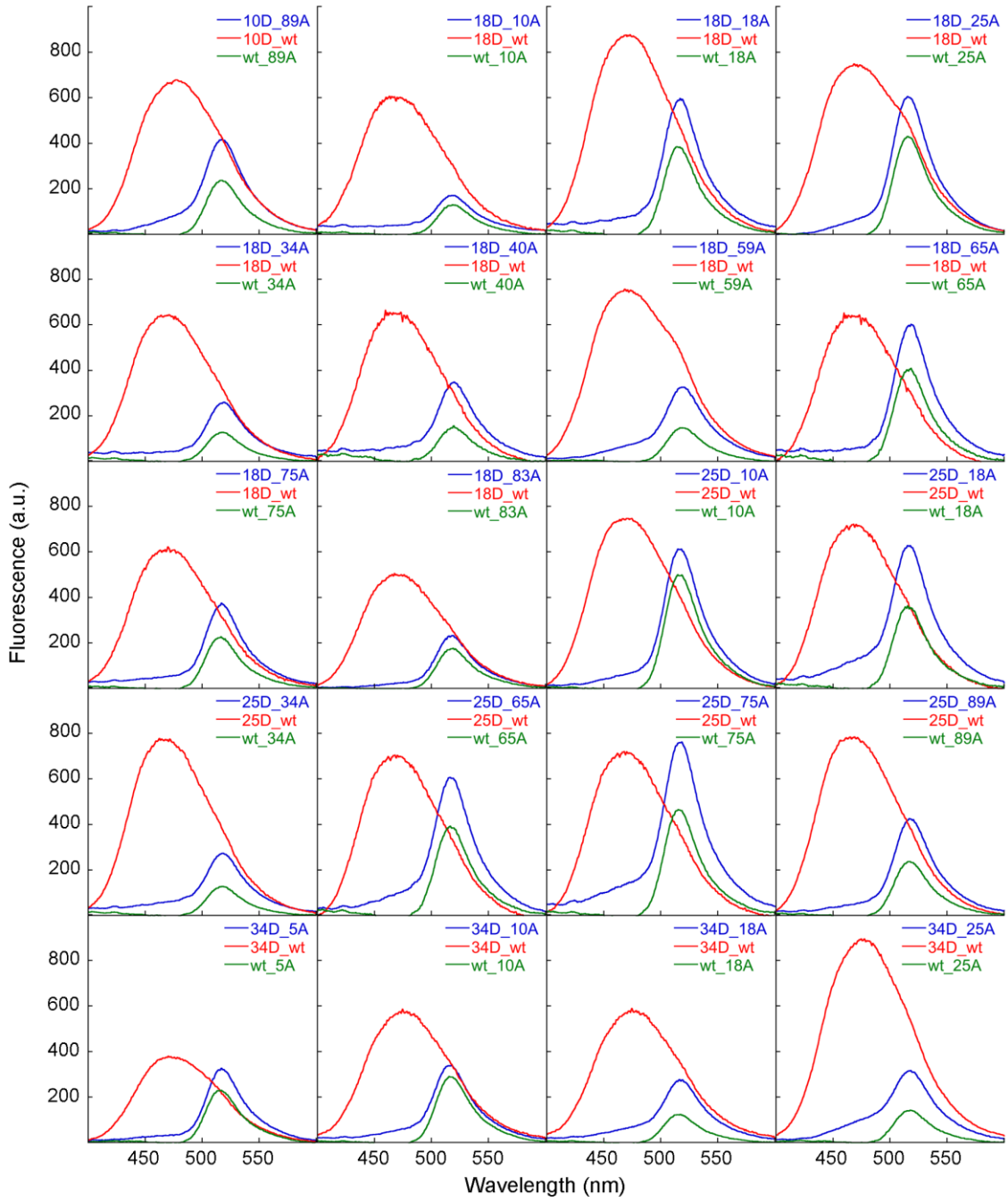
10D_89A
10D_wt
wt_89A
18D_10A
18D_wt
wt_10A
18D_18A
18D_wt
wt_18A
18D_25A
18D_wt
wt_25A
18D_34A
18D_wt
wt_34A
18D_40A
18D_wt
wt_40A
18D_59A
18D_wt
wt_59A
18D_65A
18D_wt
wt_65A
18D_75A
18D_wt
wt_75A
18D_83A
18D_wt
wt_83A
25D_10A
25D_wt
wt_10A
25D_18A
25D_wt
wt_18A
25D_34A
25D_wt
wt_34A
25D_65A
25D_wt
wt_65A
25D_75A
25D_wt
wt_75A
25D_89A
25D_wt
wt_89A
34D_5A
34D_wt
wt_5A
34D_10A
34D_wt
wt_10A
34D_18A
34D_wt
wt_18A
34D_25A
34D_wt
wt_25A
Fluorescence (a.u.)
200
400
600
800
450
500
550
Wavelength (nm)

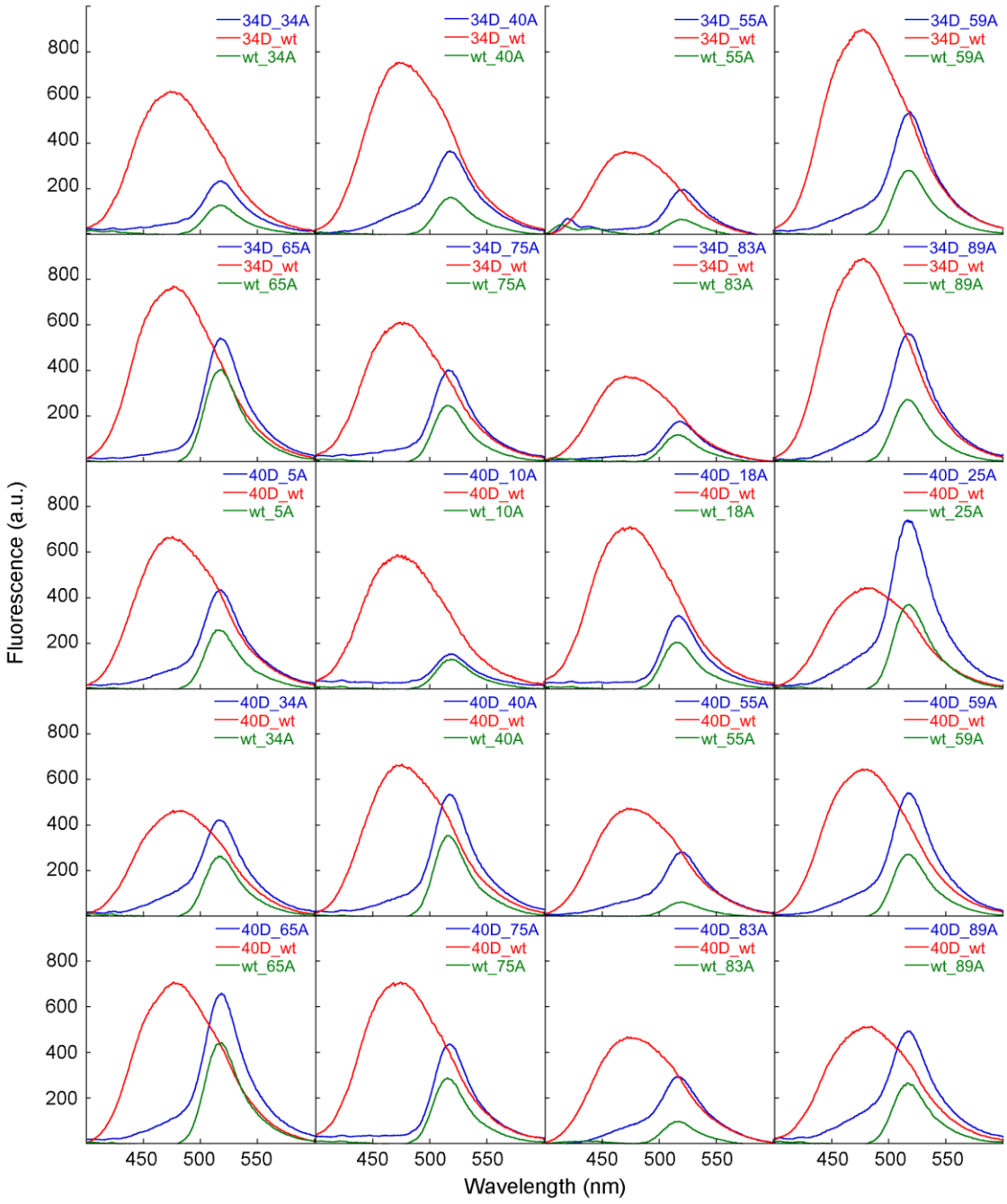
34D_34A
34D_wt
wt_34A
34D_40A
34D_wt
wt_40A
34D_55A
34D_wt
wt_55A
34D_59A
34D_wt
wt_59A
34D_65A
34D_wt
wt_65A
34D_75A
34D_wt
wt_75A
34D_83A
34D_wt
wt_83A
34D_89A
34D_wt
wt_89A
40D_5A
40D_wt
wt_5A
40D_10A
40D_wt
wt_10A
40D_18A
40D_wt
wt_18A
40D_25A
40D_wt
wt_25A
40D_34A
40D_wt
wt_34A
40D_40A
40D_wt
wt_40A
40D_55A
40D_wt
wt_55A
40D_59A
40D_wt
wt_59A
40D_65A
40D_wt
wt_65A
40D_75A
40D_wt
wt_75A
40D_83A
40D_wt
wt_83A
40D_89A
40D_wt
wt_89A
Fluorescence (a.u.)
200
400
600
800
450
500
550
Wavelength (nm)

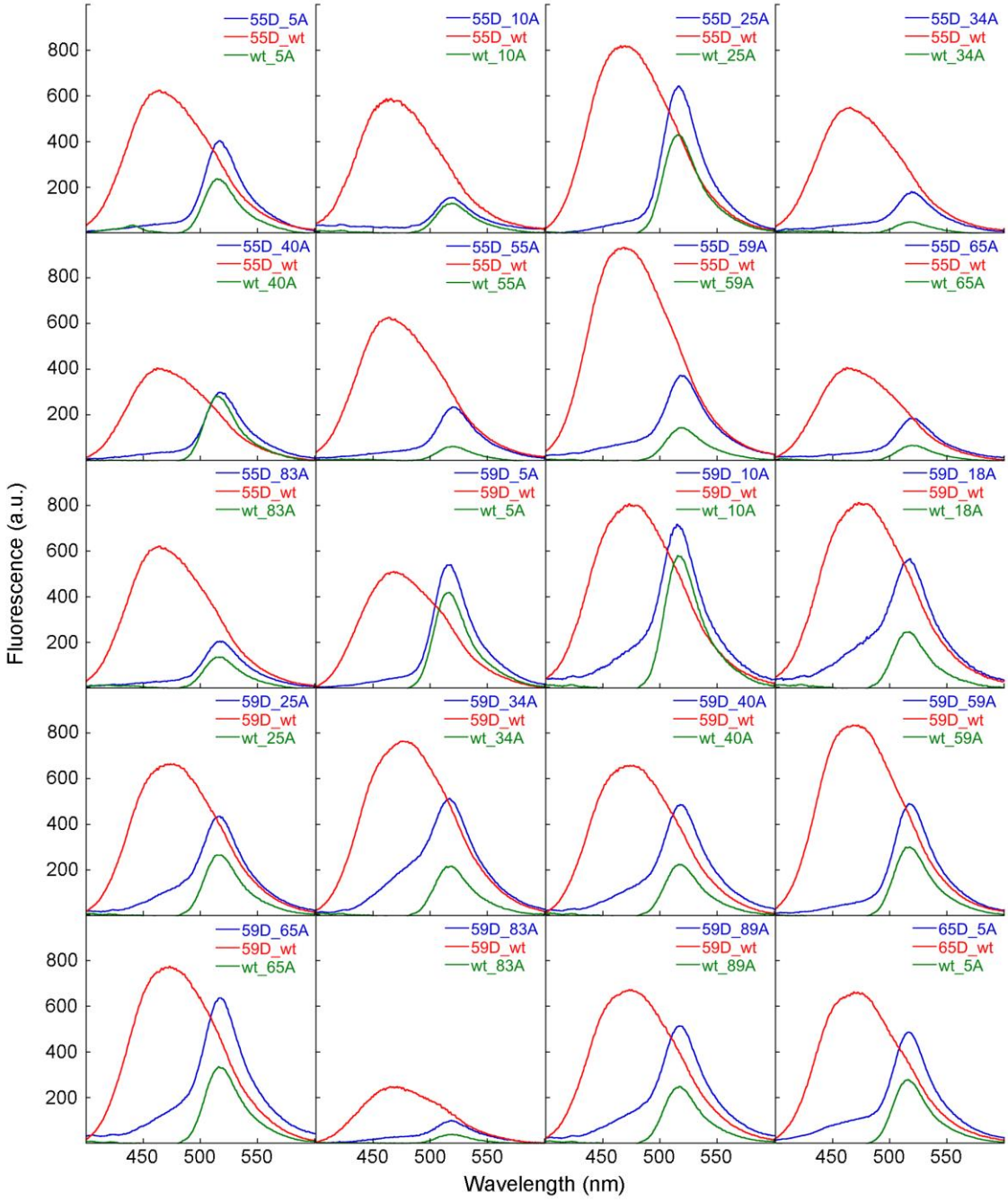
55D_5A
55D_wt
wt_5A
55D_10A
55D_wt
wt_10A
55D_25A
55D_wt
wt_25A
55D_34A
55D_wt
wt_34A
55D_40A
55D_wt
wt_40A
55D_55A
55D_wt
wt_55A
55D_59A
55D_wt
wt_59A
55D_65A
55D_wt
wt_65A
55D_83A
55D_wt
wt_83A
59D_5A
59D_wt
wt_5A
59D_10A
59D_wt
wt_10A
59D_18A
59D_wt
wt_18A
59D_25A
59D_wt
wt_25A
59D_34A
59D_wt
wt_34A
59D_40A
59D_wt
wt_40A
59D_59A
59D_wt
wt_59A
59D_65A
59D_wt
wt_65A
59D_83A
59D_wt
wt_83A
59D_89A
59D_wt
wt_89A
65D_5A
65D_wt
wt_5A
Fluorescence (a.u.)
200
400
600
800
450
500
550
Wavelength (nm)

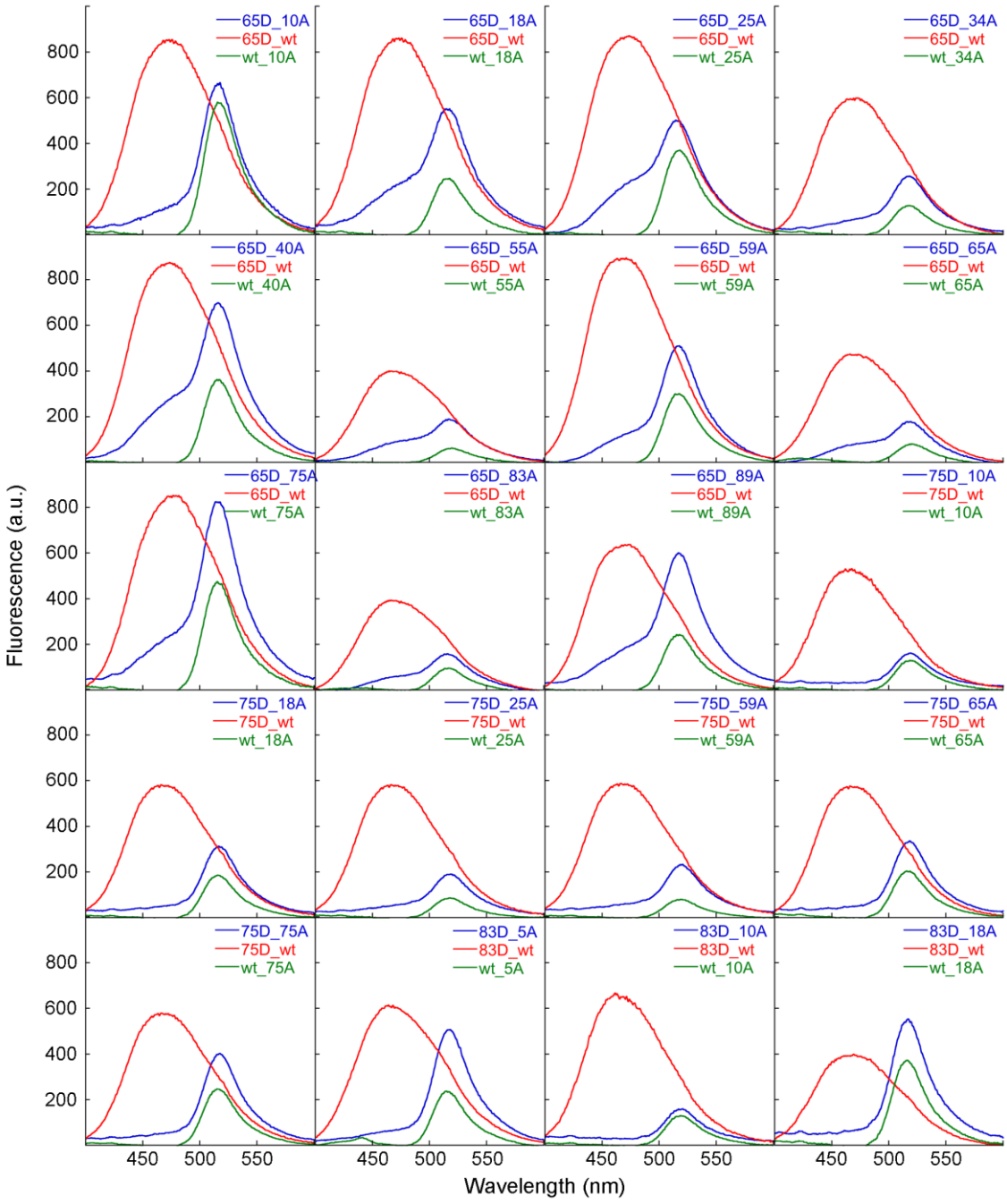
65D_10A
65D_wt
wt_10A
65D_18A
65D_wt
wt_18A
65D_25A
65D_wt
wt_25A
65D_34A
65D_wt
wt_34A
65D_40A
65D_wt
wt_40A
65D_55A
65D_wt
wt_55A
65D_59A
65D_wt
wt_59A
65D_65A
65D_wt
wt_65A
65D_75A
65D_wt
wt_75A
65D_83A
65D_wt
wt_83A
65D_89A
65D_wt
wt_89A
75D_10A
75D_wt
wt_10A
75D_18A
75D_wt
wt_18A
75D_25A
75D_wt
wt_25A
75D_59A
75D_wt
wt_59A
75D_65A
75D_wt
wt_65A
75D_75A
75D_wt
wt_75A
83D_5A
83D_wt
wt_5A
83D_10A
83D_wt
wt_10A
83D_18A
83D_wt
wt_18A
Fluorescence (a.u.)
200
400
600
800
450
500
550
Wavelength (nm)

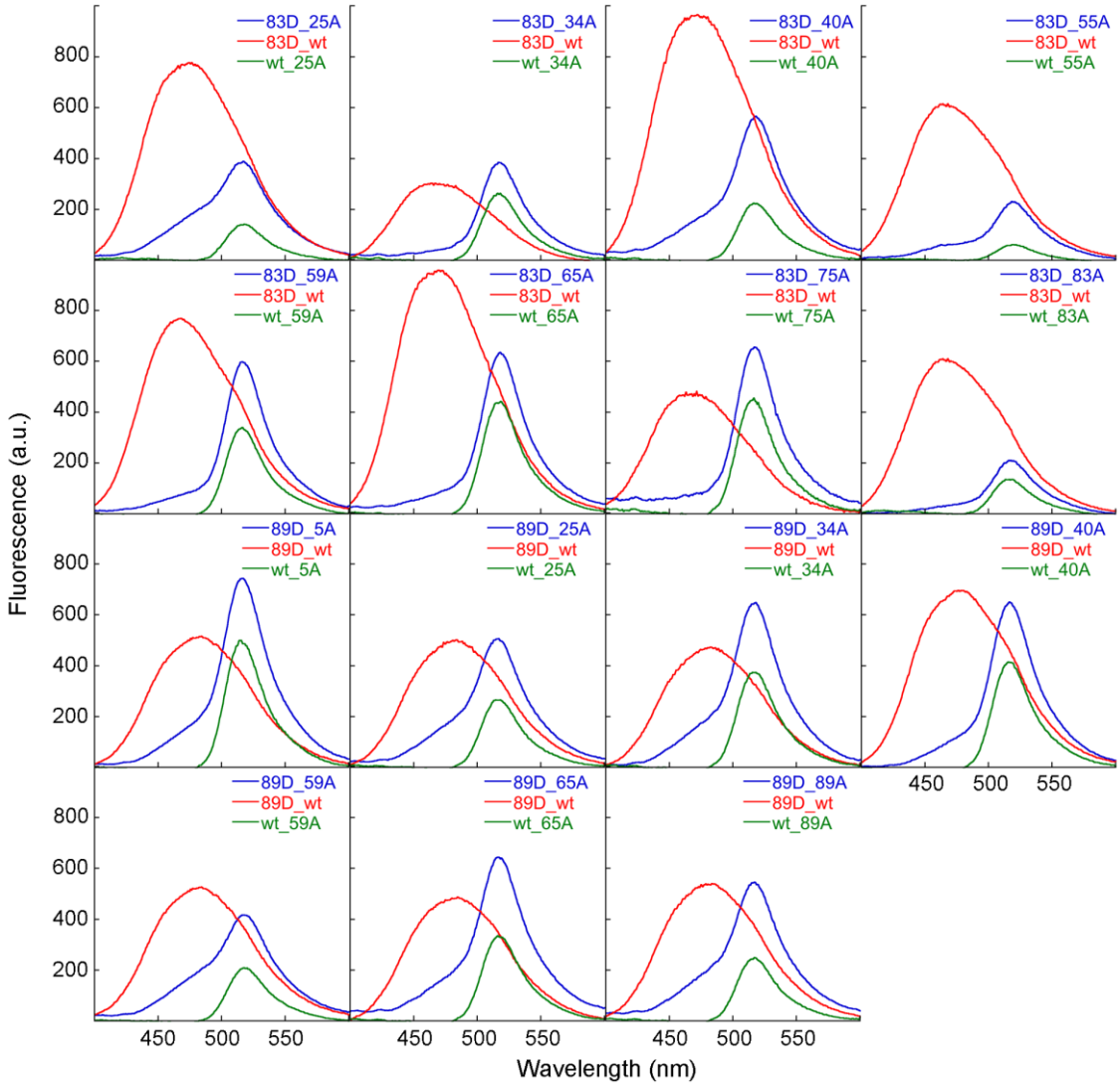
83D_25A
83D_wt
wt_25A
83D_34A
83D_wt
wt_34A
83D_40A
83D_wt
wt_40A
83D_55A
83D_wt
wt_55A
83D_59A
83D_wt
wt_59A
83D_65A
83D_wt
wt_65A
83D_75A
83D_wt
wt_75A
83D_83A
83D_wt
wt_83A
89D_5A
89D_wt
wt_5A
89D_25A
89D_wt
wt_25A
89D_34A
89D_wt
wt_34A
89D_40A
89D_wt
wt_40A
89D_59A
89D_wt
wt_59A
89D_65A
89D_wt
wt_65A
89D_89A
89D_wt
wt_89A
Fluorescence (a.u.)
Wavelength (nm)
200
400
600
800
450
500
550

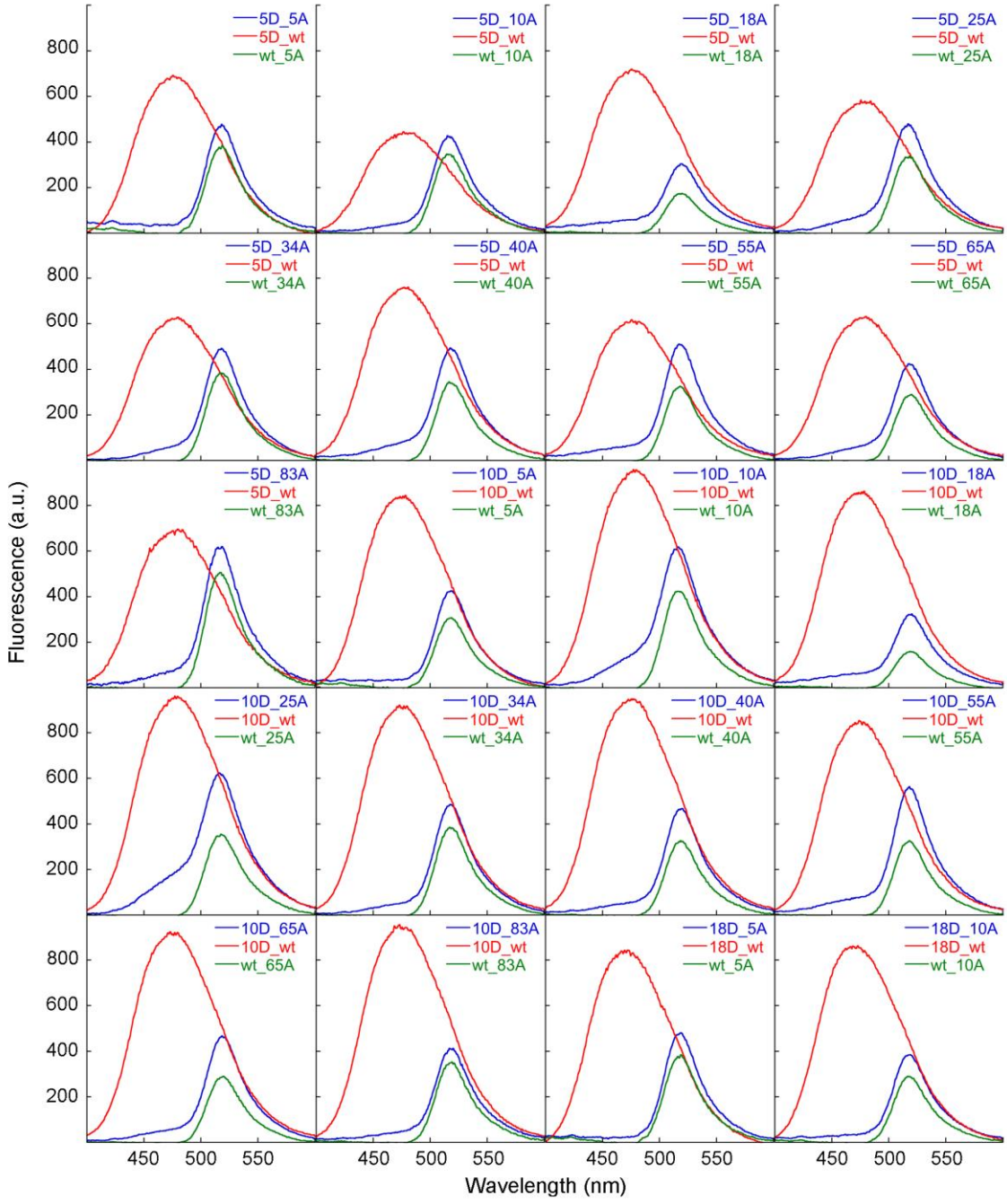

Figure 3.10. Fluorescence emission spectra obtained in the presence of type B HypF-N oligomers formed by pairs of donor-labelled variants and acceptor-labelled variants ("xD_yA") in a 1:1 molar ratio (blue spectra). Oligomers lacking the acceptor dye ("xD_wt") (red spectra) and oligomers lacking the donor dye ("wt_yA") (green spectra) are also acquired. The analysis is presented for 97 type B oligomers presenting various pairs of donor-labelled and acceptor-labelled variants and follows on the next pages.

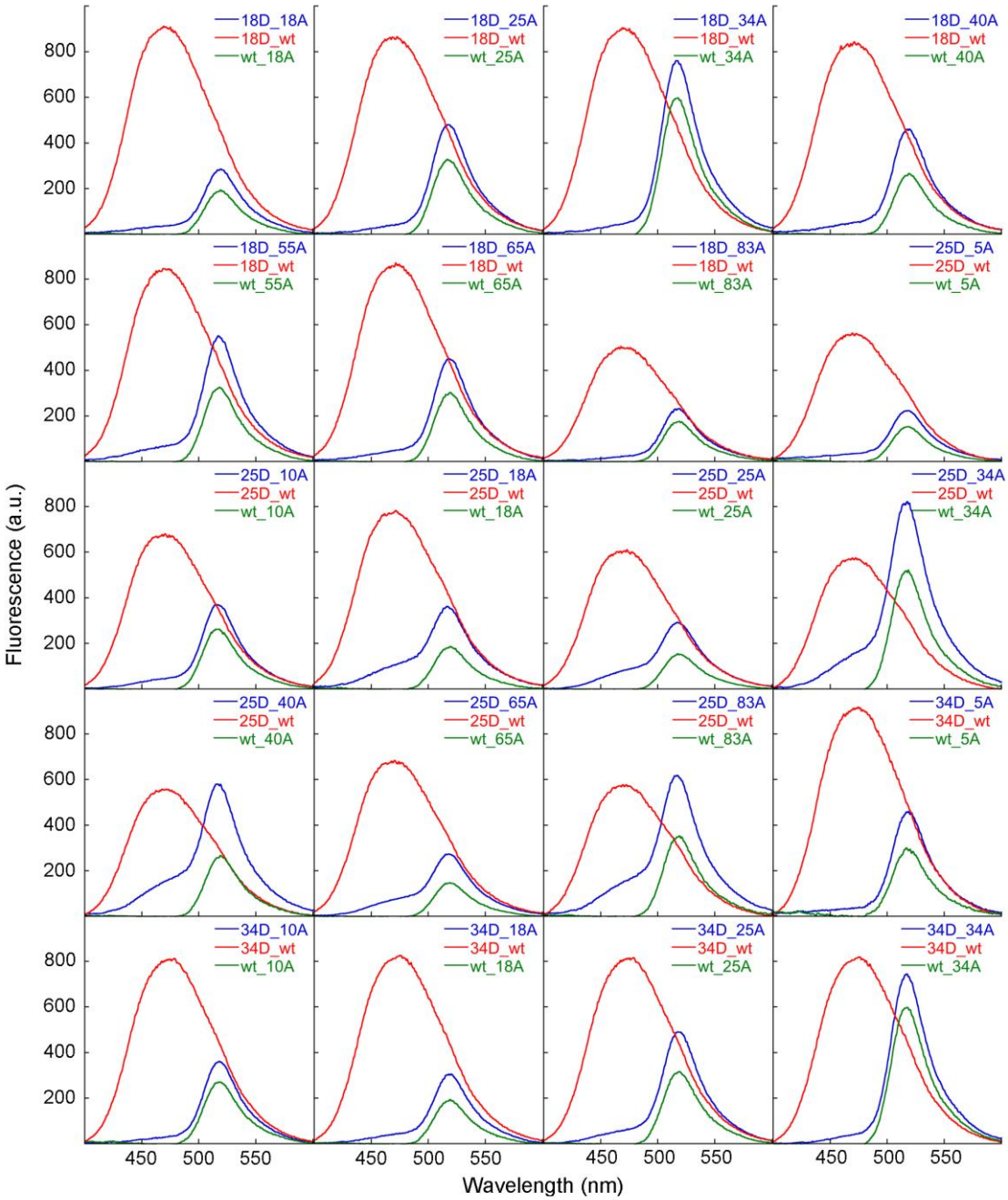
18D_18A
18D_wt
wt_18A
18D_25A
18D_wt
wt_25A
18D_34A
18D_wt
wt_34A
18D_40A
18D_wt
wt_40A
18D_55A
18D_wt
wt_55A
18D_65A
18D_wt
wt_65A
18D_83A
18D_wt
wt_83A
25D_5A
25D_wt
wt_5A
25D_10A
25D_wt
wt_10A
25D_18A
25D_wt
wt_18A
25D_25A
25D_wt
wt_25A
25D_34A
25D_wt
wt_34A
25D_40A
25D_wt
wt_40A
25D_65A
25D_wt
wt_65A
25D_83A
25D_wt
wt_83A
34D_5A
34D_wt
wt_5A
34D_10A
34D_wt
wt_10A
34D_18A
34D_wt
wt_18A
34D_25A
34D_wt
wt_25A
34D_34A
34D_wt
wt_34A
Fluorescence (a.u.)
200
400
600
800
450
500
550
Wavelength (nm)

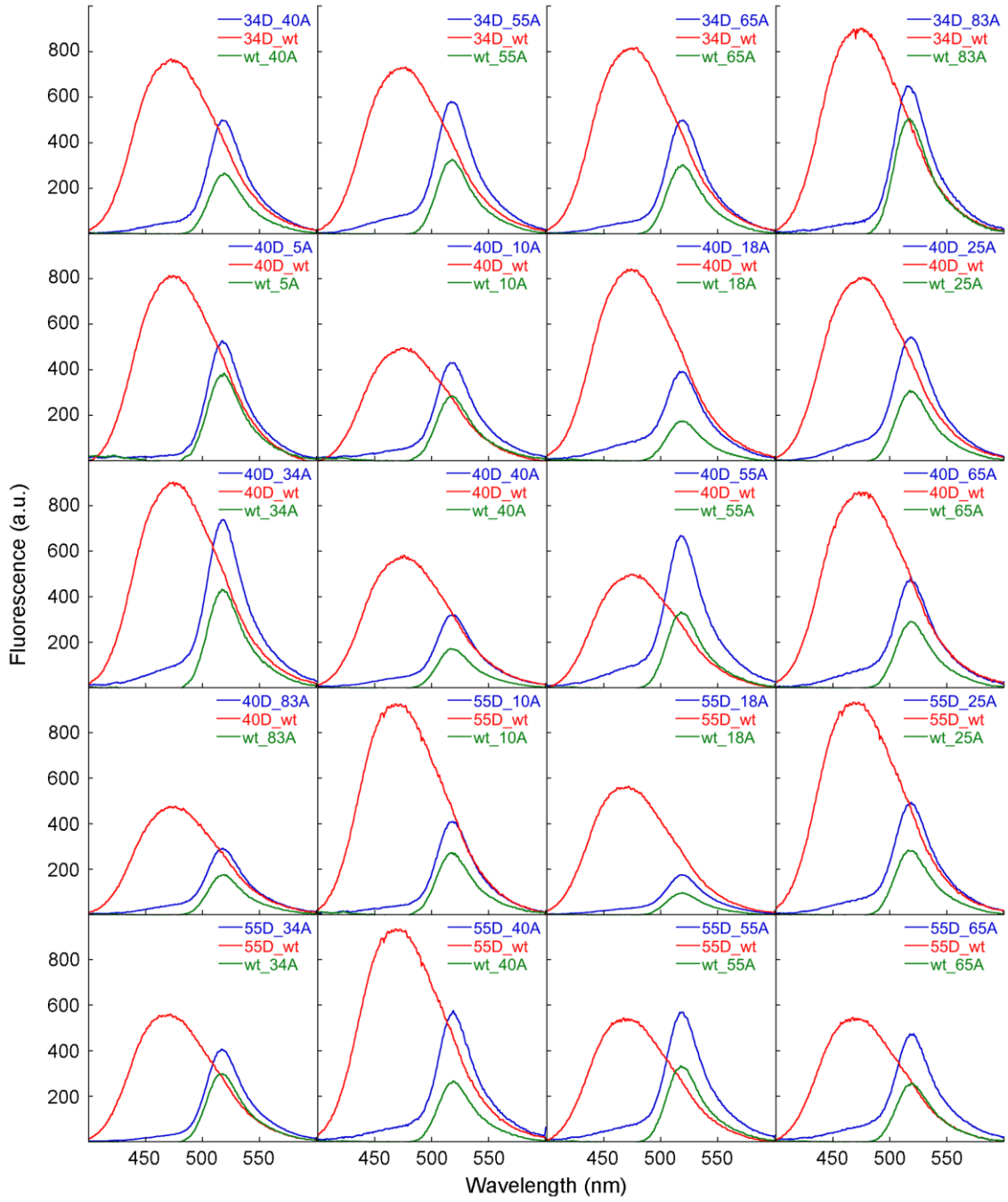
34D_40A
34D_wt
wt_40A
34D_55A
34D_wt
wt_55A
34D_65A
34D_wt
wt_65A
34D_83A
34D_wt
wt_83A
40D_5A
40D_wt
wt_5A
40D_10A
40D_wt
wt_10A
40D_18A
40D_wt
wt_18A
40D_25A
40D_wt
wt_25A
40D_34A
40D_wt
wt_34A
40D_40A
40D_wt
wt_40A
40D_55A
40D_wt
wt_55A
40D_65A
40D_wt
wt_65A
40D_83A
40D_wt
wt_83A
55D_10A
55D_wt
wt_10A
55D_18A
55D_wt
wt_18A
55D_25A
55D_wt
wt_25A
55D_34A
55D_wt
wt_34A
55D_40A
55D_wt
wt_40A
55D_55A
55D_wt
wt_55A
55D_65A
55D_wt
wt_65A
Fluorescence (a.u.)
200
400
600
800
450
500
550
Wavelength (nm)

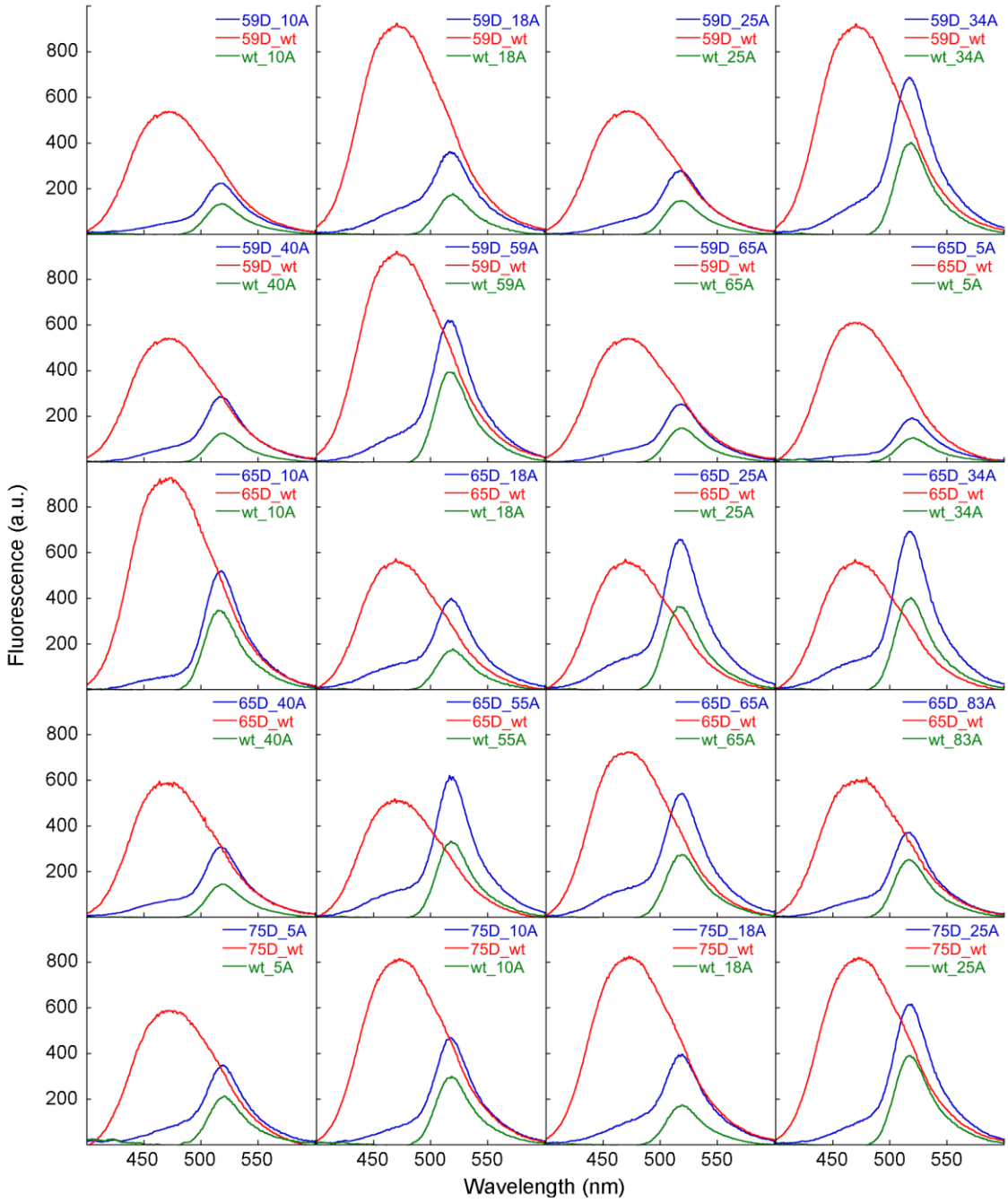
59D_10A
59D_wt
wt_10A
59D_18A
59D_wt
wt_18A
59D_25A
59D_wt
wt_25A
59D_34A
59D_wt
wt_34A
59D_40A
59D_wt
wt_40A
59D_59A
59D_wt
wt_59A
59D_65A
59D_wt
wt_65A
65D_5A
65D_wt
wt_5A
65D_10A
65D_wt
wt_10A
65D_18A
65D_wt
wt_18A
65D_25A
65D_wt
wt_25A
65D_34A
65D_wt
wt_34A
65D_40A
65D_wt
wt_40A
65D_55A
65D_wt
wt_55A
65D_65A
65D_wt
wt_65A
65D_83A
65D_wt
wt_83A
75D_5A
75D_wt
wt_5A
75D_10A
75D_wt
wt_10A
75D_18A
75D_wt
wt_18A
75D_25A
75D_wt
wt_25A
Fluorescence (a.u.)
200
400
600
800
450
500
550
Wavelength (nm)

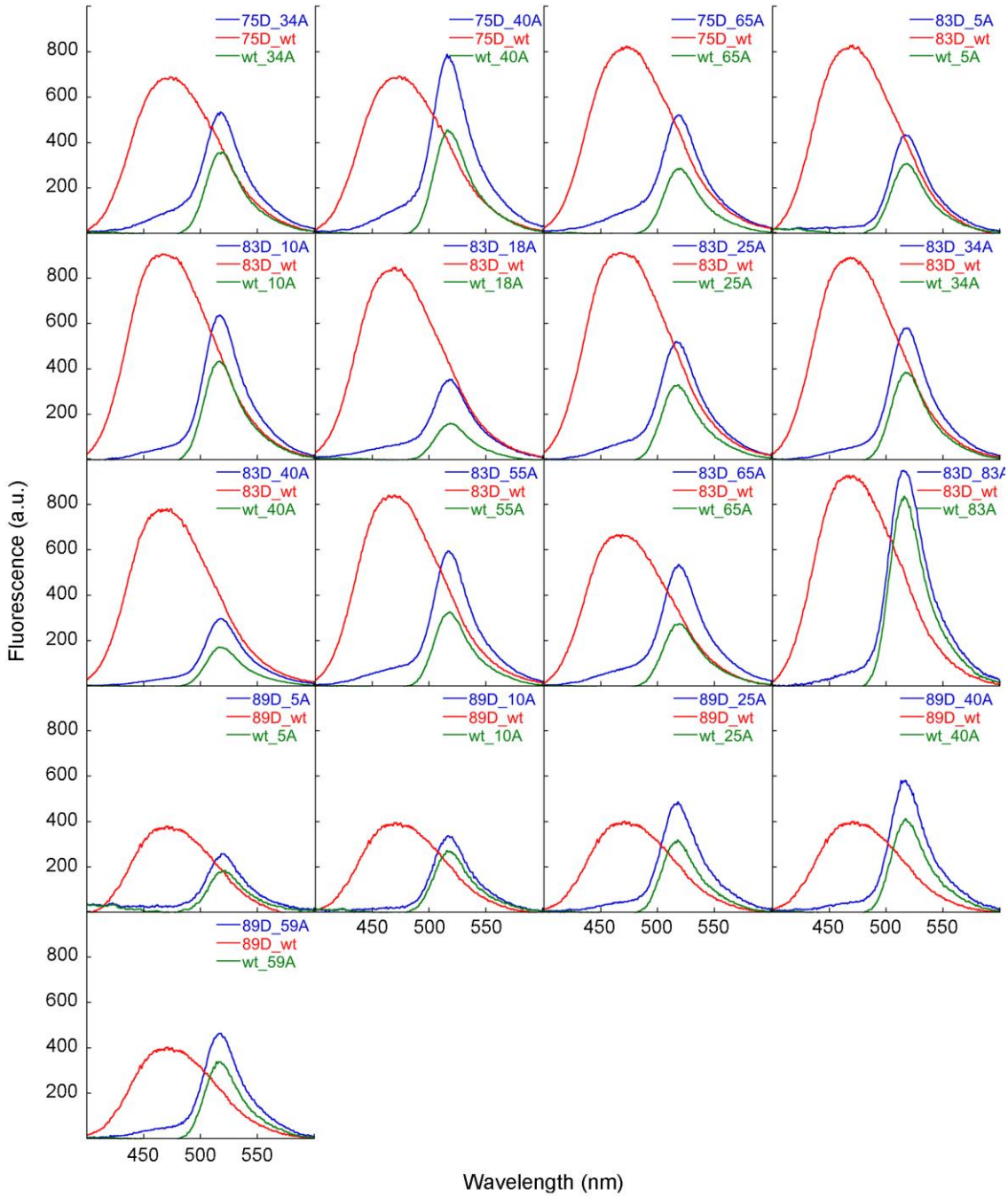
75D_34A
75D_wt
wt_34A
75D_40A
75D_wt
wt_40A
75D_65A
75D_wt
wt_65A
83D_5A
83D_wt
wt_5A
83D_10A
83D_wt
wt_10A
83D_18A
83D_wt
wt_18A
83D_25A
83D_wt
wt_25A
83D_34A
83D_wt
wt_34A
83D_40A
83D_wt
wt_40A
83D_55A
83D_wt
wt_55A
83D_65A
83D_wt
wt_65A
83D_83A
83D_wt
wt_83A
89D_5A
89D_wt
wt_5A
89D_10A
89D_wt
wt_10A
89D_25A
89D_wt
wt_25A
89D_40A
89D_wt
wt_40A
89D_59A
89D_wt
wt_59A
Fluorescence (a.u.)
200
400
600
800
450
500
550
Wavelength (nm)

The *E* values calculated for all the toxic type A and nontoxic type B labelled-oligomers investigated are reported in the Tables 3.1 and 3.2, respectively. The green cells indicate the cases in which the two *E* values obtained for the two oligomers "xD_yA" and "yD_xA" were similar, the yellow cells correspond to the cases in which the two *E* values were close, but not similar, and the red cells indicate that the two *E* values were distant from each other. Finally, the blue cells reported the *E* values obtained for oligomers formed by the same mutant (as an example, the oligomer 5D_5A) for which exist only one *E* value.

TOXIC TYPE A OLIGOMERS

	5 A	**10 A**	**18 A**	**25 A**	**34 A**	**40 A**	**55 A**	**59 A**	**65 A**	**75 A**	**83 A**	**89 A**
5 D	0.3939	~ 0	0.8923	0.4919	0.5340	0.3834	~ 1	0.4492	0.9356	0.5523	0.3669	0.7797
10 D		0.0823	0.4281	0.5341	0.4633	0.6732		~ 1	0.3984	0.4174		0.4887
18 D		0.2728	0.4102	0.5732	0.9632	~ 1		0.9046	0.4537	0.4690		
25 D		0.1790	0.4674		0.7601				0.3513	0.4042		0.7156
34 D	0.3594	0.0822	0.8351	0.6715	0.6022	0.4158	~ 1	0.8457	0.3584	0.4896	0.4129	0.8415
40 D	0.3697	0.1630	0.4238	0.9887	0.5184	0.3790	~ 1	0.8598	0.3541	0.3976	0.8089	0.9683
55 D	0.8218	0.2504		0.3787	~ 1	0.1473	~ 1	~ 1	~ 1		0.5829	
59 D	0.3406	0.0969	0.7659	0.3955	0.7877	0.6333		0.4988	0.6926		~ 1	0.7485
65 D	0.5167	0.0557	0.7226	0.0451	0.6957	0.5424	~ 1	0.6932	0.7351	0.4204	0.4181	0.9134
75 D		0.3243	0.5786	0.9558				~ 1	0.5340	0.5340		
83 D	~ 1	0.3008	0.4363	0.7854	0.7160	0.7414	~ 1	0.7900	0.3644	0.6794	0.4671	0.4778
89 D	0.4236			0.6049	0.3569	0.4052		0.6229	0.7984			0.9747

Table 3.1. *E* values calculated for type A oligomers formed by pairs of donor- and acceptor-labelled variants. The *E* value was calculated by using the following formula: $E = (I_{AD}A_A - I_AA_A)/I_AA_D$, where A_A and A_D correspond to the absorbance value of acceptor and donor, respectively, at 336 nm, at a dye concentration of 120 µM; I_{AD} and I_A represent the fluorescence emission of acceptor in the presence and in the absence, respectively, of donor. The green cells indicate the cases in which the two *E* values obtained for the two oligomers "xD_yA" and "yD_xA" were similar, the yellow cells correspond to the cases in which the two *E* values were close, but not similar, the red cells indicate that the two *E* values were distant from each other, and the blue cells reported the *E* values obtained for oligomers formed by the same mutant (as an example, the oligomer "5D_5A") for which exist only one *E* value.

NONTOXIC TYPE B OLIGOMERS

	5 A	10 A	18 A	25 A	34 A	40 A	55 A	59 A	65 A	75 A	83 A	89 A
5 D	0.2527	0.1746	0.6658	0.3413	0.2124	0.3313	0.5003		0.3909		0.1781	
10 D	0.2994	0.1861	0.7050	0.3233	0.1769	0.3241	0.4981		0.4555		0.1144	
18 D	0.2525	0.3442	0.4306	0.3705	0.2421	0.6914	0.6307		0.4364		0.2696	
25 D	0.3042	0.2594	0.7805	0.5516	0.3602	0.6183			0.5169		0.4505	
34 D	0.4011	0.2403	0.4650	0.4409	0.1936	0.6797	0.6232		0.5505		0.2434	
40 D	0.2816	0.3501	0.8439	0.5271	0.4394	0.5852	0.7204		0.3787		0.4510	
55 D		0.3653	0.6030	0.5344	0.2606	0.8764	0.5122		0.6124			
59 D		0.3991	0.6561	0.5289	0.4345	0.8119		0.3296	0.4388			
65 D	0.5850	0.2886	0.8139	0.5061	0.4722	0.6550	0.6045	0.5140	0.7385		0.2831	
75 D	0.4316	0.4090	0.9560	0.4317	0.3528	0.5777			0.6240			
83 D	0.3362	0.3316	0.9460	0.3896	0.3866	0.5487	0.6041		0.7310		0.1111	
89 D	0.3331	0.1818		0.4647		0.3423						

Table 3.2. *E* values calculated for type B oligomers formed by pairs of donor- and acceptor-labelled variants. The *E* value was calculated by using the following formula: $E = (I_{AD}A_A - I_AA_A)/I_AA_D$, where A_A and A_D correspond to the absorbance value of acceptor and donor, respectively, at 336 nm, at a dye concentration of 120 µM; I_{AD} and I_A represent the fluorescence emission of acceptor in the presence and in the absence, respectively, of donor. The green cells indicate the cases in which the two *E* values obtained for the two oligomers "xD_yA" and "yD_xA" were similar, the yellow cells correspond to the cases in which the two *E* values were close, but not similar, the red cells indicate that the two *E* values were distant from each other, and the blue cells reported the *E* values obtained for oligomers formed by the same mutant (as an example, the oligomer "5D_5A") for which exist only one *E* value.

To interpret these *E* values and their differences in the two types of oligomers, we calculated the difference between the *E* value determined for type A oligomer (E_A) and the *E* value obtained for type B oligomer (E_B), that is $\Delta E = E_A - E_B$ (Figure 3.11). The E_A and E_B values were determined as the average between the two *E* values obtained for the oligomer "xD_yA" and the oligomer "yD_xA" for both type A and type B oligomers. The results show that the *E* values are generally higher in the toxic oligomers formed under condition A than in the nontoxic oligomers formed under condition B ($\Delta E > 0$; Figure 3.11). This means that the intermolecular distances between pairs of labelled residues in adjacent protein molecules in the oligomer are lower in the case of type A oligomers, indicating that these aggregates are more compact and structured than type B oligomers. However, a number of hydrophobic interactions appear to be less structured in the toxic type A oligomers ($\Delta E < 0$; Figure 3.11), allowing the key intermolecular interactions of the nontoxic assemblies that are weak only in the toxic oligomers to be identified.

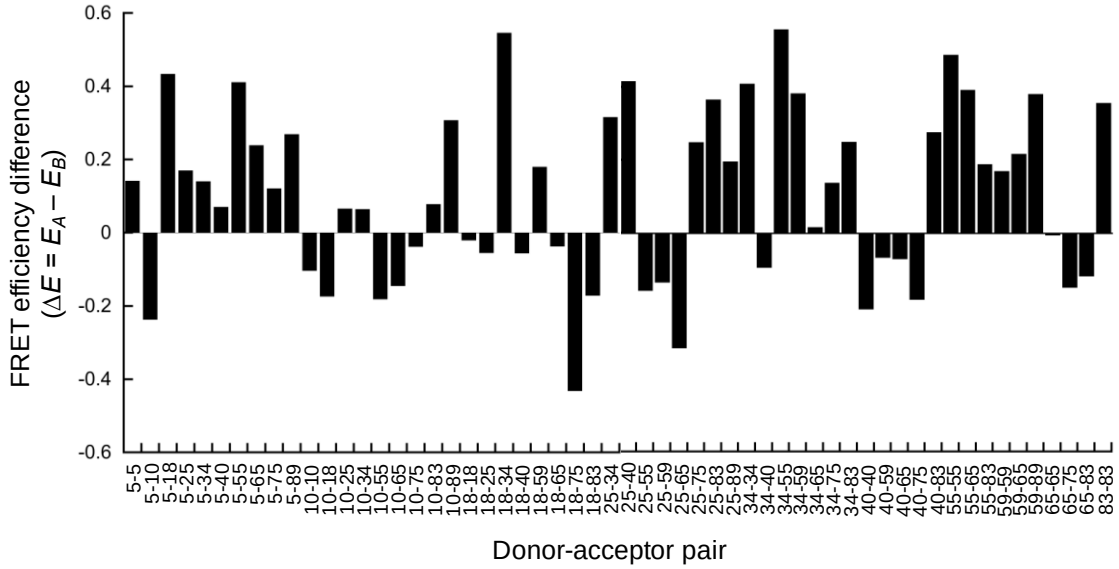

Figure 3.11. *E* difference between *E* values calculated for type A and type B oligomers ($\Delta E = E_A - E_B$) for the pairs reported on the X axis. The values are generally higher than zero; this means that the energy transfer from donor to acceptor was higher between the corresponding two labelled residues in type A oligomers compared to the same pair of labelled residues in type B oligomers.

Chapter 4

Discussion

4.1 The hydrophobicity profiles of HypF-N oligomers reveal differences between type A and type B oligomers on the hydrophobic solvent-exposure

Recent data clearly show that oligomers, rather than mature amyloid fibrils, operate as toxins in many protein misfolding diseases, particularly in neurodegenerative amyloid pathologies, such as Alzheimer's and Parkinson's disease [Chiti and Dobson, 2006]. Interestingly, toxic oligomers may originate from different proteins, that can be unrelated to disease [Bucciantini *et al*., 2002; Sirangelo *et al*., 2004], and are recognised by the same antibody [Kayed *et al*., 2009]. This means that different protein sequences are able to adopt similar aggregated structures that can impair cell viability [Stefani and Dobson, 2003; Chiti and Dobson, 2006]. It is therefore nowadays evident the importance to deeply characterize the structure of toxic oligomeric species, in order to identify new therapeutical targets.

The protein HypF-N is considered a good model system to investigate the structural basis of the cellular dysfunction caused by misfolded protein oligomers, since it is able to form oligomers *in vitro* that show similar morphological, structural and tinctorial properties to those formed by disease-related peptides and proteins [Marcon *et al.*, 2005; Campioni *et al.*, 2008]. Moreover, it was found that HypF-N is able to form two types of oligomeric assemblies under two different solution conditions, called conditions A and B, and that, despite showing similar morphological and tinctorial properties, have different biological activities [Campioni *et al*., 2010; Zampagni *et al*., 2011; Tatini *et al*., 2013]. In particular, the oligomers formed in condition A were able to impair the cell viability and to induce the cell death by apoptosis, whereas the oligomers formed in condition B did not have effect on the cell viability. The reason of this different citotoxicity arises from structural differences at the molecular level between the two types of oligomers: both HypF-N oligomers were found to possess a hydrophobic core, that is able to interact with the plasma membrane of the cell [Campioni *et al*., 2010; Zampagni *et al*., 2011]. However, it was observed that the hydrophobic regions of HypF-N are more

packed and buried in the nontoxic aggregates, whereas a higher exposure and flexibility of the same regions are present in the toxic oligomers [Campioni *et al*., 2010].

The study of the hydrophobicity profile reported in this thesis was aimed at further elucidating the differences between type A and type B oligomers, in particular about the solvent-exposure of the hydrophobic regions of the protein. The resulting hydrophobicity profiles of type A and type B oligomers labelled with the dye 1,5-IAEDANS at different positions on the primary sequence were obtained by observing the blue/red shift of the λ_{max}, which depends on the hydrophilic/hydrophobic environment around the 1,5-IAEDANS moiety. This analysis shows that the hydrophobic regions of the protein, identified by the hydropathy profile of HypF-N calculated using the Roseman hydrophobicity scale [Campioni *et al*., 2010], are more solvent-exposed in toxic type A oligomers than in nontoxic type B oligomers, and these profiles are similar to the PM excimer ratio profiles previously published [Campioni *et al*., 2010]. Considering that 1,5-IAEDANS is more hydrophilic than PM, and, thus, that the chemical nature of the dyes is different, the fact that the hydrophobicity profiles obtained by using these different approaches are consistent with each other, indicates that the labelling with this kind of dyes do not alter the structure and the physicochemical properties of the aggregates under investigation. The only differences between the two profiles regard the position 18, that is contained in the first hydrophobic region in the 1,5-IAEDANS profile, whereas it is not hydrophobic both in PM profile and in the hydropathy profile of the HypF-N sequence, and the position 65, that is contained in the second hydrophobic region of the 1,5-IAEDANS profile in accordance with the hydrophaty profile of the HypF-N sequence, whereas is not in a hydrophobic region in the PM profile. In summary, the regions spanning approximately residues 16-27, 53-67 and 73-85 are identified in the 1,5-IAEDANS profile as the hydrophobic regions potentially involved in the toxic interactions characteristic of type A oligomers, as such regions are more solvent-exposed in these type of oligomers than in type B oligomers. These regions are largely superimposable to those previously identified with the PM profile, *i.e.* 22-34, 55-59 and 75-87 [Campioni *et al*., 2010].

These data confirm the increasing evidence that a relationship exists between the exposure of hydrophobic oligomeric surface and the ability of the aggregates to cause cell dysfunction [Oma *et al*., 2005; Bolognesi *et al*., 2010; Campioni *et al*., 2010; Krishnan *et al*., 2012; Ladiwala *et al*., 2012; Mannini *et al*., 2014]. Importantly, the link between hydrophobic exposure and toxicity concernes oligomers formed by several proteins or

peptides; for instance, in a previous report two types of $A\beta_{42}$ oligomers showing similar size but dissimilar toxicity were investigated, and it was found that two hydrophobic peptide segments within Aβ (residues 16-22 and 30-42) were more solvent-exposed in the more toxic Aβ oligomer [Ladiwala *et al*., 2012]. Moreover, the less toxic oligomer was incapable of disrupting lipid bilayers, in contrast to its more toxic oligomeric counterpart [Ladiwala *et al*., 2012]. Another example is represented by the prion-determining region of yeast Sup35 (NM) [Krishnan *et al*., 2012]. During the assembly of a normal functional amyloid, NM forms a variety of oligomeric intermediates showing different sizes and conformation-specific antibody reactivities, but also different ability to impair neuronal cell viability. By using Nile Red binding, it was observed that the cytotoxic effect of the different oligomers was related to the hydrophobic nature of the aggregates, in particular the toxic oligomers were more hydrophobic, whereas the nontoxic types were more hydrophilic [Krishnan *et al*., 2012].

This leads to consider the surface hydrophobicity as a structural determinant of the oligomer toxicity. However, this is not the only factor involved in the toxic effect of the oligomers; indeed, another important determinat is recognized to be the size of the oligomer. A previous report of Mannini and co-workers, in which the introduction of hydrophobic mutations in the HypF-N sequence determined changes on the surface hydrophobicity, it was observed that such mutations also affected the size of type A and type B oligomers [Mannini *et al*., 2014]. The explanation was found considering that the increase of hydrophobicity was accompanied by the increase in the dimensions of the oligomers; the more hydrophobic exposure made the aggregates more sticky, facilitating their interactions and favouring the formations of bigger species unable to exert their toxic effect [Mannini *et al*., 2014]. Indeed, oligomer toxicity was found to correlate with both surface hydrophobicity and size in a three-dimensional plot.

4.2 Type A oligomers are more structured than type B oligomers, but some intermolecular interactions are more solvent-exposed in the toxic assemblies

The comparative analysis of the structures of type A and type B HypF-N oligomers performed by allowing the formation of the oligomers combining donor-labelled variants and acceptor-labelled variants in a 1:1 molar ratio, and by determining the energy transfer from donor to acceptor, allowed to explore the interchain interactions between pairs of labelled residues, even between residues that are distant from each other in the primary

sequence of the protein. As a result, it was possible to obtain a network of residue-residue interactions giving an overall view of the three-dimensional organization of the oligomers. Our data suggest that toxic type A oligomers present a greater degree of compactness than nontoxic type B oligomers, as indicated by the fact that the number of pairs of residues presenting a higher *E* value in type A oligomers is 34, whereas the number of pairs of residues showing a higher *E* value in type B oligomers is 23 (Figure 4.1). If we examine these interactions individually by observing the *E* difference ($\Delta E = E_A - E_B$) reported in Figure 4.1, it is possible to note that in many cases clusters of interactions exist. As an example, the pairs in which the position 5 is linked with the positions 5, 18, 25, 34, 40, 55, 65, 75 and 89, appear to be highly close to each other in type A oligomers. The only exception is the pair 5-18, that shows an *E* value higher in type B oligomers. This suggests that residue 5, known to be a solvent-exposed residue as determined by the PM excimer ratio and the λ_{max} 1,5-IAEDANS profiles, is in a environmental contest that allows its interaction with both more hydrophobic (positions 18, 25, 55, 65, 89) and more hydrophilic (positions 5, 34, 40, 75) residues of the protein in type A oligomers.

A second cluster of interactions showing higher *E* values in type A oligomers involves the position 25 and includes the pairs 25-34, 25-40, 25-75, 25-83 and 25-89. In particular, the interactions 25-75 and 25-83 involve positions that are in the first (position 25) and in the third (positions 75 and 83) hydrophobic regions of HypF-N. However, another cluster of interactions, showing lower *E* values in type A oligomers, exists. This includes the pairs 25-55, 25-59 and 25-65 and involves the first (position 25) and the second (positions 55, 59 and 65) hydrophobic regions of the protein. Thus, such interactions appear to be less structured in toxic type A oligomers. Therefore, considering the importance of the solvent-exposure of the hydrophobic regions to the ability of oligomers to permeabilize the cellular membrane and to induce cellular dysfunction as a consequence of the Ca^{2+} influx, the intermolecular hydrophobic interactions 25-55, 25-59 and 25-65 can be considered responsible for the toxic action of type A oligomers. In addition to this cluster, other two groups of hydrophobic interactions appear to be closer and, thus, buried in type B oligomers: the pairs 18-75 and 18-83, that involve the first (position 18) and the third (positions 75 and 83) regions of the hydrophaty profile, and the pairs 65-75 and 65-83, that involve the second (position 65) and the third (positions 75 and 83) regions. Therefore, similarly to the abovementioned 25-55, 25-59 and 25-65,

these interactions are more solvent-exposed in toxic type A oligomers and may be involved in the interaction of such aggregates with the cellular membrane.

Many interactions in a cluster that considers the position 34 (34-34, 34-55, 34-59, 34-65, 34-75 and 34-83) show an *E* value higher in type A oligomers, with the only exception of the pair 34-40. However, residue 34 is in a hydrophilic environment of the oligomers; hence the interactions that forms are never entirely in a hydrophobic contest. On the other hand, some interactions of a cluster involving residue 40 (40-40, 40-59, 40-65 and 40-83) show an *E* value lower in type A oligomers and, thus, can be only partially hydrophobic, as position 40 is in a hydrophilic environment. Therefore, even if this cluster present higher *E* values in type B oligomers, and, consequently, the interactions are more solvent-exposed in type A oligomers, the low hydrophobic content makes them non-significant for the toxic effect of type A oligomers. The same argument also applies to other interactions that appear closer in type B oligomers, but that are formed by one or two hydrophilic residues (10-10, 10-18, 10-55, 10-65, 10-75, 18-40, 18-75 and 65-75).

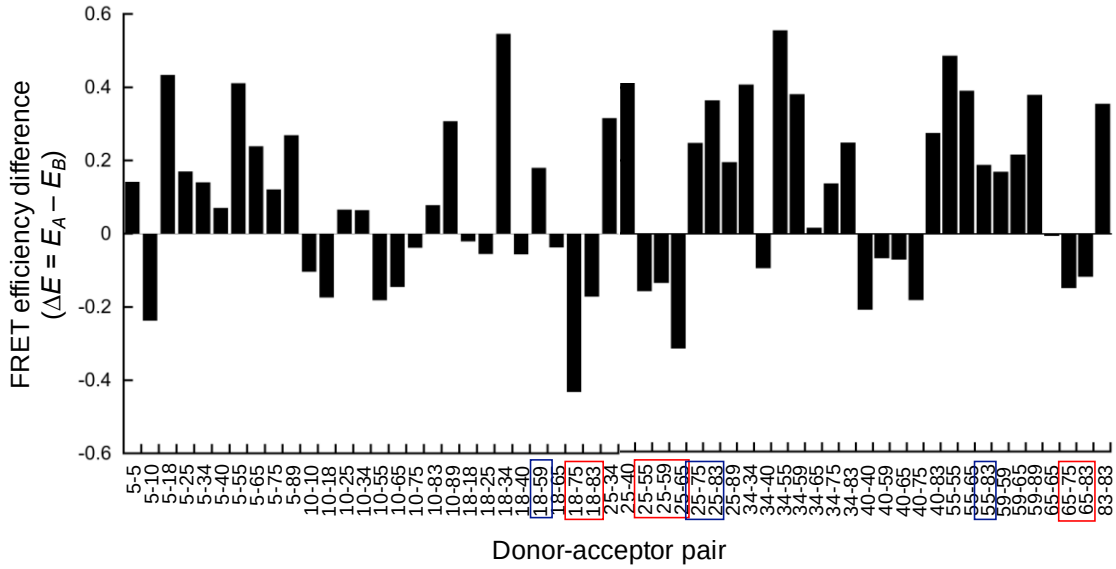

Figure 4.1. Difference between *E* values calculated for type A and type B oligomers ($\Delta E = E_A - E_B$) for the pairs reported on the X axis. The values are generally higher than zero; this means that the energy transfer from donor to acceptor was higher between the corresponding two labelled residues in type A oligomers compared to the same pair of labelled residues in type B oligomers. However, some interactions formed by hydrophobic residues located in distant regions appear to be less structured in toxic type A oligomers (red squares), whereas only a few long range hydrophobic interactions appear more structured in type A oligomers (blue squares).

Interestingly, of all 12 pairs of interactions formed by residues both located in hydrophobic regions of the sequence but far apart in the sequence (belonging to distinct hydrophobic regions) 7 interactions have *E* values lower in type A oligomers than type B oligomers (red squares in Figure 4.1, pairs 18-75, 18-83, 25-55, 25-59, 25-65, 65-75 and

65-83), 4 interactions have *E* values higher in type A oligomers (blue squares in Figure 4.1, pairs 18-59, 25-75, 25-83 and 55-83) and 1 has a *E* value similar in the two oligomer types (pair 18-65). If the analysis is repeated for the long range interactions (belonging to distinct regions of the sequence) formed by at least one hydrophilic residue, only 8 interactions have *E* values lower in type A oligomers, as many as 21 have *E* values higher and 2 have values similar in the two oligomer types. This comparative analysis indicates that although type A oligomers appear to be more compact than type B aggregates, as indicated by the overall higher *E* values, the hydrophobic interactions appear to be weakened in type A oligomers.

4.3 Conclusions

In conclusion, this analysis obtained by using the FRET approach allowed to identify two important structural characteristics of type A and type B HypF-N oligomers. First, it was possible to gain an overview of the three-dimensional organization of the two types of oligomers, that showed differences in compactness. Toxic type A oligomers appear more structured than nontoxic type B oligomers when considering all the interaction pairs studied here and involving both hydrophobic and hydrophilic residues. This evidence opens the way for some questions, for instance if the higher degree of compactness is a general characteristic that involves the entire sequence, or if it is restricted to specific regions of the protein. Second, with such analysis it was possible to uncover at least a part of the key solvent-exposed hydrophobic interactions that are probably involved in the ability of toxic assemblies to interact with the cellular membrane. Therefore, as a further direction, it will be interested to investigate specifically such hydrophobic interactions in order to clarify this aspect of the molecular basis of the cellular dysfunction induced by misfolded protein oligomers.

Bibliography

Ahmad B, Winkelmann J, Tiribilli B, Chiti F (2010) Searching for conditions to form stable protein oligomers with amyloid-like characteristics: The unexplored basic pH. *Biochim Biophys Acta* **1804**:223-34.

Alexandrescu AT (2005) Amyloid accomplices and enforces. *Protein Sci* **14**:1-12.

Amaral MD (2004) CFTR and chaperones: processing and degradation. *J Mol Neurosci* **23**:41-8.

Baglioni S, Casamenti F, Bucciantini M, Luheshi LM, Taddei N, Chiti F, Dobson CM, Stefani M (2006) Prefibrillar amyloid aggregates could be generic toxins in higher organisms. *J Neurosci* **26**:8160-7.

Balchin D, Hayer-Hartl M, Hartl FU (2016) In vivo aspects of protein folding and quality control. *Science* **353**:aac4354.

Banci L, Bertini I, D'Amelio N, Gaggelli E, Libralesso E, Matecko I, Turano P, Valentine JS (2005) Fully metallated S134N Cu,Zn-superoxide dismutase displays abnormal mobility and intermolecular contacts in solution. *J Biol Chem* **280**:35815-21.

Bauer HH, Aebi U, Häner M, Hermann R, Müller M, Merkle HP (1995) Architecture and polymorphism of fibrillar supramolecular assemblies produced by in vitro aggregation of human calcitonin. *J Struct Biol* **115**:1-15.

Bejarano E, Cuervo AM (2010) Chaperone-mediated autophagy. *Proc Am Thorac Soc* **7**:29-39.

Bemporad F, Chiti F (2012) Protein misfolded oligomers: experimental approaches, mechanism of formation, and structure-toxicity relationships. *Chem Biol* **19**:315-27.

Benson MD, Liepnieks JJ, Yazaki M, Yamashita T, Hamidi Asl K, Guenther B, Kluve-Beckerman B (2001) A new human hereditary amyloidosis: the result of a stop-codon mutation in the apolipoprotein AII gene. *Genomics* **72**:272-7.

Berger J, Hinglais N (1968) [Intercapillary deposits of IgA-IgG]. *J Urol Nephrol (Paris)* **74**:694-5.

Berriman J, Serpell LC, Oberg KA, Fink AL, Goedert M, Crowther RA (2003) Tau filaments from human brain and from in vitro assembly of recombinant protein show cross-beta structure. *Proc Natl Acad Sci U S A* **100**:9034-8.

Betcher-Lange SL, Lehrer SS (1978) Pyrene excimer fluorescence in rabbit skeletal alphaalphatropomyosin labeled with N-(1-pyrene)maleimide. A probe of sulfhydryl proximity and local chain separation. *J Biol Chem* **253**:3757-60.

Bijlmakers MJ, Marsh M (2000) Hsp90 is essential for the synthesis and subsequent membrane association, but not the maintenance, of the Src-kinase p56(lck). *Mol Biol Cell* **11**:1585-95.

Billings LM, Oddo S, Green KN, McGaugh JL, LaFerla FM (2005) Intraneuronal Abeta causes the onset of early Alzheimer's disease-related cognitive deficits in transgenic mice. *Neuron* **45**:675-88.

Bitan G, Kirkitadze MD, Lomakin A, Vollers SS, Benedek GB, Teplow DB (2003) Amyloid beta -protein (Abeta) assembly: Abeta 40 and Abeta 42 oligomerize through distinct pathways. *Proc Natl Acad Sci U S A* **100**:330-5.

Bleiholder C, Dupuis NF, Wyttenbach T, Bowers MT (2011) Ion mobility-mass spectrometry reveals a conformational conversion from random assembly to β-sheet in amyloid fibril formation. *Nat Chem* **3**:172-7.

Bolognesi B, Kumita JR, Barros TP, Esbjorner EK, Luheshi LM, Crowther DC, Wilson MR, Dobson CM, Favrin G, Yerbury JJ (2010) ANS binding reveals common features of cytotoxic amyloid species. *ACS Chem Biol* **5**:735-40.

Bouchard M, Zurdo J, Nettleton EJ, Dobson CM, Robinson CV (2000) Formation of insulin amyloid fibrils followed by FTIR simultaneously with CD and electron microscopy. *Protein Sci* **9**:1960-7.

Brodbeck J, McGuire J, Liu Z, Meyer-Franke A, Balestra ME, Jeong DE, Pleiss M, McComas C, Hess F, Witter D, Peterson S, Childers M, Goulet M, Liverton N, Hargreaves R, Freedman S, Weisgraber KH, Mahley RW, Huang Y (2011) Structure-dependent impairment of intracellular apolipoprotein E4 trafficking and its detrimental effects are rescued by small-molecule structure correctors. *J Biol Chem* **286**:17217-26.

Bucciantini M, Calloni G, Chiti F, Formigli L, Nosi D, Dobson CM, Stefani M (2004) Prefibrillar amyloid protein aggregates share common features of cytotoxicity. *J Biol Chem* **279**:31374-82.

Bucciantini M, Giannoni E, Chiti F, Baroni F, Formigli L, Zurdo J, Taddei N, Ramponi G, Dobson CM, Stefani M (2002) Inherent toxicity of aggregates implies a common mechanism for protein misfolding diseases. *Nature* **416**:507-11.

Bucciantini M, Rigacci S, Berti A, Pieri L, Cecchi C, Nosi D, Formigli L, Chiti F, Stefani M (2005) Patterns of cell death triggered in two different cell lines by HypF-N prefibrillar aggregates. *FASEB J* **19**:437-9.

Bukau B, Horwich AL (1998) The Hsp70 and Hsp60 chaperone machines. *Cell* **92**:351-66.

Calamai M, Canale C, Relini A, Stefani M, Chiti F, Dobson CM (2005) Reversal of protein aggregation provides evidence for multiple aggregated States. *J Mol Biol* **346**:603-16.

Calloni G, Lendel C, Campioni S, Giannini S, Gliozzi A, Relini A, Vendruscolo M, Dobson CM, Salvatella X, Chiti F (2008) Structure and dynamics of a partially folded protein are decoupled from its mechanism of aggregation. *J Am Chem Soc* **130**:13040-50.

Calloni G, Taddei N, Plaxco KW, Ramponi G, Stefani M, Chiti F (2003) Comparison of the folding processes of distantly related proteins. Importance of hydrophobic content in folding. *J Mol Biol* **330**:577-91.

Calloni G, Zoffoli S, Stefani M, Dobson CM, Chiti F (2005) Investigating the effects of mutations on protein aggregation in the cell. *J Biol Chem* **280**:10607-13.

Campioni S, Mannini B, López-Alonso JP, Shalova IN, Penco A, Mulvihill E, Laurents DV, Relini A, Chiti F (2012) Salt anions promote the conversion of HypF-N into amyloid-like oligomers and modulate the structure of the oligomers and the monomeric precursor state. *J Mol Biol* **424**:132-49.

Campioni S, Mannini B, Zampagni M, Pensalfini A, Parrini C, Evangelisti E, Relini A, Stefani M, Dobson CM, Cecchi C, Chiti F (2010) A causative link between the structure of aberrant protein oligomers and their toxicity. *Nat Chem Biol* **6**:140-7.

Campioni S, Mossuto MF, Torrassa S, Calloni G, de Laureto PP, Relini A, Fontana A, Chiti F (2008) Conformational properties of the aggregation precursor state of HypF-N. *J Mol Biol* **379**:554-67.

Canale C, Torrassa S, Rispoli P, Relini A, Rolandi R, Bucciantini M, Stefani M, Gliozzi A (2006) Natively folded HypF-N and its early amyloid aggregates interact with phospholipid monolayers and destabilize supported phospholipid bilayers. *Biophys J* **91**:4575-88.

Canet D, Last AM, Tito P, Sunde M, Spencer A, Archer DB, Redfield C, Robinson CV, Dobson CM (2002) Local cooperativity in the unfolding of an amyloidogenic variant of human lysozyme. *Nat Struct Biol* **9**:308-15.

Cappelli S, Penco A, Mannini B, Cascella R, Wilson MR, Ecroyd H, Li X, Buxbaum JN, Dobson CM, Cecchi C, Relini A, Chiti F (2016) Effect of molecular chaperones on aberrant protein oligomers in vitro: super-versus sub-stoichiometric chaperone concentrations. *Biol Chem* **397**:401-15.

Casalot L, Rousset M (2001) Maturation of the [NiFe] hydrogenases. *Trends Microbiol* **9**:228-37.

Cascella R, Conti S, Mannini B, Li X, Buxbaum JN, Tiribilli B, Chiti F, Cecchi C (2013) Transthyretin suppresses the toxicity of oligomers formed by misfolded proteins in vitro. *Biochim Biophys Acta* **1832**:2302-14.

Caubet C, Bousset L, Clemmensen O, Sourigues Y, Bygum A, Chavanas S, Coudane F, Hsu CY, Betz RC, Melki R, Simon M, Serre G (2010) *FASEB J* **24**:3416-26.

Cecchi C, Baglioni S, Fiorillo C, Pensalfini A, Liguri G, Nosi D, Rigacci S, Bucciantini M, Stefani M (2005) Insights into the molecular basis of the differing susceptibility of varying cell types to the toxicity of amyloid aggregates. *J Cell Sci* **118**:3459-70.

Chamcheu JC, Siddiqui IA, Syed DN, Adhami VM, Liovic M, Mukhtar H (2011) Keratin gene mutations in disorders of human skin and its appendages. *Arch Biochem Biophys* **508**:123-37.

Chamcheu JC, Wood GS, Siddiqui IA, Syed DN, Adhami VM, Teng JM, Mukhtar H (2012) Progress towards genetic and pharmacological therapies for keratin genodermatoses: current perspective and future promise. *Exp Dermatol* **21**:481-9.

Chen L, Campo P, Kupferle MJ (2015) Identification of chlorinated oligomers formed during anodic oxidation of phenol in the presence of chloride. *J Hazard Mater* **283**:574-81.

Chen HK, Ji ZS, Dodson SE, Miranda RD, Rosenblum CI, Reynolds IJ, Freedman SB, Weisgraber KH, Huang Y, Mahley RW (2011) Apolipoprotein E4 domain interaction mediates detrimental effects on mitochondria and is a potential therapeutic target for Alzheimer disease. *J Biol Chem* **286**:5215-21.

Chiarugi P, Raugei G, Fiaschi T, Taddei L, Camici G, Ramponi G (1996) Characterization of a novel nucleolytic activity of acylphosphatases. *Biochem Mol Biol Int* **40**:73-81.

Chimon S, Shaibat MA, Jones CR, Calero DC, Aizezi B, Ishii Y (2007) Evidence of fibril-like β-sheet structures in a neurotoxic amyloid intermediate of Alzheimer's β-amyloid. *Nat struct mol Biol* **14**:1157-64.

Chiti F, Bucciantini M, Capanni C, Taddei N, Dobson CM, Stefani M (2001) Solution conditions can promote formation of either amyloid protofilaments or mature fibrils from the HypF N-terminal domain. *Protein Sci* **10**:2541-7.

Chiti F, Dobson MC (2006) Protein misfolding, functional amyloid, and human disease. *Annu Rev Biochem* **75**:333-66.

Chiti F, Webster P, Taddei N, Clark A, Stefani M, Ramponi G, Dobson CM (1999) Designing conditions for in vitro formation of amyloid protofilaments and fibrils. *Proc Natl Acad Sci U S A* **96**:3590-4.

Cizas P, Budvytyte R, Morkuniene R, Moldovan R, Broccio M, Lösche M, Niaura G, Valincius G, Borutaite V (2010) Size-dependent neurotoxicity of beta-amyloid oligomers. *Arch Biochem Biophys* **496**:84-92.

Claessen JH, Kundrat L, Ploegh HL (2012) Protein quality control in the ER: balancing the ubiquitin checkbook. *Trends Cell Biol* **22**:22-32.

Cleary JP, Walsh DM, Hofmeister JJ, Shankar GM, Kuskowski MA, Selkoe DJ, Ashe KH (2005) Natural oligomers of the amyloid-beta protein specifically disrupt cognitive function. *Nat Neurosci* **8**:79-84.

Cohen-Kaplan V, Livneh I, Avni N, Cohen-Rosenzweig C, Ciechanover A (2016) The ubiquitin-proteasome system and autophagy: coordinated and independent activities. *Int J Biochem Cell Biol* **79**:403-418.

Colbeau A, Elsen S, Tomiyama M, Zorin NA, Dimon B, Vignais PM (1998) Rhodobacter capsulatus HypF is involved in regulation of hydrogenase synthesis through the HupUV proteins. *Eur J Biochem* **251**:65-71.

Collinge J, Clarke AR (2007) A general model of prion strains and their pathogenicity. *Science* **318**:930-6.

Cox TM, Cachón-González MB (2012) The cellular pathology of lysosomal diseases. *J Pathol* **226**:241-54.

Cremades N, Cohen SI, Deas E, Abramov AY, Chen AY, Orte A, Sandal M, Clarke RW, Dunne P, Aprile FA, Bertoncini CW, Wood NW, Knowles TP, Dobson CM, Klenerman D (2012) Direct observation of the interconversion of normal and toxic forms of α-synuclein. *Cell* **149**:1048-59.

Danpure CJ, Purdue PE, Fryer P, Griffiths S, Allsop J, Lumb MJ, Guttridge KM, Jennings PR, Scheinman JI, Mauer SM, et al. (1993) Enzymological and mutational analysis of a complex primary hyperoxaluria type 1 phenotype involving alanine:glyoxylate aminotransferase peroxisome-to-mitochondrion mistargeting and intraperoxisomal aggregation. *Am J Hum Genet* **53**:417-32.

Danzer KM, Haasen D, Karow AR, Moussaud S, Habeck M, Giese A, Kretzschmar H, Hengerer B, Kostka M (2007) Different species of alpha-synuclein oligomers induce calcium influx and seeding. *J Neurosci* **27**:9220-32.

De Gracia R, Fernández EJ, Riñón C, Selgas R, Garcia-Bustos J (2006) Hereditary renal amyloidosis associated with a novel mutation in the apolipoprotein AII gene. *QJM* **99**:274.

Deshpande A, Mina E, Glabe C, Busciglio J (2006) Different conformations of amyloid beta induce neurotoxicity by distinct mechanisms in human cortical neurons. *J Neurosci* **26**:6011-8.

Diaz-Espinoza R, Soto C (2012) High-resolution structure of infectious prion protein: the final frontier. *Nat Struct Mol Biol* **19**:370-7.

Dykes G, Crepeau RH, Edelstein SJ (1978) Three-dimensional reconstruction of the fibres of sickle cell haemoglobin. *Nature* **272**:506-10.

Dobson CM, Sali A, Karplus M (1998) Protein folding: a perspective from theory and experiment. *Angew Chem Int Ed Eng* **37**:868-93.

Dobson CM (2003) Protein folding and misfolding. *Nature* **426**:884-90.

Dobson CM (2004) Principles of protein folding, misfolding and aggregation. *Semin Cell Dev Biol* **15**:3-16.

Dong LM, Weisgraber KH (1996) Human apolipoprotein E4 domain interaction. Arginine 61 and glutamic acid 255 interact to direct the pre ference for very low density lipoproteins. *J Biol Chem* **271**:19053-7.

Dwyer JJ, Gittis AG, Karp DA, Lattman EE, Spencer DS, Stites WE, García-Moreno EB (2000) High apparent dielectric constants in the interior of a protein reflect water penetration. *Biophys J* **79**:1610-20.

Eanes ED, Glenner GG (1968) X-ray diffraction studies on amyloid filaments. *J Histochem Cytochem* **16**:673-7.

Eisenberg D, Jucker M (2012) The amyloid state of proteins in human diseases. *Cell* **148**:1188-203.

Ellis RJ (2001) Macromolecular crowding: an important but neglected aspect of the intracellular environment. *Curr Opin Struct Biol* **11**:114-9.

Ellis RJ, Minton AP (2006) Protein aggregation in crowded environments. *Biol Chem* **387**:485-97.

Evangelisti E, Cascella R, Becatti M, Marrazza G, Dobson CM, Chiti F, Stefani M, Cecchi C (2016) Binding affinity of amyloid oligomers to cellular membranes is a generic indicator of cellular dysfunction in protein misfolding diseases. *Sci Rep* **6**:32721.

Evangelisti E, Cecchi C, Cascella R, Sgromo C, Becatti M, Dobson CM, Chiti F, Stefani M (2012) Membrane lipid composition and its physicochemical properties define cell vulnerability to aberrant protein oligomers. *J Cell Sci* **125**:2416-27.

Fändrich M, Dobson CM (2002) The behaviour of polyamino acids reveals an inverse side chain effect in amyloid structure formation. *EMBO J* **21**:5682-90.

Fändrich M, Forge V, Buder K, Kittler M, Dobson CM, Diekmann S (2003) Myoglobin forms amyloid fibrils by association of unfolded polypeptide segments. *Proc Natl Acad Sci U S A* **100**:15463-8.

Farrer LA, Cupples LA, Haines JL, Hyman B, Kukull WA, Mayeux R, Myers RH, Pericak-Vance MA, Risch N, van Duijn CM (1997) Effects of age, sex, and ethnicity on the association between apolipoprotein E genotype and Alzheimer disease. A meta-analysis. APOE and Alzheimer Disease Meta Analysis Consortium. *JAMA* **278**:1349-56.

Flagmeier P, Meisl G, Vendruscolo M, Knowles TP, Dobson CM, Buell AK, Galvagnion C (2016) Mutations associated with familial Parkinson's disease alter the initiation and amplification steps of α-synuclein aggregation. *Proc Natl Acad Sci U S A* **113**:10328-33.

Fowler DM, Koulov AV, Alory-Jost C, Marks MS, Balch WE, Kelly JW (2006) Functional amyloid formation within mammalian tissue. *PLoS Bioli* **4**:e6.

Freed-Pastor WA, Prives C (2012) Mutant p53: one name, many proteins. *Genes Dev* **26**:1268-86.

Friedrich B, Schwartz E (1993) Molecular biology of hydrogen utilization in aerobic chemolithotrophs. *Annu Rev Microbiol* **47**:351-83.

Futerman AH, van Meer G (2004) The cell biology of lysosomal storage disorders. *Nat Rev Mol Cell Biol* **5**:554-65.

Fu XL, Gao DS (2014) Endoplasmic reticulum proteins quality control and the unfolded protein response: the regulative mechanism of organisms against stress injuries. *Biofactors* **40**:569-85.

Gavrin LK, Denny RA, Saiah E (2012) Small molecules that target protein misfolding. *J Med Chem* **55**:10823-43.

Glenner GG, Terry W, Harada M, Isersky C, Page D (1971) Amyloid fibril proteins: proof of homology with immunoglobulin light chains by sequence analyses. *Science* **172**:1150-1.

Goldsbury C, Frey P, Olivieri V, Aebi U, Müller SA (2005) Multiple assembly pathways underlie amyloid-beta fibril polymorphisms. *J Mol Biol* **352**:282-98.

Gong H, Yang X, Zhao Y, Petersen RB, Liu X, Liu Y, Huang K (2015) Amyloidogenicity of p53: a hidden link between protein misfolding and cancer. *Curr Protein Pept Sci* **16**:135-46.

Grabowski GA (2008) Phenotype, diagnosis, and treatment of Gaucher's disease. *Lancet* **372**:1263-71.

Guijarro JI, Sunde M, Jones JA, Campbell ID, Dobson CM (1998) Amyloid fibril formation by an SH3 domain. *Proc Natl Acad Sci U S A* **95**:4224-8.

Haass C, Selkoe DJ (2007) Soluble protein oligomers in neurodegeneration: lessons from the Alzheimer's amyloid beta-peptide. *Nat Rev Mol Cell Biol* **8**:101-12.

Hammarström P, Kalman B, Jonsson BH, Carlsson U (1997) Pyrene excimer fluorescence as a proximity probe for investigation of residual structure in the unfolded state of human carbonic anhydrase II. *FEBS Lett* **420**:63-8.

Hammarström P, Owenius R, Måstensson LG, Carlsson U, Lindgren M (2001) High-resolution probing of local conformational changes in proteins by the use of multiple labeling: unfolding and self-assembly of human carbonic anhydrase II monitored by spin, fluorescent, and chemical reactivity probes. *Biophys J* **80**:2867-85.

Hammarström P, Persson M, Freskgård PO, Mårtensson LG, Andersson D, Jonsson BH, Carlsson U (1999) Structural mapping of an aggregation nucleation site in a molten globule intermediate. *J Biol Chem* **274**:32897-903.

Hardesty B, Kramer G (2001) Folding of a nascent peptide on the ribosome. *Prog Nucleic Acid Res Mol Biol* **66**:41-66.

Hartl FU, Hayer-Hartl M (2002) Molecular chaperones in the cytosol: from nascent chain to folded protein. *Science* **295**:1852-8.

Hervás R, Li L, Majumdar A, Fernández-Ramírez Mdel C, Unruh JR, Slaughter BD, Galera-Prat A, Santana E, Suzuki M, Nagai Y, Bruix M, Casas-Tintó S, Menéndez M, Laurents DV, Si K, Carrión-Várquez M (2016) Molecular basis of Orb2 amyloidogenesis and blockade of memory consolidation. *PLoS Biol* **14**:e1002361.

Hidvegi T, Ewing M, Hale P, Dippold C, Beckett C, Kemp C, Maurice N, Mukherjee A, Goldbach C, Watkins S, Michalopoulos G, Perlmutter DH (2010) An autophagy-enhancing drug promotes degradation of mutant alpha1-antitrypsin Z and reduces hepatic fibrosis. *Science* **329**:229-32.

Hidvegi T, Schmidt BZ, Hale P, Perlmutter DH (2005) Accumulation of mutant alpha1-antitrypsin Z in the endoplasmic reticulum activates caspases-4 and -12, NFkappaB, and BAP31 but not the unfolded protein response. *J Biol Chem* **280**:39002-15.

Hinton DR, Polk RK, Linse KD, Weiss MH, Kovacs K, Garner JA (1997) Characterization of spherical amyloid protein from a prolactin-producing pituitary adenoma. *Acta Neuropathol* **93**:43-9.

Hirschfield GM, Hawkins PN (2003) Amyloidosis: new strategies for treatment. *Int J Biochem Cell Biol* **35**:1608-13.

Hoseki J, Ushioda R, Nagata K (2010) Mechanism and components of endoplasmic reticulum-associated degradation. *J Biochem* **147**:19-25.

Iijima K, Chiang HC, Hearn SA, Hakker I, Gatt A, Shenton C, Granger L, Leung A, Iijima-Ando K, Zhong Y (2008) Abeta42 mutants with different aggregation profiles induce distinct pathologies in Drosophila. *PLoS One* **3**:e1703.

Itoh-Watanabe H, Kamihira-Ishijima M, Javkhlantugs N, Inoue R, Itoh Y, Endo H, Tuzi S, Saitô H, Ueda K, Naito A (2013) Role of aromatic residues in amyloid fibril formation of human calcitonin by solid-state 13C NMR and molecular dynamics simulation. *Phys Chem Chem Phys* **15**:8890-901.

Jahn TR, Radford SE (2008) Folding versus aggregation: polypeptide conformations on competing pathways. *Arch Biochem Biophys* **469**:100-17.

Jaroniec CP, MacPhee CE, Astrof NS, Dobson CM, Griffin RG (2002) Molecular conformation of a peptide fragment of transthyretin in an amyloid fibril. *Proc Natl Acad Sci U S A* **99**:16748-53.

Jarosz DF, Taipale M, Lindquist S (2010) Protein homeostasis and the phenotypic manifestation of genetic diversity: principles and mechanisms. *Annu Rev Genet* **44**:189-216.

Jimenez-Zepeda VH (2012) Light chain deposition disease: novel biological insights and treatment advances. *Int J Lab Hematol* **34**:347-55.

Jones EM, Surewicz WK (2005) Fibril conformation as the basis of species- and strain-dependent seeding specificity of mammalian prion amyloids. *Cell* **121**:63-72.

Kamada R, Toguchi Y, Nomura T, Imagawa T, Sakaguchi K (2016) Tetramer formation of tumor suppressor protein p53: Structure, function, and applications. *Biopolymers* **106**:598-612.

Kapoor A, Sanyal AJ (2009) Endoplasmic reticulum stress and the unfolded protein response. *Clin Liver Dis* **13**:581-90.

Karplus M (1997) The Levinthal paradox, yesterday and today. *Fold Des* **2**:569-76.

Kayed R, Pensalfini A, Margol L, Sokolov Y, Sarsoza F, Head E, Hall J, Glabe C (2009) Annular protofibrils are a structurally and functionally distinct type of amyloid oligomer. *J Biol Chem* **284**:4230-7.

Kaylor J, Bodner N, Edridge S, Yamin G, Hong DP, Fink AL (2005) Characterization of oligomeric intermediates in alpha-synuclein fibrillation: FRET studies of Y125W/Y133F/Y136F alpha-synuclein. *J Mol Biol* **353**:357-72.

Kelly JW, Balch WE (2003) Amyloid as a natural product. *J Cell Biol* **161**:461-2.

Keshet B, Yang IH, Good TA (2010) Can size alone explain some of the differences in toxicity between beta-amyloid oligomers and fibrils? *Biotechnol Bioeng* **106**:333-7.

Klunk WE, Pettegrew JW, Abraham DJ (1989) Quantitative evaluation of congo red binding to amyloid-like proteins with a beta-pleated sheet conformation. *J Histochem Cytochem* **37**:1273-81.

Koffie RM, Meyer-Luehmann M, Hashimoto T, Adams KW, Mielke ML, Garcia-Alloza M, Micheva KD, Smith SJ, Kim ML, Lee VM, Hyman BT, Spires-Jones TL (2009) Oligomeric amyloid beta associates with postsynaptic densities and correlates with excitatory synapse loss near senile plaques. *Proc Natl Acad Sci U S A* **106**:4012-7.

Koga H, Kaushik S, Cuervo AM (2011) Protein homeostasis and aging: The importance of exquisite quality control. *Ageing Res Rev* **10**:205-15.

Konno T, Murata K, Nagayama K (1999) Amyloid-like aggregates of a plant protein: a case of a sweet-tasting protein, monellin. *FEBS Lett* **454**:122-6.

Krishnan R, Goodman JL, Mukhopadhyay S, Pacheco CD, Lemke EA, Deniz AA, Lindquist S (2012) Conserved features of intermediates in amyloid assembly determine their benign or toxic states. *Proc Natl Acad Sci U S A* **109**:11172-7.

Krishnan R, Lindquist SL (2005) Structural insights into a yeast prion illuminate nucleation and strain diversity. *Nature* **435**:765-72.

Kubbutat MH, Jones SN, Vousden KH (1997) Regulation of p53 stability by Mdm2. *Nature* **387**:299-303.

Labbadia J, Morimoto RI (2015) The biology of proteostasis in aging and disease. *Annu Rev Biochem* **84**:435-64.

Ladiwala AR, Dordick JS, Tessier PM (2011) Aromatic small molecules remodel toxic soluble oligomers of amyloid beta through three independent pathways. *J Biol Chem* **286**:3209-18.

Ladiwala AR, Litt J, Kane RS, Aucoin DS, Smith SO, Ranjan S, Davis J, Van Nostrand WE, Tessier PM (2012) Conformational differences between two amyloid β oligomers of similar size and dissimilar toxicity. *J Biol Chem* **287**:24765-73.

Lakowicz JR (1999) Principles of Fluorescence Spectroscopy, 2nd Ed. Kluwer, New York.

Larson J, Lynch G, Games D, Seubert P (1999) Alterations in synaptic transmission and long-term potentiation in hippocampal slices from young and aged PDAPP mice. *Brain Res* **840**:23-35.

Lee J, Culyba EK, Powers ET, Kelly JW (2011) Amyloid-β forms fibrils by nucleated conformational conversion of oligomers. *Nat Chem Biol* **7**:602-9.

Lesné S, Koh MT, Kotilinek L, Kayed R, Glabe CG, Yang A, Gallagher M, Ashe KH (2006) A specific amyloid-beta protein assembly in the brain impairs memory. *Nature* **440**:352-7.

LeVine H 3rd (1993) Thioflavine T interaction with synthetic Alzheimer's disease beta-amyloid peptides: detection of amyloid aggregation in solution. *Protein Sci* **2**:404-10.

LeVine H 3rd (1995) Thioflavine T interaction with amyloid β-sheet structures. *Amyloid* **2**:1-6.

Levinthal C (1968) Are there pathways for protein folding? *J Chim Phys* **65**:44-5.

Li J, McQuade T, Siemer AB, Napetschnig J, Moriwaki K, Hsiao YS, Damko E, Moquin D, Walz T, McDermott A, Chan FK, Wu H (2012) The RIP1/RIP3 necrosome forms a functional amyloid signaling complex required for programmed necrosis. *Cell* **150**:339-50.

Lindgren M, Hammarström P (2010) Amyloid oligomers: spectroscopic characterization of amyloidogenic protein states. *FEBS J* **277**:1380-8.

Liu X, Wilcken R, Joerger AC, Chuckowree IS, Amin J, Spencer J, Fersht AR (2013) Small molecule induced reactivation of mutant p53 in cancer cells. *Nucleic Acids Res* **41**:6034-44.

Lomas DA, Carrell RW (2002) Serpinopathies and the conformational dementias. *Nat Rev Genet* **3**:759-68.

Lomas DA, Evans DL, Finch JT, Carrell RW (1992) The mechanism of Z alpha 1-antitrypsin accumulation in the liver. *Nature* **357**:605-7.

Lubin DJ, Butler JS, Loh SN (2010) Folding of tetrameric p53: oligomerization and tumorigenic mutations induce misfolding and loss of function. *J Mol Biol* **395**:705-16.

Lue LF, Kuo YM, Roher AE, Brachova L, Shen Y, Sue L, Beach T, Kurth JH, Rydel RE, Rogers J (1999) Soluble amyloid beta peptide concentration as a predictor of synaptic change in Alzheimer's disease. *Am J Pathol* **155**:853-62.

Ma J, Yee A, Brewer HB Jr, Das S, Potter H (1994) Amyloid-associated proteins alpha 1-antichymotrypsin and apolipoprotein E promote assembly of Alzheimer beta-protein into filaments. *Nature* **372**:92-4.

Maji SK, Perrin MH, Sawaya MR, Jessberger S, Vadodaria K, Rissman RA, Singru PS, Nilsson KP, Simon R, Schubert D, Eisenberg D, Rivier J, Sawchenko P, Vale W, Riek R (2009) Functional amyloids as natural storage of peptide hormones in pituitary secretory granules. *Science* **325**:328-32.

Makin OS, Atkins E, Sikorski P, Johansson J, Serpell LC (2005) Molecular basis for amyloid fibril formation and stability. *Proc Natl Acad Sci U S A* **102**:315-20.

Mannini B, Cascella R, Zampagni M, van Waarde-Verhagen M, Meehan S, Roodveldt C, Campioni S, Boninsegna M, Penco A, Relini A, Kampinga HH, Dobson CM, Wilson MR, Cecchi C, Chiti F (2012) Molecular mechanisms used by chaperones to reduce the toxicity of aberrant protein oligomers. *Proc Natl Acad Sci U S A* **109**:12479-84.

Mannini B, Mulvihill E, Sgromo C, Cascella R, Khodarahmi R, Ramazzotti M, Dobson CM, Cecchi C, Chiti F (2014) Toxicity of protein oligomers is rationalized by a function combining size and surface hydrophobicity. *ACS Chem Biol* **9**:2309-17.

Marcon G, Plakoutsi G, Canale C, Relini A, Taddei N, Dobson CM, Ramponi G, Chiti F (2005) Amyloid formation from HypF-N under conditions in which the protein is initially in its native state. *J Mol Biol* **347**:323-35.

Mastrangelo IA, Ahmed M, Sato T, Liu W, Wang C, Hough P, Smith SO (2006) High-resolution atomic force microscopy of soluble Abeta42 oligomers. *J Mol Biol* **358**:106-19.

McLean CA, Cherny RA, Fraser FW, Fuller SJ, Smith MJ, Beyreuther K, Bush AI, Masters CL (1999) Soluble pool of Abeta amyloid as a determinant of severity of neurodegeneration in Alzheimer's disease. *Ann Neurol* **46**:860-6.

Meacham GC, Patterson C, Zhang W, Younger JM, Cyr DM (2001) The Hsc70 co-chaperone CHIP targets immature CFTR for proteasomal degradation. *Nat Cell Biol* **3**:100-5.

Milner J, Medcalf EA (1991) Cotranslation of activated mutant p53 with wild type drives the wild-type p53 protein into the mutant conformation. *Cell* **65**:765-74.

Missmahl HP, Hartwig M (1953) Optical polarization studies of amyloid substance. *Virchows Arch Pathol Anat Physiol Klin Med* **324**:489-508.

Moechars D, Dewachter I, Lorent K, Reversé D, Baekelandt V, Naidu A, Tesseur I, Spittaels K, Haute CV, Checler F, Godaux E, Cordell B, Van Leuven F (1999) Early phenotypic changes in transgenic mice that overexpress different mutants of amyloid precursor protein in brain. *J Biol Chem* **274**:6483-92.

Mohanca M, Khemasuwan D, Stoller JK (2012) A review of augmentation therapy for alpha-1 antitrypsin deficiency. *Expert Opin Biol Ther* **12**:685-700.

Morris AM, Watzky MA, Finke RG (2009) Protein aggregation kinetics, mechanism, and curve-fitting: a review of the literature. *Biochim Biophys Acta* **1794**:375-97.

Naiki H, Hashimoto N, Suzuki S, Kimura S, Nakakuki K, Gejyo F (1997) Establishment of a kinetic model of dialysis-related amyloid fibril extension in vitro. *Amyloid* **4**:223-32.

Nathan BP, Bellosta S, Sanan DA, Weisgraber KH, Mahley RW, Pitas RE (1994) Differential effects of apolipoproteins E3 and E4 on neuronal growth in vitro. *Science* **264**:850-2.

Nelson R, Eisenberg D (2006) Recent atomic models of amyloid fibril structure. *Curr Opin Struct Biol* **16**:260-5.

Nelson R, Sawaya MR, Balbirnie M, Madsen AØ, Riekel C, Grothe R, Eisenberg D (2005) Structure of the cross-beta spine of amyloid-like fibrils. *Nature* **435**:773-8.

Nicolet Y, Piras C, Legrand P, Hatchikian CE, Fontecilla-Camps JC (1999) Desulfovibrio desulfuricans iron hydrogenase: the structure shows unusual coordination to an active site Fe binuclear center. *Structure* **7**:13-23.

Nilsberth C, Westlind-Danielsson A, Eckman CB, Condron MM, Axelman K, Forsell C, Stenh C, Luthman J, teplow DB, Younkin SG, Näslund J, Lannfelt L (2001) The 'Arctic' APP mutation (E693G) causes Alzheimer's disease by enhanced Abeta protofibril formation. *Nat Neurosci* **4**:887-93.

Nilsson MR (2004) Techniques to study amyloidfibril formation in vitro. *Methods* **34**:151-60.

Nyitrai M, Hild G, Hartvig N, Belágyi J, Somogyi B (2000) Conformational and dynamic differences between actin filaments polymerized from ATP- or ADP-actin monomers. *J Biol Chem* **275**:41143-9.

Ojha J, Masilamoni G, Dunlap D, Udoff RA, Cashikar AG (2011) Sequestration of toxic oligomers by HspB1 as a cytoprotective mechanism. *Mol Cell Biol* **31**:3146-57.

Olofsson A, Ippel JH, Wijmenga SS, Lundgren E, Ohman A (2004) Probing solvent accessibility of transthyretin amyloid by solution NMR spectroscopy. *J Biol Chem* **279**:5699-707.

Olzscha H, Schermann SM, Woerner AC, Pinkert S, Hecht MH, Tartaglia GG, Vendruscolo M, Hayer-Hartl M, Hartl FU, Vabulas RM (2011) Amyloid-like aggregates sequester numerous metastable proteins with essential cellular functions. *Cell* **144**:67-78.

Oma Y, Kino Y, Sasagawa N, Ishiura S (2005) Comparative analysis of the cytotoxicity of homopolymeric amino acids. *Biochim Biophys Acta* **1748**:174-9.

Oropesa-Nuñez R, Seghezza S, Dante S, Diaspro A, Cascella R, Cecchi C, Stefani M, Chiti F, Canale C (2016) Interaction of toxic and non-toxic HypF-N oligomers with lipid bilayers investigated at high resolution with atomic force microscopy. *Oncotarget* **7**:44991-45004.

Orte A, Birkett NR, Clarke RW, Devlin GL, Dobson CM, Klenerman D (2008) Direct characterization of amyloidogenic oligomers by single-molecule fluorescence. *Proc Natl Acad Sci U S A* **105**:14424-9.

Pagano K, Bemporad F, Fogolari F, Esposito G, Viglino P, Chiti F, Corazza A (2010) Structural and dynamics characteristics of acylphosphatase from Sulfolobus solfataricus in the monomeric state and in the initial native-like aggregates. *J Biol Chem* **285**:14689-700.

Palm T, Sale K, Brown L, Li H, Hambly B, Fajer PG (1999) Intradomain distances in the regulatory domain of the myosin head in prepower and postpower stroke states: fluorescence energy transfer. *Biochemistry* **38**:13026-34.

Paoli P, Camici G, Manao G, Giannoni E, Ramponi G (2000) Acylphosphatase possesses nucleoside triphosphatase and nucleoside diphosphatase activities. *Biochem J* **349**:43-9.

Paschos A, Glass RS, Böck A (2001) Carbamoylphosphate requirement for synthesis of the active center of [NiFe]-hydrogenases. *FEBS Lett* **488**:9-12.

Pedersen JS, Christensen G, Otzen DE (2004) Modulation of S6 fibrillation by unfolding rates and gatekeeper residues. *J Mol Biol* **341**:575-88.

Pedersen JS, Dikov D, Flink JL, Hjuler HA, Christiansen G, Otzen DE (2006a) The changing face of glucagon fibrillation: structural polymorphism and conformational imprinting. *J Mol Biol* **355**:501-23.

Pedersen JS, Flink JM, Dikov D, Otzen DE (2006b) Sulfates dramatically stabilize a salt-dependent type of glucagon fibrils. *Biophys J* **90**:4181-94.

Pellistri F, Bucciantini M, relini A, Nosi D, Gliozzi A, Robello M, Stefani M (2008) Nonspecific interaction of prefibrillar amyloid aggregates with glutamatergic receptors results in Ca2+ increase in primary neuronal cells. *J Biol Chem* **283**:29950-60.

Perlmutter DH (2011) Alpha-1-antitrypsin deficiency: importance of proteasomal and autophagic degradative pathways in disposal of liver disease-associated protein aggregates. *Annu Rev Med* **62**:333-45.

Pertinhez TA, Bouchard M, Tomlinson EJ, Wain R, Ferguson SJ, Dobson CM, Smith LJ (2001) Amyloid fibril formation by a helical cytochrome. *FEBS Lett* **495**:184-6.

Petkova AT, Ishii Y, Balbach JJ, Antzutkin ON, Leapman RD, Delaglio F, Tycko R (2002) A structural model for Alzheimer's beta-amyloid fibrils based on experimental constraints from solid state NMR. *Proc Natl Acad Sci U S A* **99**:16742-7.

Plakoutsi G, Bemporad F, Calamai M, Taddei N, Dobson CM, Chiti F (2005) Evidence for a mechanism of amyloid formation involving molecular reorganisation within native-like precursor aggregates. *J Mol Biol* **351**:910-22.

Pountney DL, Voelcker NH, Gai WP (2005) Annular alpha-synuclein oligomers are potentially toxic agents in alpha-synucleinopathy. Hypothesis. *Neurotox Res* **7**:59-67.

Putilina T, Skouri-Panet F, Prat K, Lubsen NH, Tardieu A (2003) Subunit exchange demonstrates a differential chaperone activity of calf alpha-crystallin toward beta LOW- and individual gamma-crystallins. *J Biol Chem* **278**:13747-56.

Qi W, Zhang A, Patel D, Lee S, Harrington JL, Zhao L, Schaefer D, Good TA, Fernandez EJ (2008) Simultaneous monitoring of peptide aggregate distributions, structure, and kinetics using amide hydrogen exchange: application to Abeta(1-40) fibrillogenesis. *Biotechnol Bioeng* **100**:1214-27.

Qu BH, Strickland EH, Thomas PJ (1997) Localization and suppression of a kinetic defect in cystic fibrosis transmembrane conductance regulator folding. *J Biol Chem* **272**:15739-44.

Raimondi S, Guglielmi F, Giorgetti S, Di Gaetano S, Arciello A, Monti DM, Relini A, Nichino D, Doglia SM, Natalello A, Pucci P, Mangione P, Obici L, Merlini G, Stoppini M, Robustelli P, Tartaglia GG, Vendruscolo M, Dobson CM, Piccoli R, Bellotti V (2011) Effects of the known pathogenic mutations on the aggregation pathway of the amyloidogenic peptide of apolipoprotein A-I. *J Mol Biol* **407**:465-76.

Ramakrishna D, Prasad MD, Bhuyan AK (2012) Hydrophobic collapse overrides Coulombic repulsion in ferricytochrome c fibrillation under extremely alkaline condition. *Arch Biochem Biophys* **528**:67-71.

Ramshini H, Parrini C, Relini A, Zampagni M, Mannini B, Pesce A, Saboury AA, Nemat-Gorgani M, Chiti F (2011) Large proteins have a great tendency to aggregate but a low propensity to form amyloid fibrils. *PLoS One* **6**:e16075.

Reissmann S, Hochleitner E, Wang H, Paschos A, Lottspeich F, Glass RS, Böck A (2003) Taming of a poison: biosynthesis of the NiFe-hydrogenase cyanide ligands. *Science* **299**:1067-70.

Relini A, Torrassa S, Ferrando R, Rolandi R, Campioni S, Chiti F, Gliozzi A (2010) Detection of populations of amyloid-like protofibrils with different physical properties. *Biophys J* **98**:1277-84.

Relini A, Torrassa S, Rolandi R, Gliozzi A, Rosano C, Canale C, Bolognesi M, Plakoutsi G, Bucciantini M, Chiti F, Stefani M (2004) Monitoring the process of HypF fibrillization and liposome permeabilization by protofibrils. *J Mol Biol* **338**:943-57.

Ritter C, Maddelein ML, Siemer AB, Lührs T, Ernst M, Meier BH, Saupe SJ, Riek R (2005) Correlation of structural elements and infectivity of the HET-s prion. *Nature* **435**:844-8.

Ron I, Horowitz M (2005) ER retention and degradation as the molecular basis underlying Gaucher disease heterogeneity. *Hum Mol Genet* **14**:2387-98.

Rosano C, Zuccotti S, Bucciantini M, Stefani M, Ramponi G, Bolognesi M (2002) Crystal structure and anion binding in the prokaryotic hydrogenase maturation factor HypF acylphosphatase-like domain. *J Mol Biol* **321**:785-96.

Russell D, Andrews PD, James J, Lane EB (2004) Mechanical stress induces profound remodelling of keratin filaments and cell junctions in epidermolysis bullosa simplex keratinocytes. *J Cell Sci* **117**:5233-43.

Saiki M, Honda S, Kawasaki K, Zhou D, Kaito A, Konakahara T, Morii H (2005) Higher-order molecular packing in amyloid-like fibrils constructed with linear arrangements of hydrophobic and hydrogen-bonding side-chains. *J Mol Biol* **348**:983-98.

Saridaki T, Zampagni M, Mannini B, Evangelisti E, Taddei N, Cecchi C, Chiti F (2012) Glycosaminoglycans (GAGs) suppress the toxicity of HypF-N prefibrillar aggregates. *J Mol Biol* **421**:616-30.

Sawkar AR, Adamski-Werner SL, Cheng WC, Wong CH, Beutler E, Zimmer KP, Kelly JW (2005) Gaucher disease-associated glucocerebrosidases show mutation-dependent chemical chaperoning profiles. *Chem Biol* **12**:1235-44.

Sawkar AR, Cheng WC, Beutler E, Wong CH, Balch WE, Kelly JW (2002) Chemical chaperones increase the cellular activity of N370S beta-glucosidase: a therapeutic strategy for Gaucher disease. *Proc Natl Sci U S A* **99**:15428-33.

Sawkar AR, D'Haeze W, Kelly JW (2006) Therapeutic strategies to ameliorate lysosomal storage disorders – a focus on Gaucher disease. *Cell Mol Life Sci* **63**:1179-92.

Schiene C, Fischer G (2000) Enzymes that catalyse the restructuring of proteins. *Curr Opin Struct Biol* **10**:40-45.

Selvin PR (2000) The renaissance of fluorescence resonance energy transfer. *Nat Struct Biol* **7**:730-4.

Serio TR, Cashikar AG, Kowal AS, Sawicki GJ, Moslehi JJ, Serpell L, Arnsdorf MF, Lindquist SL (2000) Nucleated conformational conversion and the replication of conformational information by a prion determinant. *Science* **289**:1317-21.

Serpell LC (2000a) Alzheimer's amyloid fibrils: structure and assembly. *Biochim Biophys Acta* **1502**:16-30.

Serpell LC, Berriman J, Jakes R, Goedert M, Crowther RA (2000b) Fiber diffraction of synthetic alpha-synuclein filaments shows amyloid-like cross-beta conformation. *Proc Natl Acad Sci U S A* **97**:4897-902.

Serpell LC, Sunde M, Benson MD, Tennent GA, Pepys MB, Fraser PE (2000c) The protofilament substructure of amyloid fibrils. *J Mol Biol* **300**:1033-9.

Singh S, Trikha S, Bhowmick DC, Sarkar AA, Jeremic AM (2015) Role of Cholesterol and Phospholipids in Amylin Misfolding, Aggregation and Etiology of Islet Amyloidosis. *Adv Exp Med Biol* **855**:95-116.

Sirangelo I, Malmo C, Iannuzzi C, Mezzogiorno A; Bianco MR, Papa M, Irace G (2004) Fibrillogenesis and cytotoxic activity of the amyloid-forming apomyoglobin mutant W7FW14F. *J Biol Chem* **279**:13183-9.

Soldi G, Bemporad F, Chiti F (2008) The degree of structural protection at the edge beta-strands determines the pathway of amyloid formation in globular proteins. *J Am Chem Soc* **130**:4295-302.

Solomon JP, Page LJ, Balch WE, Kelly JW (2012) Gelsolin amyloidosis: genetics, biochemistry, pathology and possible strategies for therapeutic intervention. *Crit Rev Biochem Mol Biol* **47**:282-96.

Spillantini MG, Goedert M (2013) Tau pathology and neurodegeneration. *Lancet Neurol* **12**:609-22.

Stefani M (2010) Biochemical and biophysical features of both oligomer/fibril and cell membrane in amyloid cytotoxicity. *FEBS J* **277**:4602-13.

Stefani M, Dobson CM (2003) Protein aggregation and aggregate toxicity: new insights into protein folding, misfolding diseases and biological evolution. *J Mol Med (Berl)* **81**:678-99.

Stefani M, Ramponi G (1995) Acylphosphate phosphohydrolases. *Life Chem Rep* **12**:271-301.

Sunde M, Blake C (1997) The structure of amyloid fibrils by electron microscopy and X-ray diffraction. *Adv Protein Chem* **50**:123-59.

Sunde M, Serpell LC, Bartlam M, Fraser PE, Pepys MB, Blake CC (1997) Common core structure of amyloid fibrils by synchrotron X-ray diffraction. *J Mol Biol* **273**:729-39.

Tatini F, Pugliese AM, Traini C, Niccoli S, Maraula G, Ed Dami T, Mannini B, Scartabelli T, Pedata F, Casamenti F, Chiti F (2013) Amyloid-β oligomer synaptotoxicity is mimicked by oligomers of the model protein HypF-N. *Neurobiol Aging* **34**:2100-9.

Tomiyama T, Nagata T, Shimada H, Teraoka R, Fukushima A, Kanemitsu H, Takuma H, Kuwano R, Imagawa M, Ataka S, Wada Y, Yoshioka E, Nishizaki T, Watanabe Y, Mori H (2008) A new amyloid beta variant favoring oligomerization in Alzheimer's-type dementia. *Ann Neurol* **63**:377-87.

Toyama BH, Weissman JS (2011) Amyloid structure: conformational diversity and consequences. *Annu Rev Biochem* **80**:557-85.

Tycko R (2003) Insights into the amyloid folding problem from solid-state NMR. *Biochemistry* **42**:3151-9.

Tycko R, Wickner RB (2013) Molecular structures of amyloid and prion fibrils: consensus versus controversy. *Acc Chem Res* **46**:1487-96.

Usmani SM, Zirafi O, Müller JA, Sandi-Monroy NL, Yadav JK, Meier C, Weil T, Roan NR, Greene WC, Walther P, Nilsson KP, Hammarström P, Wetzel R, Pilcher CD, Gagsteiger F, Fändrich M, Kirchhoff F, Münch J (2014) Direct visualization of HIV-enhancing endogenous amyloid fibrils in human semen. *Nat Commun* **5**:3508.

Uversky VN, Fink AL (2004) Conformational constraints for amyloid fibrillation: the importance of being unfolded. *Biochim Biophys Acta* **1698**:131-53.

Uversky VN (2014) The triple power of D^3: protein intrinsic disorder in degenerative diseases. *Front Biosci (Landmark Ed)* **19**:181-258.

Van Der Meer BW (1994) Resonance Energy Transfer: Theory and Data, VCH, New York.

van Rooijen BD, Claessens MM, Subramaniam V (2010) Membrane Permeabilization by Oligomeric α-Synuclein: In Search of the Mechanism. *PLoS One* **5**:e14292.

Vassilev LT, Vu BT, Graves B, Carvajal D, Podlaski F, Filipovic Z, Kong N, Kammlott U, Lukacs C, Klein C, Fotouhi N, Liu EA (2004) In vivo activation of the p53 pathway by small-molecule antagonists of MDM2. *Science* **303**:844-8.

Vestergaard B, Groenning M, Roessle M, Kastrup JS, van de Weert M, Flink JM, Frokjaer S, Gajhede M, Svergun DI (2007) A helical structural nucleus is the primary elongating unit of insulin amyloid fibrils. *PLoS Biol* **5**:e134.

Voellmy R, Boellmann F (2007) Chaperone regulation of the heat shock protein response. *Adv Exp Med Biol* **594**:89-99.

Wang J, Dickson DW, Trojanowski JQ, Lee VM (1999) The levels of soluble versus insoluble brain Abeta distinguish Alzheimer's disease from normal and pathologic aging. *Exp Neurol* **158**:328-37.

Wang X, Venable J, LaPointe P, Hutt DM, Koulov AV, Coppinger J, Gurkan C, Kellner W, Matteson J, Plutner H, Riordan JR, Kelly JW, Yates JR 3rd, Balch WE (2006) Hsp90 cochaperone Aha1 downregulation rescues misfolding of CFTR in cystic fibrosis. *Cell* **127**:803-15.

Werner NS, Windoffer R, Strnad P, Grund C, Leube RE, Magin TM (2004) Epidermolysis bullosa simplex-type mutations alter the dynamics of the keratin cytoskeleton and reveal a contribution of actin to the transport of keratin subunits. *Mol Biol Cell* **15**:990-1002.

Westermark P, Benson MD, Buxbaum JN, Cohen AS, Frangione B, Ikeda S, Masters CL, Merlini G, Saraiva MJ, Sipe JD (2005) Amyloid: toward terminology clarification. Report from the Nomenclature Committee of the International Society of Amyloidosis. *Amyloid* **12**:1-4.

Whitesell L, Mimnaugh EG, De Costa B, Myers CE, Neckers LM (1994) Inhibition of heat shock protein HSP90-pp60v-src heteroprotein complex formation by benzoquinone

ansamycins: essential role for stress proteins in oncogenic transformation. *Proc Natl Acad Sci U S A* **91**:8324-8.

Winkelmann J, Calloni G, Campioni S, Mannini B, Taddei N, Chiti F (2010) Low-level expression of a folding-incompetent protein in Escherichia coli: search for the molecular determinants of protein aggregation in vivo. *J Mol Biol* **398**:600-13.

Winner B, Jappelli R, Maji SK, Desplats PA, Boyer L, Aigner S, Hetzer C, Loher T, Vilar M, Campioni S, Tzitzilonis C, Soragni A, Jessberger S, Mira H, Consiglio A, Pham E, Masliah E, Gage FH, Riek R (2011) In vivo demonstration that alpha-synuclein oligomers are toxic. *Proc Natl Acad Sci U S A* **108**:4194-9.

Wishner BC, Ward KB, Lattman EE, Love WE (1975) Crystal structure of sickle-cell deoxyhemoglobin at 5 A resolution. *J Mol Biol* **98**:179-94.

Xu Y, Lindquist S (1993) Heat-shock protein hsp90 governs the activity of pp60v-src kinase. *Proc Natl Acad Sci U S A* **90**:7074-8.

Yu L, Edalji R, Harlan JE, Holzman TF, Lopez AP, Labkovsky B, Hillen H, Barghorn S, Ebert U, Richardson PL, Miesbauer L, Solomon L, Bartley D, Walter K, Johnson RW, Hajduk PJ, Olejniczak ET (2009) Structural characterization of a soluble amyloid beta-peptide oligomer. *Biochemistry* **48**:1870-7.

Zampagni M, Cascella R, Casamenti F, Grossi C, Evangelisti E, Wright D, Becatti M, Liguri G, Mannini B, Campioni S, Chiti F, Cecchi C (2011) A comparison of the biochemical modifications caused by toxic and non-toxic protein oligomers in cells. *J Cell Mol Med* **15**:2106-16.

Zraika S, Hull RL, Verchere CB, Clark A, Potter KJ, Fraser PE, Raleigh DP, Kahn SE (2010) Toxic oligomers and islet beta cell death: guilty by association or convicted by circumstantial evidence? *Diabetologia* **53**:1046-56.